

## University of Southampton Research Repository

Copyright © and Moral Rights for this thesis and, where applicable, any accompanying data are retained by the author and/or other copyright owners. A copy can be downloaded for personal non-commercial research or study, without prior permission or charge. This thesis and the accompanying data cannot be reproduced or quoted extensively from without first obtaining permission in writing from the copyright holder/s. The content of the thesis and accompanying research data (where applicable) must not be changed in any way or sold commercially in any format or medium without the formal permission of the copyright holder/s.

When referring to this thesis and any accompanying data, full bibliographic details must be given, e.g.

Thesis: Author (Year of Submission) "Full thesis title", University of Southampton, name of the University Faculty or School or Department, MPhil Thesis, pagination.

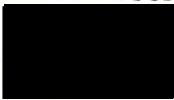
Data: Author (Year) Title. URI [dataset]

Library Loan and Photocopying Permit

Title of Thesis .. STUDIES OF ADSORBED SPECIES BY ELECTROCHEMICALLY MODULATED INFRARED SPECTROSCOPY.

Candidate ... Catherine GIBILARO .....

Three copies of the above thesis are now formally submitted for the degree of ..... Should the Senate of the University award me either this degree or another higher degree in respect of this thesis, I hereby agree that from the date of the award the thesis may be made available for inter-library loan or for photocopying and that the abstract may be made available for publication.

Signature .....  ..... Date .. 6<sup>th</sup> December 19.82 ..



UNIVERSITY OF SOUTHAMPTON

DEPARTMENT OF CHEMISTRY

STUDIES OF ADSORBED SPECIES BY ELECTROCHEMICALLY  
MODULATED INFRARED SPECTROSCOPY.

By

Catherine GIBILARO

A thesis submitted for the degree of  
Master of Philosophy

December 1982



A mes sweet parents,

UNIVERSITY OF SOUTHAMPTON

ABSTRACT

FACULTY OF SCIENCE

CHEMISTRY

Master of Philosophy

STUDIES OF ADSORBED SPECIES BY  
ELECTROCHEMICALLY MODULATED  
INFRARED SPECTROSCOPY

by Catherine GIBILARO

Electrochemically modulated infrared spectroscopy has been used to obtain infrared spectra of adsorbates in different electrochemical systems. This very sensitive technique provides direct information on the identity and the molecular structure of the adsorbed species present at the electrode surface, as well as their orientation and bonding to the electrode surface.

Systems studied included the adsorption of acrylonitrile on a gold electrode in aqueous sulphuric acid, and the adsorption of cyanide on silver and gold electrodes in aqueous potassium cyanide.

The results reported for the gold/acrylonitrile system have shown that the entire molecule is adsorbed over the potential range investigated with a molecular orientation parallel to the electrode surface.

The study of the adsorption of cyanide on a silver electrode has shown that the nature of the adsorbed species is dependent on the concentration of cyanide ions. The nature of the surface complex species, which is thought to be formed on silver and gold electrodes in concentrated solution, is discussed.

## ACKNOWLEDGEMENTS

I would like to express my thanks to Dr. A. Bewick for his guidance and encouragement throughout the course of this work.

I am very grateful to Dr. P. Hendra for inviting me to study at the University of Southampton.

I would also like to thank Dr. K. Kunimatsu, Dr. J. Russell, Dr. M. Razaq and Dr. B. Beden for their helpful suggestions and guidance in the course of my work.

I am grateful to all the people who have been working in this group since I joined it for providing a friendly atmosphere in which to work.

Without the collaboration and unfailing encouragements of Mr. Francis Lasserre this research would not have been completed.

Thanks are due to Mrs. K. Welfare for her patience to type this thesis.

Finally, I would like to thank all my family, for their continuous support throughout my student life.

## C O N T E N T S

Page

### CHAPTER ONE

	Vibrational Spectroscopies for Studying the Electrode/Electrolyte Interphase and Electrode Surface.	1.
1.1	Introduction	1.
1.2	Optical " <u>in-situ</u> " Methods	2.
1.2.1	Ellipsometry	2.
1.2.2	Internal Reflection Spectroscopy (IRS)	3.
1.2.3	Specular External Reflectance Spectroscopy	6.
1.2.4	Laser Raman Spectroscopy	9.
1.2.4.1	The Raman Effect	9.
1.2.4.2	Resonance Raman Effect	11.
1.2.4.3	Surface Enhanced Raman Spectroscopy	12.
1.3	" <u>Ex-situ</u> " Techniques	13.
1.3.1	Introduction	13.
1.3.2	X-Ray Photoelectron Spectroscopy	13.
1.3.3	Auger Electron Spectroscopy	15.
1.3.4	Low Energy Electron Diffraction	16.
1.3.5	Conclusion	17.
1.4	Conclusion	18.

### CHAPTER TWO

	Theoretical Considerations	19.
2.1	Introduction	19.
2.2	The Electrical Double Layer	19.
2.3	A.C. Impedance Measurement of Differential Capacitance	23.
2.4	Infra Red Modulated Specular Reflectance Spectroscopy	27.
2.4.1	Introduction - Earlier Work in MSRS	27.
2.4.2	Vibrational and Surface Selection Rules	30.
2.4.2.1	Infra Red Selection Rules	30.
2.4.2.2	Surface Selection Rule	32.



	<u>Page</u>
2.4.3 Electrochemically Modulated Infra Red Spectroscopy (EMIRS)	36.
2.4.3.1 Description of the EMIRS Technique	36.
2.4.3.2 Earlier Work in EMIRS	43.
2.4.4 Subtractively Normalized Interfacial Fourier Transform Infra Red Spectroscopy (SNIFTIRS)	48.
2.4.5 Infra Red Reflection Absorption Spectroscopy (IRRAS)	49.
 <u>CHAPTER THREE</u> 	
Experimental	53.
3.1 Infra Red/Electrochemical Cells and Electrodes	53.
3.1.1 Cells	53.
3.1.2 Electrodes	55.
3.2 Preparation of Solutions, Glassware and Electrodes	57.
3.3 EMIRS Experimental Apparatus	58.
3.3.1 The Optical Equipment	58.
3.3.2 The Electrode Potential Modulation Equipment	63.
3.3.3 The Signal Recovery and Processing Systems	64.
3.4 Experimental Procedures	67.
3.5 Electrode Capacitance Measurements	70.
 <u>CHAPTER FOUR</u> 	
Acrylonitrile Adsorption on a Gold Electrode	73.
4.1 Introduction	73.
4.2 Double Layer Capacity Measurements	73.
4.3 EMIRS Experiments	80.
4.3.1 Experimental	80.
4.3.2 Results and Discussion	80.
4.4 Conclusion	92.

CHAPTER FIVE

	Cyanide Adsorption on Silver and Gold Electrodes	94.
5.1	Introduction - Earlier work in Raman	94.
5.2	EMIRS Experiments	102.
5.2.1	Experimental	102.
5.2.2	Results and Discussion	103.
5.2.2.1	The Silver/Cyanide System	103.
5.2.2.2	The Gold/Cyanide System	112.
5.3	Conclusion	122.

CHAPTER SIX

	Conclusion	123.
--	------------	------

	<u>REFERENCES</u>	125.
--	-------------------	------

## CHAPTER ONE

### Vibrational Spectroscopies for Studying the Electrode/ Electrolyte Interphase and Electrode Surface

#### 1.1 Introduction

The most serious test for modern day science is that of meeting the world's present needs for energy. In this problem, electrochemistry has an important part to play in providing newer and more efficient means of obtaining energy and utilising present resources.

Fuel cells<sup>(1,2)</sup> constitute one of the most promising areas for research, and a complete understanding of the processes occurring in these cells is the required condition for their development and improvement. Therefore, a detailed insight into the electronic and molecular structure of the electrode-solution interface must be obtained in order to understand the important factors controlling electrocatalytic processes.

Unfortunately, none of the direct electrochemical methods usually employed to study a system will provide such data, and the majority of the physical methods, recently developed for surface characterization<sup>(3)</sup>, involve high vacuum conditions which are unsuitable for in-situ studies of an electrode immersed in an electrolyte solution. This led to the development of several in-situ methods capable of giving molecular information concerning electrochemical interfaces and processes occurring thereat. Optical spectroscopy, one of the powerful tools currently used by scientists to elucidate the structure of molecules, lends itself to in-situ studies. The majority of the presently used in-situ spectroscopic techniques were recently reviewed by Yeager<sup>(4,5)</sup>.

Infra red spectroscopy was used throughout the work reported in this thesis to study adsorbed species on gold and silver electrodes. The technique used and described in chapter two is a modulated external reflectance spectroscopic technique. The remainder of this chapter presents a brief review of some of the other current and prospective in-situ techniques, and a summary of the related helpful work provided by the ex-situ spectroscopies carried out in the ultra-high vacuum environment.

## 1.2 Optical "in-situ" Methods (6-8)

The simplest way of looking at electrode surfaces in-situ is to shine a beam of light, u.v., visible or infra red, at the electrode and to detect either the reflected or transmitted beam which will have been perturbed by any change in the structure of the electrode-electrolyte solution interphase. A number of optical techniques have been used in this way; some of those which have found extensive use for in-situ studies of electrochemical interfaces are described in the following parts. Only the electrochemical aspect of their application will be considered.

### 1.2.1 Ellipsometry (9-14)

Reflection of a plane polarized light from a surface generally produces elliptically polarized light, because the parallel and perpendicular components are reflected with different efficiencies and with different phase shifts.

Reflectance ellipsometry is a technique concerned with the measurement of three parameters: the change in relative amplitude ( $\psi$ ) and relative phase ( $\Delta$ ) of two orthogonal components of light due to reflection, and the change in relative reflectivity of the surface  $\left(\frac{\delta R}{R}\right)$  (15-17). These changes are interpreted in terms of the properties of the reflecting surface.

This optical technique has been in existence for at least 100 years<sup>(18)</sup> and its first application to electrochemistry was made 50 years ago<sup>(19)</sup> in a study by Tronstad of the passivation and corrosion of metals. The technique was not taken up again until the end of the 1960's when the availability of high-speed computers and comprehensive programs<sup>(20)</sup>, capable of solving the rather complex equations involved<sup>(21)</sup>, brought a renewed interest in it.

In order to calculate the optical properties of an interface from the ellipsometric measurements a model is required, which is assumed to describe as adequately as possible the interface. A three-layer model is usually used, where the three layers are: the substrate, a film, and the ambient<sup>(17)</sup>. Many

ellipsometric investigations are in fact concerned with the characterization of the optical constants and thickness of this intermediate film layer as a means to probe its structure.

Ideally, it can be possible to follow ellipsometrically the adsorption of various sorts of species from the environment onto the surface. There have been few ellipsometric studies of specific adsorption of ions<sup>(22-25)</sup>, and very few investigations have been made of the adsorption of organic molecules<sup>(26-30)</sup>. It was clearly shown that the interpretation of ellipsometric measurements of partial monolayer films depends essentially on the choice of the optical model for the layer and the value assumed for its thickness. Unfortunately, it appears recently<sup>(16,31)</sup> that the widely used three-layer model is adequate only for relatively thick layers, such as those encountered in corrosion and passivation studies<sup>(12)</sup>.

Ellipsometry is therefore best suited to the accurate determination of optical constants, and to the study of thick surface films. Its application elsewhere in electrochemistry is somewhat limited.

### 1.2.2 Internal Reflection Spectroscopy (IRS)<sup>(14,32-35)</sup>

This technique sometimes referred to as "Attenuated total reflectance" (ATR) made possible the optical and spectroscopic observation of the region within about a tenth of a wavelength of the electrochemical interface, without any interference whatever from the rest of the electrolyte. The idea is to detect, identify, and/or quantitatively measure concentration of electroactive species within this region as they come and go during electrochemical manipulation.

The theory and application of internal reflection spectroscopy have been thoroughly covered in a book by Harrick<sup>(32)</sup>, and more recently by Hansen<sup>(34,36)</sup>; no more than a brief summary will be given here.

As shown in Figure I.1, the monochromatic light enters the internal reflection element, i.e. the optically more dense phase ( $n_1$ ), and then undergoes multiple reflection if the angle of

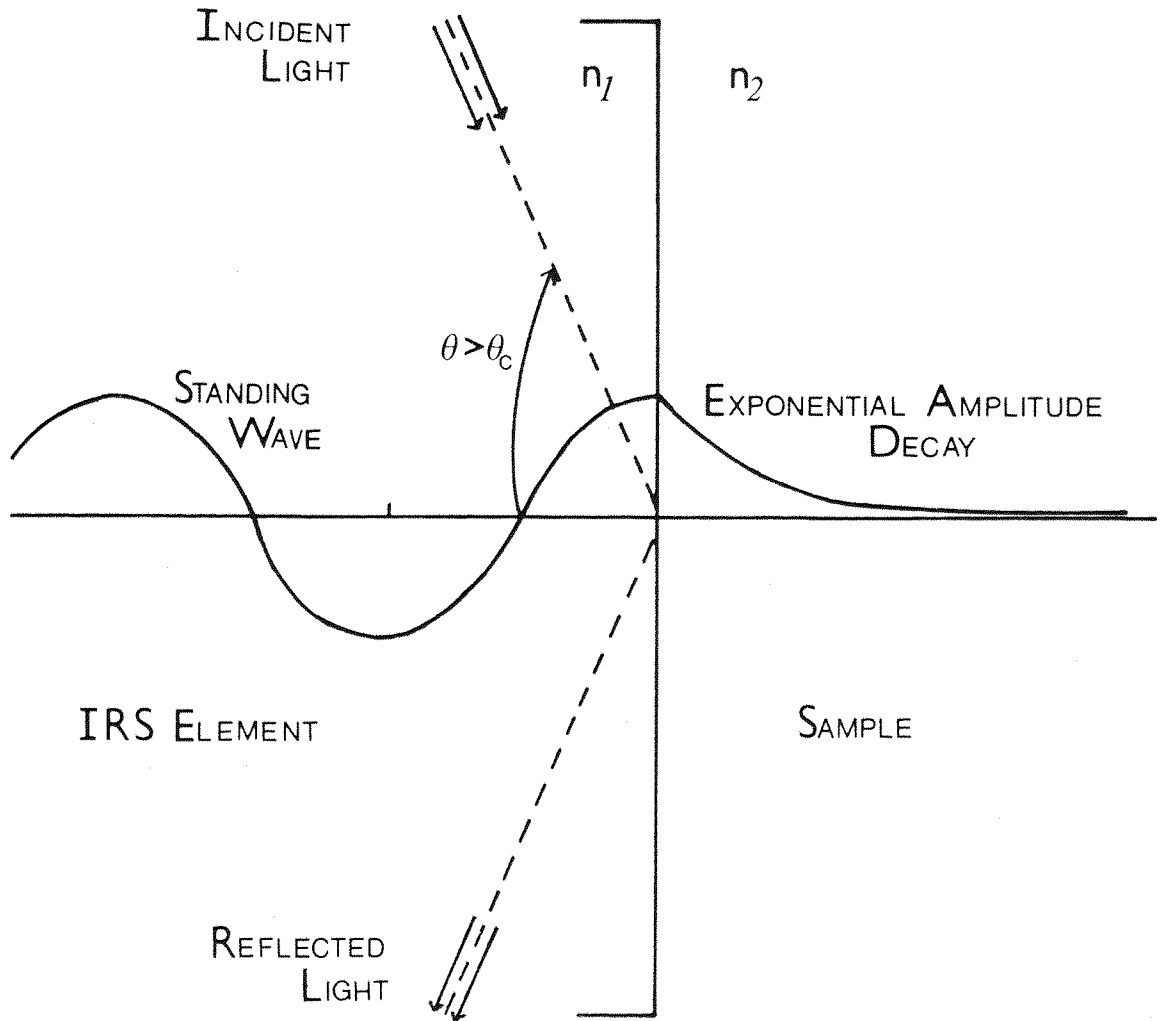


FIGURE I.1— Attenuated total internal reflection. Energy is transferred to an absorbing sample via the evanescent wave.  $n_1$  = refractive index of the IRS element and  $n_2$  = refractive index of the sample;  $n_1 > n_2$ .

incidence is greater than the critical angle  $\theta_c$  (defined by  $\sin \theta_c = \frac{n_2}{n_1}$ ). Components of the incident and reflected waves combine to form a standing wave in the denser medium, normal to the reflecting boundary, and there is an intense evanescent non-propagating field produced in the rarer medium, whose intensity falls exponentially with distance with a characteristic length of the order of one-tenth of a wavelength of the source radiation. Depending on the system and its parameters, the internal reflection element can be an electrical conductor used directly as the electrode or the thin layer electrode of an optically transparent electrode or the transparent substrate of it.

The presence of photo-active species on the sample side of the interface will cause absorption of energy from the evanescent wave, and transfer of energy across the interface; the interaction being greatest within the compact double layer. This loss of energy to the absorbing species is seen as an attenuation of the reflected beam<sup>(32)</sup>. The attenuation of the light passing through an IRS cell is monitored and recorded just as in a transmission spectrum.

Several types of optically transparent electrodes (OTE) have been used as working electrodes<sup>(56)</sup>, these are :

- very thin carbon<sup>(51)</sup> and metal films, e.g. platinum, palladium or gold, deposited on to transparent substrates by vacuum evaporation methods<sup>(38-41)</sup>.
- Transparent substrates coated with thin films of semi-conductor, e.g. doped tin or indium oxides<sup>(52)</sup>.
- Solid plates of semi-conductor, such as germanium<sup>(47,50)</sup>; and minigrids of gold<sup>(53)</sup> or mercury-coated gold or nickel<sup>(54,55)</sup>.

In an electrochemical context the use of IRS allows the monitoring of the surface concentration of electroactive species within the diffusion region in various electrochemical operations<sup>(42)</sup>. Most of the work published concerns the use of IRS to observe intermediates and products produced during an electrochemical reaction, e.g. oxidation, reduction<sup>(46,57)</sup> or polymer

film formation<sup>(44)</sup>.

Although successful IRS experiments have been reported<sup>(34)</sup>, this technique is somewhat limited by the use of optically transparent electrodes with their attendant, substantial disadvantages<sup>(45, 46)</sup>. IRS method was applied a few times in the infra red region<sup>(47-51)</sup> using germanium plate-electrodes, but as the electrochemical properties of these electrodes are quite complex, some difficulties were reported<sup>(38, 43)</sup>.

### 1.2.3 Specular External Reflectance Spectroscopy<sup>(14, 46, 58, 60)</sup>

Specular reflection spectroscopy is an analytical technique which has been widely applied to the study of the optical properties of solids, e.g. metals, semiconductors, for many years. Since its first successful application to electrochemistry in the mid 1960's<sup>(59)</sup> this technique has received increased attention as a method of studying in-situ the formation and optical properties of very thin films on surfaces and for detecting intermediates and products of heterogeneous chemical and electrochemical reactions<sup>(58, 60-66)</sup>.

The principles of physical optics on which the method is based are identical to those of the classical ellipsometric method of studying surface films, the changes in the polarization state of the light reflected from the surface being recorded using differential reflection spectroscopy. The normalized reflectivity changes,  $\left(\frac{\Delta R}{R}\right)_P$  and  $\left(\frac{\Delta R}{R}\right)_S$ , are determined by measurement of the intensity ratios of rays specularly reflected from the filmed surfaces and bare surfaces or electrode surfaces in a known state. The normalized reflectance change is therefore defined by,

$$\frac{\Delta I_R}{I_R} = \frac{\Delta R}{R} = \frac{R(d) - R(o)}{R(o)} = \frac{R(d)}{R(o)} - 1 \quad (1.0)$$

where  $I_R$  is the measured intensity of the reflected beam,  $R(d)$  is the reflectance of the three-phase system (ambient-film-substrate) and  $R(o)$  is the reflectance of the corresponding film-free two phase system.

For very thin films ( $d \ll \lambda$ ) as it is often the case in electro-



chemical situations, McIntyre and Aspnes<sup>(67)</sup> have shown that, using linear approximation theory, the complicated reflectance relations reduce to,

$$\left(\frac{\Delta R}{R}\right)_P = \frac{8\pi dn_1 \cos\phi_1}{\lambda} \operatorname{Im} \left[ X \left( \frac{1 - (\epsilon_1/\hat{\epsilon}_2 \hat{\epsilon}_3)(\hat{\epsilon}_2 + \hat{\epsilon}_3)\sin^2\phi_1}{1 - (1/\hat{\epsilon}_3)(\epsilon_1 + \hat{\epsilon}_3)\sin^2\phi_1} \right) \right] \quad (1.1)$$

and

$$\left(\frac{\Delta R}{R}\right)_S = \frac{8\pi dn_1 \cos\phi_1}{\lambda} \operatorname{Im} [X] \quad (1.2)$$

For parallel (p) and perpendicular (s) polarized radiation and where  $\operatorname{Im}[X]$  refers to the imaginary part of  $X$ ,

$$X = \left( \frac{\hat{\epsilon}_2 - \hat{\epsilon}_3}{\epsilon_1 - \hat{\epsilon}_3} \right) \quad (1.3)$$

$\phi_1$  is the angle of incidence in the ambient phase with real dielectric constant  $\epsilon_1$  and refractive index  $n_1$ , and  $\hat{\epsilon}_2$ ,  $\hat{\epsilon}_3$  are the complex dielectric constants of the absorbing thin film and substrate phases, respectively.

McIntyre<sup>(60)</sup> has shown that the relative reflectivity change as a film grows on a surface and for normal incidence is given by,

$$\frac{\Delta R}{R} = \frac{\theta 8\pi dn_1}{\lambda} \operatorname{Im}[X] \quad (1.4)$$

it follows that  $\frac{\Delta R}{R}$  is linearly proportional to the surface coverage,  $\theta$ , provided that the physical properties ( $\hat{\epsilon}_2$ ) of the film does not vary with  $\theta$ .

In general  $(\Delta R/R)$  can be written as,

$$\frac{\Delta R}{R} = \frac{R_{(A)} - R_{(B)}}{R} \quad (1.5)$$

which refers simply to the relative reflectivity change between two states of the electrode, A and B, and implies nothing about the model used to describe them. This form of representation will be used throughout the work reported in this thesis (see section 2.4.3.1).

The application of the above equations to a number of systems of interest in surface chemistry and physics have been described in detail<sup>(67)</sup>. Bewick et al have discussed the application of this theory to electrochemical systems<sup>(46,68-70)</sup>, by comparing experimental results with theoretical ones from computer calculations.

In practice changes in the structure of the interphase produce only very small changes in the reflectivity and these are often so small that they are buried in noise generated in the detection equipment. Two different means of improving the sensitivity have been approached.

The first of these was to use multiple reflections whereby two working electrodes held at the same potential are mounted in parallel and the light beam is obliquely reflected many times between them before being detected. Takamura et al<sup>(64)</sup> have used this technique to study oxide formation, specific adsorption of iodide ions and under-potential deposition of lead and cadmium on a gold electrode. Cahar et al<sup>(71)</sup> have examined the gold/electrolyte interface with both single and multiple reflection techniques. After the initial popularity, multiple reflection techniques have largely been dropped, being very difficult to interpret<sup>(72)</sup>, in favour of electrode potential modulation, a technique previously successfully employed<sup>(73)</sup>.

Modulated specular reflectance spectroscopy is the technique used in the present work and the experimental and theoretical details are given in subsequent chapters. Briefly, the potential of the reflecting electrode is repeatedly modulated permitting correlation techniques (phase sensitive detection or/and signal averaging) to be used. In this way relative reflectivity changes ( $\Delta R/R$ ) as small as  $1 \times 10^{-6}$  can be detected<sup>(45)</sup>. This optical technique has the great advantage that, like ellipsometry normal bulk-type electrodes can be used, whilst very much simpler optics are required. Also electrodes in contact with absorbing solutions can be studied and wavelength and potential scanning are readily accomplished. A considerable amount of work has concentrated on the electronic structure of the electrode surface and a number of

theories have been proposed to account for the results<sup>(60,74-78)</sup>. A number of systems involving the underpotential deposition of metals, and particularly lead, have been investigated<sup>(79-82)</sup>. Modulated specular reflectance spectroscopy has also been increasingly employed in kinetic studies of electrode processes and in electrosorption and specific adsorption studies. This work will be reviewed in chapter two.

#### 1.2.4 Laser Raman Spectroscopy<sup>(14,83-86)</sup>

##### 1.2.4.1 The Raman effect

When an intense beam of monochromatic light ( $\nu_0$ ) is passed through a transparent medium, a small fraction of the light is scattered in all directions. Most of this light is elastically scattered, i.e. without a change in photon energy, that is, the Rayleigh effect ( $\nu_0$ ) which gives an intense line in the scattered spectra. However, some photons exchange energy with the vibrating molecules of the sample ( $\nu_{\text{vib}}$ ) and are inelastically scattered, with a change in wavelength reflecting the loss ( $\nu_0 - \nu_{\text{vib}}$ ) or gain ( $\nu_0 + \nu_{\text{vib}}$ ) in energy. These two frequencies, characteristic of the sample, are identified as the Raman scattering frequencies, first observed by C.V. Raman in 1928<sup>(87)</sup>, and are known respectively as the 'Stokes' and 'anti-Stokes' lines, Figure I.2.

The classical theory of the Raman effect fully described in many comprehensive texts<sup>(85,86)</sup> leads to an understanding of the basic concept of this form of spectroscopy, i.e. its relationship to the polarizability of a molecule,  $\alpha$ . This parameter can be defined as the ease with which a dipole may be induced in the electron cloud of a molecule by an externally applied electric or magnetic vector. For a vibration to be Raman active, i.e. for the frequencies  $\nu_0 \pm \nu_{\text{vib}}$  to appear in the scattered radiation, there must be some change in the molecular polarizability during the vibration. Similar selection rules may be formulated for the infra red spectra where in place of the polarizability it is the components of the molecular dipole moment which are involved. The important consequence of these two different selection rules will be discussed later.

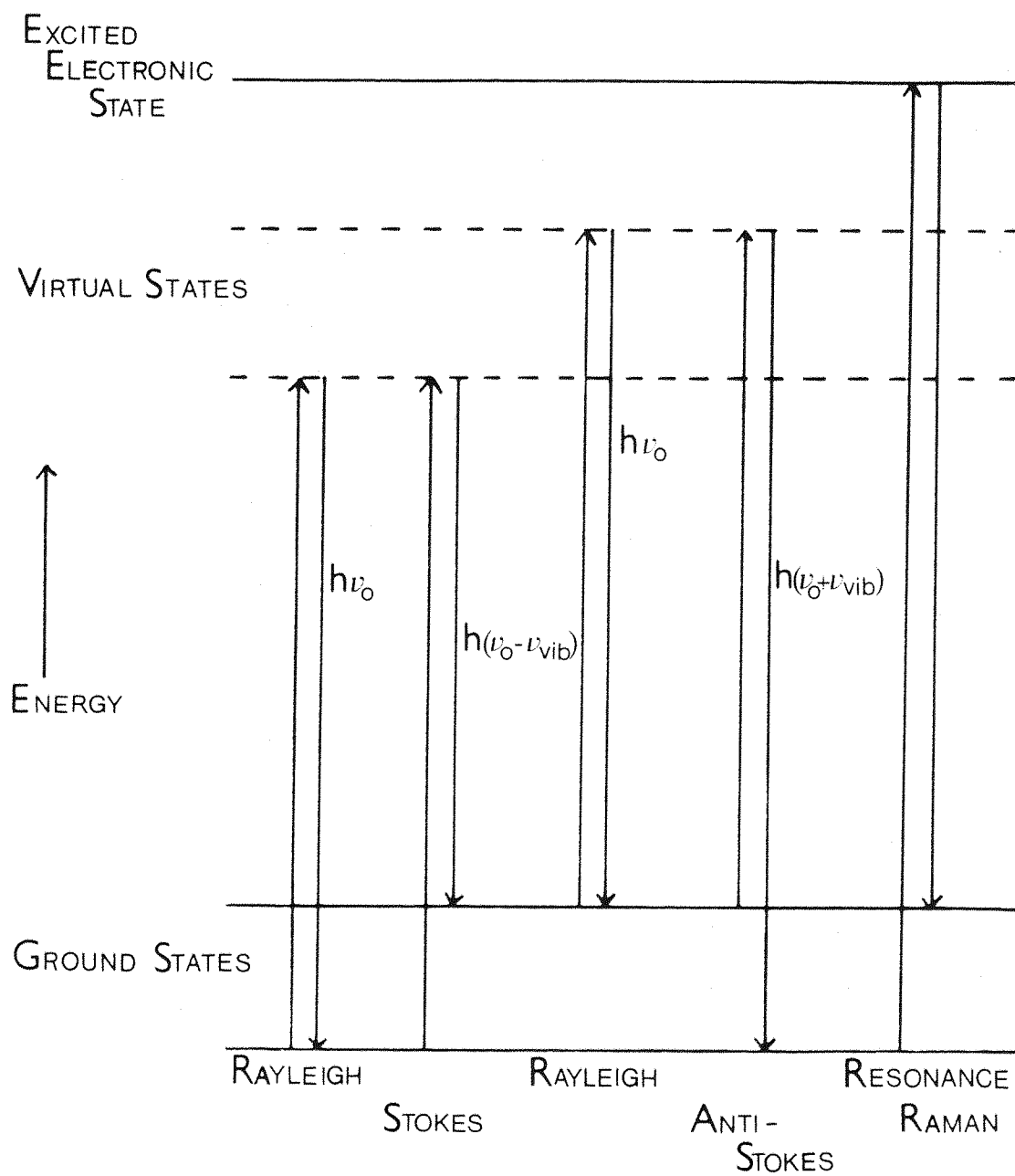


FIGURE I.2 — Energy level diagram for the quantum mechanical interpretation of the Raman effect.

The Raman effect is an inelastic light scattering phenomenon, produced typically by one incident photon out of  $10^{10}$ , and hence is a very unlikely event. The total Raman scattered radiation is therefore very small, and long path lengths ( $\sim 2$  mm) and high scattering cross-sections are required for a typical experiment on a liquid. Applications of Raman spectroscopy to electrode/electrolyte studies with their very short double layer path length, would therefore appear to be quite impossible. Although in the first investigations of adsorbed species on an electrode surface spectra were obtained from a few monolayers of very strong Raman scatterers<sup>(88)</sup>, the majority of spectra reported to date<sup>(83)</sup> have involved special enhancement phenomena of the Raman intensity. Two different types of enhancement have been observed and very intense spectra from electrode adsorbates have been obtained.

#### 1.2.4.2 Resonance Raman Effect

Resonance Raman scattering occurs when the frequency of excitation of a coloured sample is close to an allowed electronic transition of the scattering molecule. By absorbing incident laser radiation efficiently, the population density of the excited state is greatly increased (Figure I.2). The efficiency of Raman scattering is improved between  $10^4$  and  $10^6$  times when a resonance condition exists<sup>(89)</sup>, and its intensity becomes dependent on the proximity of the excitation frequency to an electronic transition rather than the usual intensity-frequency dependence of  $\nu^4$ . A tunable laser is normally used in order to adjust the frequency of the incident radiation to lie within an electronic absorption band of the sample.

Van Duyne and coworkers<sup>(90)</sup> have demonstrated the efficiency of the resonance Raman effect for "in-situ" characterization. They have developed resonance Raman spectroelectrochemistry to study electrogenerated species both in the bulk electrolyte and the diffusion layer. By monitoring intensity changes in specific Raman bands as the electrode potential is modulated, optical voltammograms and optical current-time transients can be obtained. This makes resonance Raman spectroelectrochemistry a very promising tool for investigating electrode reaction kinetics, particularly

when used in conjunction with conventional electrochemical techniques.

#### 1.2.4.3 Surface Enhanced Raman Spectroscopy

The first successful attempt to couple Raman spectroscopy and electrochemistry was performed by Fleischmann *et al* who obtained good quality spectra from films of a few monolayers of  $\text{Hg}_2\text{Cl}_2$ ,  $\text{Hg}_2\text{Br}_2$  and  $\text{HgO}$  formed on droplets of mercury electro-deposited onto platinum electrodes<sup>(88)</sup>. Clearly some scattering enhancement phenomenon was involved and is now known as surface enhanced Raman scattering or SERS.

Since this first successful record of an in-situ Raman spectrum many research groups have started work in Raman spectroscopic studies of species at electrode-solution interfaces and SERS spectra have been obtained from many different molecules and ions adsorbed to silver, copper and gold electrodes. A list of electrochemical systems, investigated using SERS is given in reference (83). Results show that laser Raman spectroscopy is an appropriate tool for examining the metal electrode/electrolyte interface. Structural and chemical information can be yielded particularly when a complementary electrochemical technique is used simultaneously.

The most widely studied system has been pyridine adsorbed on an electrochemically roughened silver electrode in aqueous potassium chloride solution<sup>(91)</sup>. This has been aimed to clarify the nature of the enhancement process, but in spite of intensive investigation<sup>(83)</sup>, a definitive explanation of the enhancement mechanism has still not been achieved. SERS spectra have also been obtained in air and under ultra-high vacuum conditions<sup>(92)</sup>.

Finally, it should be emphasized that in spite of the enhancement observed, the weakness of the Raman signals emanating from the layers immediately adjoining the electrode surface is such that extreme conditions are required; i.e. large mechanical slitwidth, extreme sensitivities, etc. The development of multiplexing spectrographs and of signal processing techniques, as well as improvements in the optical performance of the overall system,

will allow the extension of the range of systems which can be studied by Raman spectroscopy.

### 1.3 "Ex-Situ" Techniques

#### 1.3.1 Introduction

The development since 1965 of new methods for analyzing surfaces, based on electron and ion spectroscopies, has revolutionized the study of the surface chemistry of solids.

Electrode surfaces including single crystal systems can be characterized before and after electrochemical measurements by using one of these spectroscopic techniques listed in reference (5). A common feature of all of them is that for the study of these clean or adsorbate-covered metal surfaces the samples have to be analysed in high vacuum ( $10^{-5}$  -  $10^{-7}$  torr) or ultra-high vacuum ( $< 10^{-8}$  torr). The critical question is whether the electrode surface can be transferred from the ultra-high vacuum environment and vice versa without substantial restructuring of the surface as well as chemical changes and contamination.

The most important techniques, which give direct information on the chemical composition of the surface and near-surface layers of a solid, are X-ray photoelectron spectroscopy (XPS), also called electron spectroscopy for chemical analysis (ESCA), Auger electron spectroscopy (AES), and low energy electron diffraction (LEED).

#### 1.3.2 X-Ray Photoelectron Spectroscopy (3,14,93-95)

The XPS experiment involves the measurement of binding energies of electrons photoejected from the sample into the surrounding vacuum by interaction of a molecule with a mono-energetic beam of soft X-rays. The basic process is the emission of a core electron of an atom which has absorbed a photon of sufficient energy. The photoemission process is illustrated in Figure I.3 by the ionization at a K-shell level. Since energy is conserved, the kinetic energy,  $E$ , of the electron, measured with the electron spectrometer, plus the energy required to remove it from its orbital to the spectrometer vacuum,  $E_b$ , must

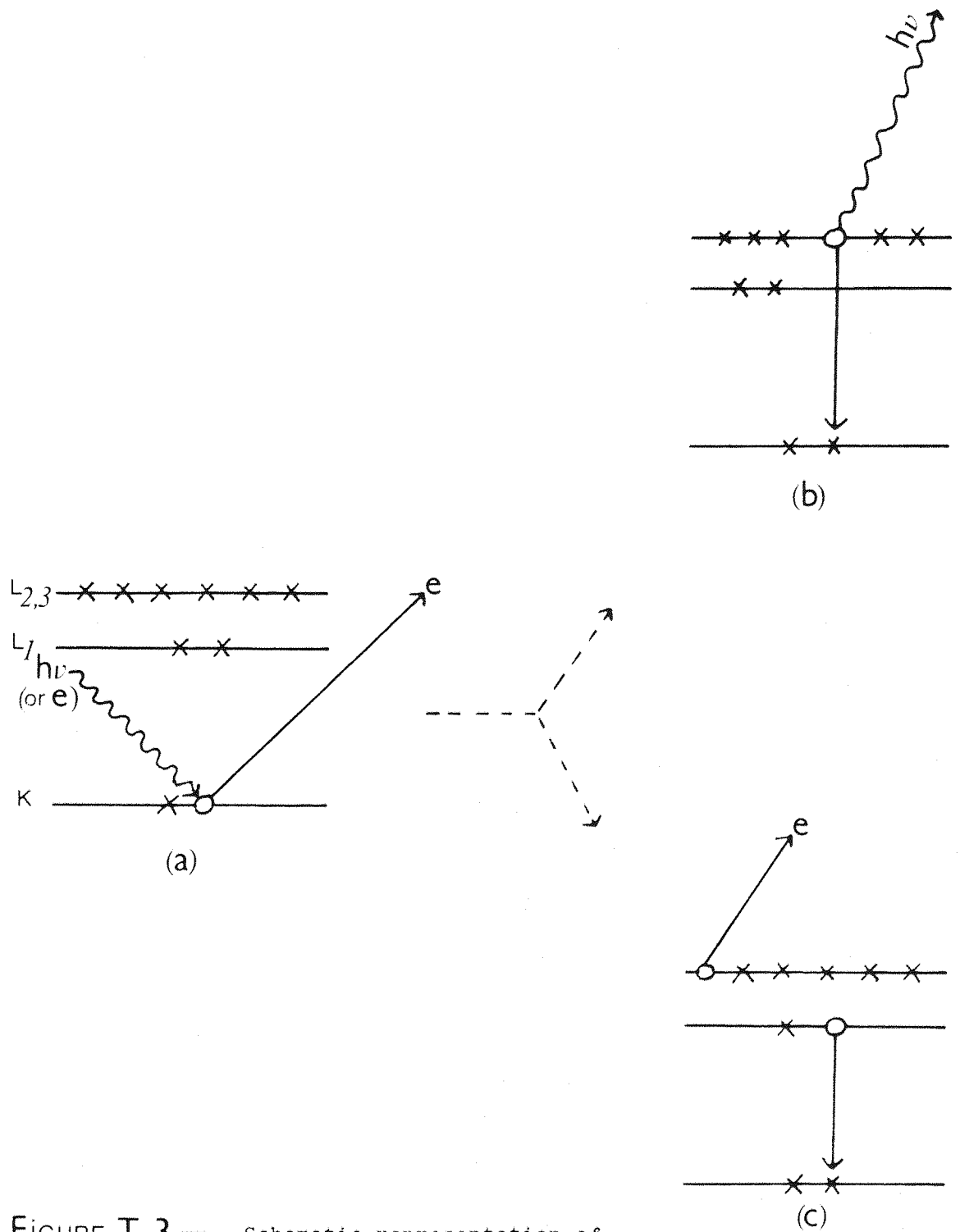


FIGURE I.3 — Schematic representation of  
 (a) Photoelectron emission,  
 (b) X-ray fluorescence,  
 (c) Auger electron emission.



equal the X-ray energy ( $h\nu$ ). A correction for the spectrometer work function,  $\phi_s$ , must also be applied, normally as part of the spectrometer calibration procedure. Thus, one obtains:

$$E_b = h\nu - E + \phi_s \quad (1.6)$$

$E_b$  is called the binding energy of the core electron in the atomic orbital. These electron energy levels are characteristic of the atomic species so that, for a constant incident photon energy, the identity of the atom is readily determined. However, chemical bonds generally cause shifts in core levels ionization energy. These "chemical shifts" can be detected and related, with varying degrees of success, to atomic oxidation states, formal oxidation numbers, etc.

The extreme surface sensitivity of this technique, typically sampling the top  $\sim 50 \text{ \AA}$  of material and its ability to supply information about the chemical forms in which atoms are present in this surface region without seriously damaging it, has made it useful for electrochemical applications. Characterization of anodic films<sup>(96)</sup> and structure analysis of adsorbed species<sup>(97)</sup> or deposited species<sup>(98)</sup> are the electrochemical areas where XPS has been successfully applied. Various other applications are very useful, e.g. in studies of surface structure of polymers<sup>(99)</sup>, and of catalysis<sup>(93)</sup>.

### 1.3.3 Auger Electron Spectroscopy<sup>(3,93,94,99)</sup>

As illustrated in Figure I.3, if a vacancy is created in an atomic core level, for example, by irradiation with X-rays, as above, or with electrons, then an electron from an upper level will immediately fill the hole in order to stabilize the system. The energy from this relaxation, depicted by an  $L_1 \rightarrow K$  transition in Figure I.3(c), can be released wholly in the form of a photon (X-ray fluorescence) or be transferred to another electron, e.g. in the  $L_2$  level, which is ejected from the atom as the Auger electron. Thus this process is termed the  $KL_1L_2$  Auger transition.

The measured kinetic energy of Auger electrons originating from a WXY transition can be estimated from the empirical relation:

$$E_{WXY} = E_W(Z) - E_X(Z) - E_Y(Z + \Delta) - \phi_A \quad (1.7)$$

where  $\phi_A$  is the work function of the analyser material,  $Z$  is the atomic number of the atom involved and  $\Delta$  is a correction factor lying between  $\frac{1}{2}$  and  $\frac{3}{4}$ .

By measuring the distribution of electrons versus kinetic energy, we can obtain a spectrum that should show sharp peaks at the discrete Auger energies. Each Auger line is characteristic of the originating atom and can be used analytically to indicate the presence of that species. In practice, measurable and frequently large shifts in Auger energies corresponding to changes in chemical environment are observed. But because more than one level is involved these chemical shifts are much more complex to analyse than in XPS.

A technique called depth profiling, carried out by etching the sample with a beam of high-energy ions (e.g.  $\text{Ar}^+$ ) through a sputtering process is widely used, coupled with XPS or AES, in order to follow the distribution of a particular element with depth. The Auger depth profiling method is particularly employed for the characterization of anodic films, e.g. in corrosion studies, and to study the properties of films such as passivating layers or insulating barriers<sup>(100)</sup>.

Numerous applications of AES have appeared in the literature during the past few years and they are presented in references (93,99). Combined with LEED, AES has often been utilized to provide chemical identification of surface species<sup>(101)</sup>; and in many adsorption and desorption studies (mainly of gases on solid surfaces) AES has been used to monitor surface coverage<sup>(102)</sup>.

#### 1.3.4 Low Energy Electron Diffraction (3,14,103,104)

Electrons travelling in vacuum at kinetic energies in the range 10 to 500 eV have de Broglie wavelengths in the order of a few angstroms, i.e. of the lattice constant of the solid; hence a monochromatic beam of these electrons will be reflected from an ordered solid in a diffraction pattern that provides information

about the structure of the solid. This effect is the basis of the LEED method. The beam cannot penetrate the sample to a distance greater than a few  $\text{\AA}$  without being scattered inelastically and hence losing energy. Thus only diffraction spectra due to the two-dimensional order of the surface will be observed.

LEED is a very specific tool for examining the geometric pattern of atoms on a surface and it has been widely used for studies of adsorption from the gas phase and catalysis of gas-phase/solid-surface reactions. Recently, electrochemists have begun to use this technique for the characterization of surfaces of interest to them<sup>(105-107)</sup>, and particularly to define the structure of a single crystal electrode surface before and after electrochemical treatment<sup>(105,108)</sup>. Combined LEED/Auger systems are frequently used because it is convenient to be able to monitor surface contamination or adsorption by AES during LEED studies<sup>(101)</sup>.

#### 1.3.5 Conclusion

These very powerful methods for surface and thin-film analysis are sure to be more extensively applied to electrochemical problems in the future. However, the necessity for transferring the sample into a system where there is no electrolyte always raises the possibility that the analyzed interface differs significantly from the one in the cell, which is actually the point of interest.

Special apparatus has been designed to minimize these problems, and several research groups<sup>(105-108)</sup> have carried out electrochemical measurements such as hydrogen electrosorption and lead underpotential electrodeposition on single crystal surfaces using a two vacuum chamber system; but one must always be alert for artifacts engendered by the transfer even if special precautions have been used.

In fact these new spectroscopic methods can, at best, be used as ex-situ techniques in the electrochemical context. Very useful comparison of the data obtained for the metal/electrolyte solution interface, and for the metal/gas interface, using

in-situ and ex-situ techniques respectively can be done when adsorption of a gas is studied<sup>(109)</sup>.

#### 1.4 Conclusion

All of the previously mentioned in-situ techniques seem likely to offer valuable methods of studying the electrode/electrolyte interphase.

Infra red specular reflection spectroscopy stands alone among these techniques in offering a relatively simple method which can provide specifically molecular information about the structure and composition of the electrode/electrolyte interphase. It also offers the possibility of studying electrochemical reactions by optical means, in conjunction with conventional electrochemical methods.

The only in-situ technique to rival infra red specular reflection spectroscopy is Raman spectroscopy, and the development of surface enhanced Raman spectroscopy, SERS, as an in-situ electrochemical method, will have to be followed.

An external reflectance technique, electrochemically modulated infra red spectroscopy (EMIRS) was used in this study. It is therefore separately reviewed in chapter two, in addition to the conventional electrochemical techniques employed in this study.

## CHAPTER TWO

### Theoretical Considerations

#### 2.1 Introduction

Success in extending the established and essentially simple technique, modulated specular reflectance spectroscopy, into the true vibrational infra-red region, was reported a few years ago<sup>(110)</sup>. This new technique, electrochemically modulated infra-red spectroscopy (EMIRS), has been applied to a number of electrochemical systems and very useful IR spectra from the electrode/electrolyte interphase have been obtained (section 2.4.3.2).

EMIRS and an electrochemical technique, differential capacitance measurement, have been used in this work, to obtain complementary information about the electrode/electrolyte solution interface of the gold and silver/adsorbate systems studied.

This chapter reviews both the electrochemical and spectroscopic background of the techniques employed.

#### 2.2 The Electrical Double Layer<sup>(14,111-114)</sup>

The simplest model that can be imagined for the electrode/electrolyte solution interface is of two semi-infinite phases with a plane as the boundary. In reality however, the interface is a region of extreme heterogeneity as a result of the electric field normal to the electrode surface. Many models have been proposed attempting to describe the distribution of all those charged species and oriented dipoles existing at the metal-solution interface called the electrical double layer. The model proposed by Gouy and Chapman<sup>(113)</sup> in the 1910's has been later modified by Stern<sup>(115)</sup> and Grahame<sup>(116)</sup> and this modified form, shown in Figure II.1 is accepted as a good model today.

If a potential  $\phi_m$  is applied to a metal electrode surface, the resulting charge  $q_m$  will represent an excess or deficiency of electrons in a very thin layer ( $< 0.7 \text{ \AA}$ ) adjacent to the solution. The electrolyte solution near to this electrode surface can be divided into distinct zones:

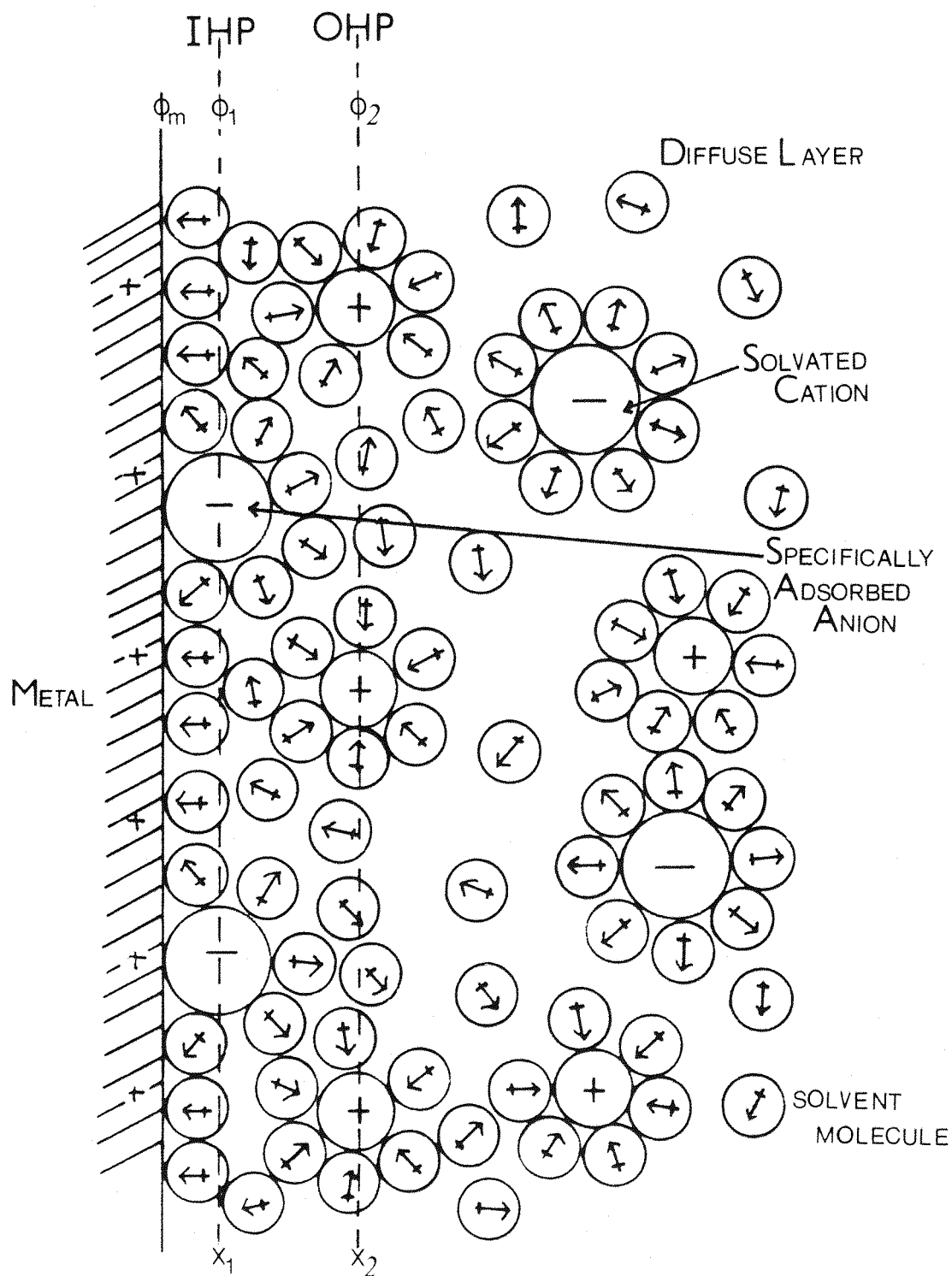


FIGURE II.1 — The electrical double-layer.

- (a) The inner Helmholtz plane (IHP) which contains specifically adsorbed species (ions or molecules) and solvent molecules and has a potential  $\phi_1$ .
- (b) The outer Helmholtz plane (OHP) which contains non-specifically or physisorbed solvated ions and solvent molecules and has a potential  $\phi_2$ .
- (c) Beyond the OHP extends the diffuse layer, a three dimensional region of solvated ions, disturbed by thermal agitation and still under the influence of the electrode potential. The thickness of this layer will depend on the total ionic concentration in the solution.

The total charge on the solution side of the double layer must balance that of the metal electrode, so that

$$q_m = -(q_1 + q_2 + q_D) \quad (2.1)$$

where  $q_1$ ,  $q_2$  and  $q_D$  are respectively the excess ionic charges of the layers described above. If the extent of specific adsorption is negligible,

$$q_m = -(q_2 + q_D) \quad (2.2)$$

and if  $\phi_s$  is the potential in the bulk electrolyte, the potential drop across the interface is given by:

$$(\phi_m - \phi_s) = (\phi_m - \phi_2) + (\phi_2 - \phi_s) \quad (2.3)$$

where  $(\phi_m - \phi_2)$  is the potential drop across the inner layer and  $(\phi_2 - \phi_s)$  is the potential drop across the diffuse layer.

At a given potential the electrode-solution interface is characterized by a double layer capacitance which is difficult to measure without disturbing the equilibrium of the interface. Therefore, a quantity called the differential capacitance is defined  $C_{Diff}$ .

Knowing that the capacitance of a capacitor is given by

$$C = q/V \quad (2.4)$$

then the differential capacitance  $C_{\text{Diff}}$ , in response to a small change in potential is

$$C_{\text{Diff}} = \frac{\delta q}{\delta V} \quad (2.5)$$

Differentiating (2.3) with respect to charge,

$$\frac{\delta(\phi_m - \phi_s)}{\delta q} = \frac{\delta(\phi_m - \phi_2)}{\delta q} + \frac{\delta(\phi_2 - \phi_s)}{\delta q} \quad (2.6)$$

Applying (2.5) to the molecular capacitor equation (2.6) gives us

$$\frac{1}{C_{\text{Diff}}} = \frac{1}{C_i} + \frac{1}{C_d} \quad (2.7)$$

The observed capacity is therefore a series combination of the inner layer capacity  $C_i$ , and the diffuse layer capacity,  $C_d$ . This differential capacitance equation is very useful, since determination of actual capacitance values of the electrochemical diffuse layer is difficult. Methods for measuring differential capacitance will be discussed in the next section. Unlike real capacitors, whose capacitances are independent of the voltage across them,  $C_{\text{Diff}}$  is a function of potential as the molecules adsorb, desorb and reorientate when the potential changes.

The mathematical formulation of the diffuse layer region, worked out by Gouy and Chapman and fully treated in several reviews<sup>(14,112)</sup> can be written for dilute aqueous solutions at 25°C.

$$C_d = 228.5 |z| (C_s)^{\frac{1}{2}} \cosh(19.46 |z| \phi_2) \quad (2.8)$$

where  $C_d$  is in  $\mu\text{F}/\text{cm}^2$ ,  $C_s$ , the bulk electrolyte concentration in moles per litre and  $\phi_2$  in volts,  $z$  being the ionic charge. When expression (2.8) is plotted it shows a minimum in differential capacitance at the point of zero charge (pzc), where  $q_m = 0$  and the number of cations and anions in the diffuse layer is equal. Experimentally this point is only observed for very dilute solutions of non-chemisorbed ions (e.g. 0.001M and 0.01M



NaF solutions<sup>(117)</sup>); otherwise the differential capacitance terms for the outer Helmholtz species and the inner Helmholtz specifically adsorbed species, must become dominant.

The Gouy-Chapman equation (2.8) has been modified by Stern who postulated that ions cannot reach the electrode beyond the plane of closest approach at some distance  $x_2$ . This plane called the outer Helmholtz plane is an important concept particularly with more concentrated electrolytes for which the charge in solution becomes more tightly compressed against this boundary at  $x_2$ , and equation (2.9) yields differential capacitance curves which agree closely with experimental results for many systems<sup>(118)</sup>;

$$\frac{1}{C_{\text{Diff}}} = \frac{x_2}{\epsilon\epsilon_0} + \frac{1}{(2\epsilon\epsilon_0 z^2 e^2 n^0/kT)^{\frac{1}{2}} \cosh\left(\frac{ze\phi_2}{2kT}\right)} \quad (2.9)$$

where  $\epsilon$  is the dielectric constant of the medium,  $\epsilon_0$  is the permittivity of free space,  $\phi_2$  is the potential at  $x_2$  and  $n^0$  is the number of adsorbed species per litre.

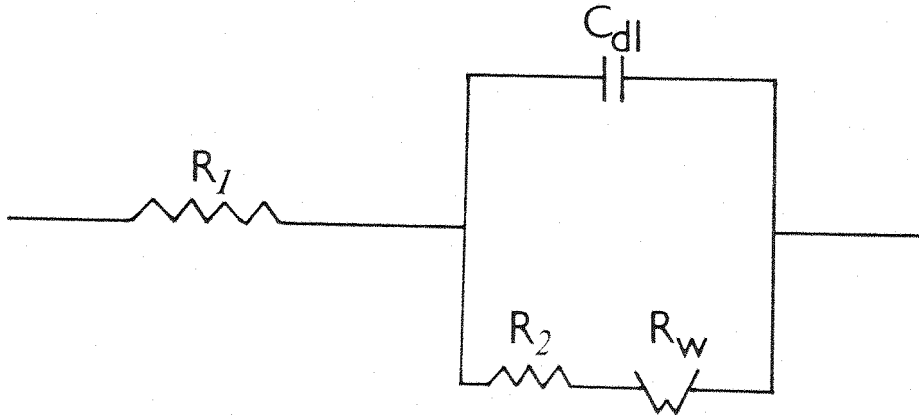
In cases where specific adsorption is substantial, the thermodynamics of adsorption is important, and adsorption isotherms such as Langmuir, Frumkin and Temkin are used to model the potential dependence of the adsorption process and hence the differential capacitance. Close agreements<sup>(119)</sup> have been reported which demonstrate that such theories may be successfully applied to model the structure of the metal and adsorbates themselves.

### 2.3 A.C. Impedance Measurement of Differential Capacitance

Measurement of electrode impedance, in terms of the response to a small sinusoidal modulation, yields useful information about electrochemical processes occurring at the electrode and also about the nature of the electrical double layer.

In a general sense, an electrochemical cell is simply an impedance to a small sinusoidal excitation. It is therefore possible to represent its performance by an equivalent circuit

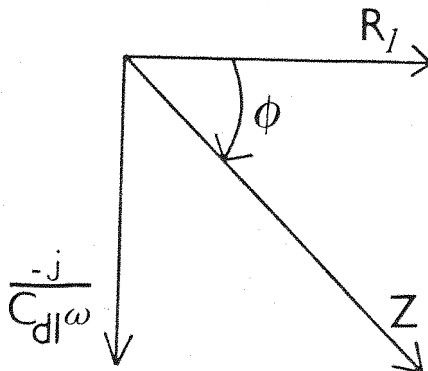
of resistors and capacitors that pass current with the same amplitude and phase angle as the real cell. A typical circuit is shown below



where  $R_1$  represents the resistive drop between the working and reference electrode,  $C_{dl}$  represents the double-layer capacitance of the working electrode interface.  $R_2$ , the charge transfer resistance and  $R_w$  the Warburg impedance due to diffusion of electroactive species to the electrode surface, can be neglected if no Faradaic process is occurring at the electrode. In this case the impedance of the cell which can be defined as its "resistance" towards an alternating current of frequency  $\omega$ , is given by

$$z = R_1 - \frac{j}{C_{dl}\omega} \quad (2.10)$$

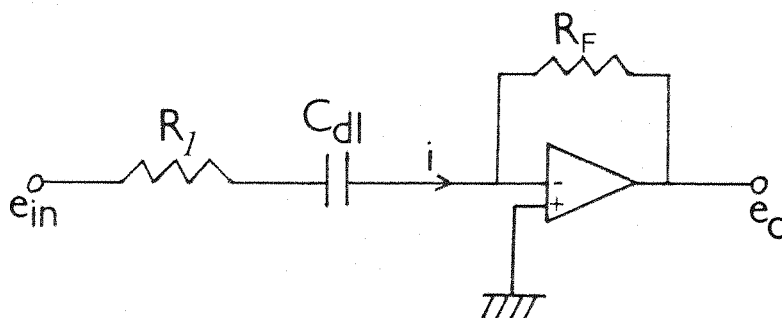
The impedance, as is shown in the vector diagram below, is therefore resolved into a resistive in phase component,  $R_1$  (real) and a capacitive quadrature component  $\left(\frac{1}{C_{dl}\omega}\right)$  which as an imaginary component is multiplied by  $j=(-1)^{\frac{1}{2}}$



The magnitude of  $z$  is  $\left(R_1^2 + \frac{1}{(C_{dl}\omega)^2}\right)^{\frac{1}{2}}$  and the phase angle between the alternating voltage applied to the cell ( $e_{in} = E\sin\omega t$ ) and the related current passing through the cell ( $i = I\sin(\omega t + \phi)$ ) is given by

$$\tan\phi = \frac{1}{\omega R_1 C_{dl}} \quad (2.11)$$

The figure below represents the electrochemical cell under potentiostatic control when no Faradaic process is occurring and where  $R_F$  is the current follower feedback resistance.



The output voltage of the current follower can be expressed by

$$e_o = -iR_F \quad (2.12)$$

and since Ohm's law always holds, the current is given by

$$i = \frac{e_{in}}{z} = \frac{e_{in}}{R_1 - \frac{j}{C_{dl}\omega}} \quad (2.13)$$

then

$$e_o = -e_{in} \frac{R_F}{R_1 - \frac{j}{C_{dl}\omega}} \quad (2.14)$$

$e_o$  can be resolved into in phase and quadrature components

$$e_{in \text{ phase}} = -e_{in} \frac{(\omega C_{dl})^2 R_1 R_F}{1 + (\omega C_{dl} R_1)^2} \quad (2.15)$$

$$e_{\text{quadrature}} = -e_{\text{in}} \frac{\omega C_{\text{dl}} R_{\text{F}}}{1 + (\omega C_{\text{dl}} R_{\text{F}})^2} \quad (2.16)$$

(90° out of phase)

If the cell was represented by a pure capacitor the output voltage would be exactly in quadrature with the phase of the current response of the electrode and in this case the output voltage would be

$$e_{\text{o}} = -e_{\text{in}} j\omega C_{\text{dl}} R_{\text{F}} \quad (2.17)$$

rewriting this as

$$e_{\text{ideal,quadr.}} = e_{\text{in}} \omega C_{\text{dl}} R_{\text{F}} = \text{const. } C_{\text{dl}} \quad (2.18)$$

then, it can be deduced from equations (2.15) and (2.16) that

$$e_{\text{ideal,quadr.}} = e_{\text{quadr.}} \left( 1 + \left( \frac{e_{\text{inph}}}{e_{\text{quadr.}}} \right)^2 \right) = \text{const. } C_{\text{dl}} \quad (2.19)$$

Therefore, as explained in section 3.5, and using the experimental circuit shown in Figure III.11, before each experiment a resistive dummy cell was used to set the phase of the system (adjusting  $e_{\text{quadr}}$  to zero) and the constant defined in equation (2.18) was evaluated, using equation (2.19), from measured values of  $e_{\text{inph}}$  and  $e_{\text{quadr.}}$  for different known capacitance dummy cell. The double layer capacitance measurements were carried out by recording the two components of the output voltage of the current follower and for each point the  $C_{\text{dl}}$  value was calculated applying equation (2.19). The values obtained are normally divided by the geometrical area of the electrode, and the double layer capacity is plotted versus the D.C. potential applied to the electrode (a very slow ramp from the waveform generator).

The principal advantage of this method is that only the impedance of the working electrode and the solution between the working electrode and the reference electrode is measured. The alternative method of measuring differential capacitance involves the use of an A.C. impedance Wheatstone bridge and is more accurate<sup>(120)</sup> but it has the disadvantage that the AC

modulation and the DC ramp is applied across the whole cell.

## 2.4 Infra Red Modulated Specular Reflectance Spectroscopy

### 2.4.1 Introduction - Earlier work in MSRS

As has been seen previously, modulated specular reflectance spectroscopy (MSRS) overcomes most of the problems met with the other in situ optical methods, described in chapter one, and has the greatest sensitivity of the group. This technique has been extensively used in the ultra violet-visible wavelength range, where the optical effect due to a thin film on a metal substrate is optimized<sup>(46)</sup>.

Bewick and co-workers in this laboratory have investigated the mechanisms, kinetics and obtained spectra of intermediates, of a number of reactions including the oxidation of thianthrene<sup>(121)</sup>, alkoxybenzenes and alkylbenzenes<sup>(122-124)</sup> in acetonitrile and the reduction of carbon dioxide<sup>(121)</sup>. Very interesting results were obtained and MSRS was shown to enable the distinction to be made between different possible mechanisms in organic electrochemical reactions, such as the anodic oxidation of hydrocarbons<sup>(125)</sup>.

Investigating the electrode-electrolyte solution inter-phase using MSRS, Bewick et al<sup>(70)</sup> demonstrated the practicability of using this technique to separate and identify the various effects that can give rise to reflectance changes and to establish their relative importance in different systems. In general, when the electrolyte is not specifically adsorbed, three optical effects are present:

- (a) the electroreflectance effect (ER) arising from a perturbation of the dielectric constant of the surface region of the metal as the charge density is varied. This effect contains both a free electron and a bound electron component and the most satisfactory complete theoretical treatment has been given very recently by Brodsky<sup>(126)</sup>;
- (b) optical effects from the variation with charge of the surface excesses of non-specifically adsorbed ions in the diffuse layer;

(c) optical effects caused by the changing surface excess and orientation of the solvent on the electrode.

In a study<sup>(70)</sup> where the reflectivity changes at a lead electrode in contact with aqueous sodium fluoride were measured at two angles of incidence, it was shown that the adsorbed water layer did not perturb the ER effect, and therefore the two effects could be identified and described separately, the contribution from the diffuse layer being very small compared to the two other effects. In an earlier work<sup>(68)</sup> it has been shown that adsorption of hydrogen on platinum did perturb the ER effect, and separation of the two effects under these conditions is impossible. The changes in reflectivity of a platinum electrode in molar perchloric and sulphuric acid solutions accompanying the formation of adsorbed hydrogen were investigated by Bewick et al<sup>(62,68,69)</sup> and McIntyre<sup>(74)</sup> using MSRS and the two types of adsorbed hydrogen, which are readily distinguishable by their electrochemical behaviour, were also observed to show distinct optical properties.

Many other research groups have done interesting work, studying by MSRS the specific adsorption of halides on gold, platinum<sup>(127)</sup> and on mercury film electrodes<sup>(128)</sup>; the electro-sorption of aromatic hydrocarbons on a gold electrode<sup>(129)</sup>; the adsorption of thiourea on a mercury thin film electrode<sup>(128)</sup>. Underpotential deposition of metals has also been widely investigated<sup>(58,79-82)</sup>.

Many electrode surfaces have been studied and a number of theories have been proposed to account for the potential dependence of the reflectivity at the electrode-solution inter-phase<sup>(60,71,74-78)</sup>.

In fact, it is readily seen that although visible-uv spectroscopy of electrode-solution interphases has provided a large amount of valuable information concerning the structure and properties of the interphase, infra red spectra would be even more important. As of yet, there is no experimental means to obtain direct information on the identity, the actual bonding and the molecular structure of species at the surface and their

modes of deformation during an applied electric field. Infra red studies of adsorbed species could be of great importance in many electrochemical processes. Previous attempts<sup>(47,49)</sup> to apply IR spectroscopy to species at the electrode surface made use of internal reflectance at germanium electrodes; little useful data was obtained and the method has not been developed further. It has always been assumed that the presence of an aqueous electrolyte solution would cause insuperable problems to the development of external reflectance infra red spectroscopy as an in-situ technique, and even recently<sup>(130)</sup> some negative assessments were reported into the feasibility of studying adsorbed layers on metal electrodes in aqueous electrolyte by IR spectroscopy.

During the past few years, however, an external reflectance technique, electrochemically modulated infra red spectroscopy (EMIRS), has been successfully demonstrated and applied to a number of aqueous electrochemical systems, reviewed in section 2.4.3.2.

Since the simple technique, modulated specular reflectance spectroscopy has been proved to be successfully extended into the infra red region, the range of external reflectance infra red methods has been expanded with the development of a modified technique which used the advantages of Fourier Transform Infra Red Spectroscopy (SNIFTIRS)<sup>(131,132)</sup>, and by the application to electrochemical systems of a polarisation modulation method (IRRAS)<sup>(133)</sup> previously applied to study adsorption of gases on metal surfaces<sup>(135)</sup>. The work described in this thesis is concerned with the application of EMIRS to the study of the electrode/electrolyte solution interphase of gold and silver/adsorbate aqueous systems. The description of the EMIRS, SNIFTIRS and IRRAS techniques will be given in subsequent sections. In order to interpret the data from the EMIRS experiments, the selection rules related to infra red spectroscopy and reflection of electromagnetic infra red radiation at a metal surface will be described.

## 2.4.2 Vibrational and Surface Selection Rules

### 2.4.2.1 Infra red selection rules (86,136,137)

It is well-known that a molecule composed of  $N$  atoms has  $3N-6$  fundamental vibrations also called normal modes of vibration ( $3N-5$  for a linear molecule). Provided these vibrations satisfy the selection rule stated below, the molecule will absorb electromagnetic radiation of the same frequency as each fundamental vibration, giving rise to at least  $3N-6$  absorption bands in the infra red region, the usual range of an infra red spectrum being between  $4000\text{ cm}^{-1}$  at the high frequency end and  $625\text{ cm}^{-1}$  at the low frequency end.

In fact absorption of infra red radiation ( $\nu$ ) by a vibrating molecule will only take place if the vibration produces an alternating electric field ( $\nu$ ), i.e. if the vibration is coupled with a periodical changing dipole moment. As an illustration of this selection rule, consider a carbon dioxide molecule which as a linear triatomic molecule has four normal modes of vibration, Table II.2. The arrows refer to motions of atoms in the plane of the page and +, - refer to movements in a perpendicular plane. The permanent dipole moment of  $\text{CO}_2$  is zero and the dipole moment of the molecule will not change during the symmetric stretching vibration ( $\nu_1$ ) whilst the  $\nu_2$ ,  $\nu_3$  and  $\nu_4$  vibrational modes involve a periodic fluctuation in the electric dipole,  $\mu$ , with respect to the normal coordinates expressing the motions of the atoms during the vibration,  $Q_k$ . Thus  $\left(\frac{\partial \mu}{\partial Q_k}\right) \neq 0$  for  $\nu_2$ ,  $\nu_3$  and  $\nu_4$  vibrational modes and if the molecule is infra red irradiated these oscillating electric dipoles will interact with the electromagnetic radiation of the same frequency leading to absorption of some of this radiation. These vibrations are thus "infra red active",  $\nu_1$  being "infra red inactive". As an example, the fluctuation in the dipole moment during the asymmetric stretching vibration of the carbon dioxide molecule is shown in Figure II.3.

Comparing the infra red and Raman selection rules (see section 1.2.4.1) it is interesting to note that in a molecule



Vibrational Mode Number	Motion of Atoms During the Half Period	Description of Vibration
$\nu_1$	$\leftarrow \text{O} = \text{C} = \text{O} \rightarrow$	Symmetric Stretching Mode
$\nu_2$	$\leftarrow \text{O} = \text{C} = \text{O} \leftarrow$	Asymmetric Stretching Mode
$\nu_3$	$\begin{array}{c} \uparrow \\ \text{O} = \text{C} = \text{O} \\ \downarrow \end{array}$	} Bending Modes
$\nu_4$	$\begin{array}{c} \text{O} = \text{C} = \text{O} \\ + \quad - \quad + \end{array}$	

TABLE II.2 — The normal modes of vibration of carbon dioxide.

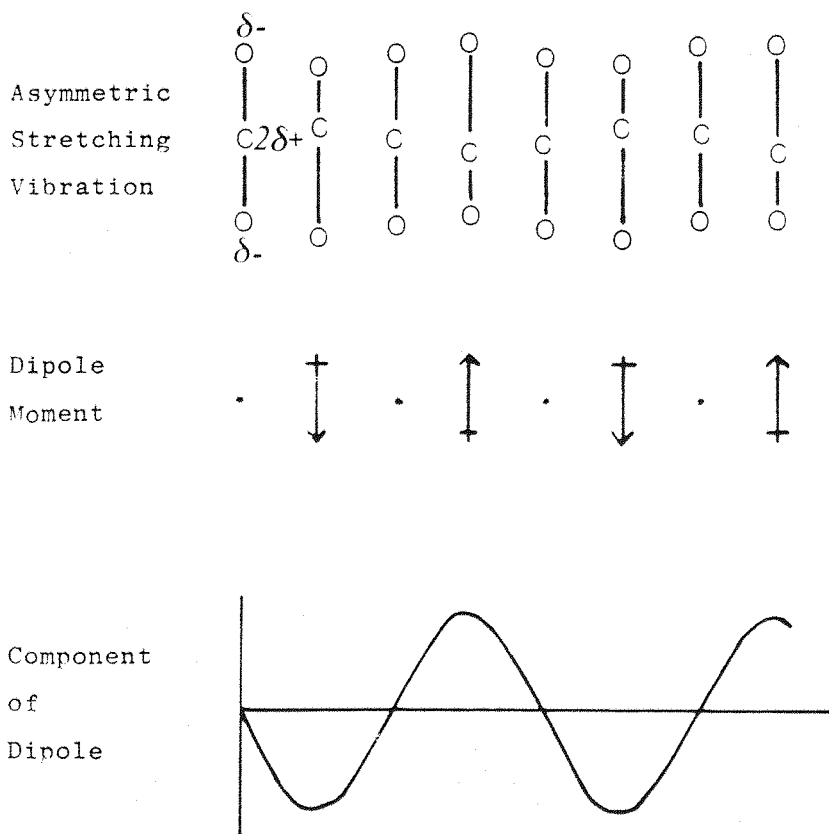


FIGURE II.3 — The asymmetric stretching vibration of the carbon dioxide molecule and its associated dipole fluctuation.

with a centre of symmetry, like  $\text{CO}_2$ , those vibrations symmetrical about the centre of symmetry are active in Raman and inactive in the infra red, e.g.  $\nu_1$  in  $\text{CO}_2$ ; those vibrations which are not centrosymmetric are inactive in Raman and usually active in the infra red, e.g.  $\nu_2$ ,  $\nu_3$  and  $\nu_4$  in  $\text{CO}_2$ . This is doubly useful, for it means that the two types of spectroscopy are complementary, the infra red being most informative in general because most functional groups are not centrosymmetric.

In practice the activity of a particular vibration of a molecule is readily ascertained by reference to character tables. In fact, the symmetry group (or point group) to which a molecule belongs is determined by the symmetry elements it possesses, e.g. plane of symmetry, centre of symmetry, rotation axes, etc. For each of the point groups, character tables have been worked out<sup>(138)</sup>, which designate the symmetry species into which the vibrations divide. Each symmetry species describes the behaviour of the normal mode with respect to the various symmetry operations. It is therefore possible, from these tables, to determine the number of normal modes of various types, i.e. rotation, vibration and translation which are to be found in each symmetry species, and their activity in the infra red and Raman spectrum.

It is very important to note that the symmetry properties of a molecule can change with its physical state, i.e. solid, liquid, gas, and its environment. In adsorption studies, the effects of the metal substrate on the IR and Raman activity of adsorbate vibrations have been discussed recently by Richardson<sup>(139)</sup> with benzene as an example. He has shown that molecular configuration and adsorption site dictate the number of bands in the vibrational spectrum and that from the intensity of certain bands, particular aspects of the adsorbate/metal interaction can be revealed.

#### 2.4.2.2 Surface Selection Rule<sup>(140,171)</sup>

The selectivity of reflection-absorption spectroscopy for dipole components perpendicular to the metal surfaces constitutes an important selection rule. It is a consequence of the dielectric response of the metal in which the screening effect of

the conduction electrons prevents a tangential field being established at the metal surface. The basis of this effect follows from a simple consideration of the electric fields produced by the radiation at a bare metal surface. Figure II.4 illustrates the incident and reflected electric vectors of s- and p-polarised radiation. For other than normal incidence, the effective intensity of the radiation very close to the surface is different for the p-polarised and s-polarised states, respectively parallel and perpendicular to the plane of incidence.

As seen in Figure II.5, at all angles of incidence the s-polarised component is practically reversed in phase upon reflection, and since the reflection coefficient is near unity, the resultant vector of the incident and reflected vectors is close to zero at the surface. Consequently, the s-component of the radiation cannot interact significantly with vibrating dipoles near the surface. The only radiation effective for studies at metal surfaces is therefore the p-polarised radiation which suffers a phase change upon reflection that varies strongly with angle of incidence. As we can see in Figure II.6 the p-component can yield an enhanced resultant vector  $E_{p\perp}$  perpendicular to the surface when the angle of incidence  $\theta$  is large and a very much weaker tangential vector  $E_{p\parallel}$ .

The p-polarised infra red radiation can therefore interact strongly with vibrational modes of adsorbed species having a non-zero component of the dipole derivative perpendicular to the surface  $\left(\frac{\partial\mu}{\partial Q}\right)_{\perp}$ , i.e. only these vibrational modes will give rise to absorption bands in the infra red. A very interesting consequence of this selection rule is that the relative intensities of the absorption band shown by an adsorbed molecule will vary as its orientation with respect to the surface is changed. This sensitivity towards orientation is a very valuable feature of the EMIRS method. Very high angles of incidence which confer greatly enhanced sensitivity to reflection-absorption measurements, as shown in Figure II.6, are often difficult to achieve in spectrometers because of other essential optical requirements. In EMIRS, the constraints imposed by the electrochemical cell provide a further impediment (see chapter three).

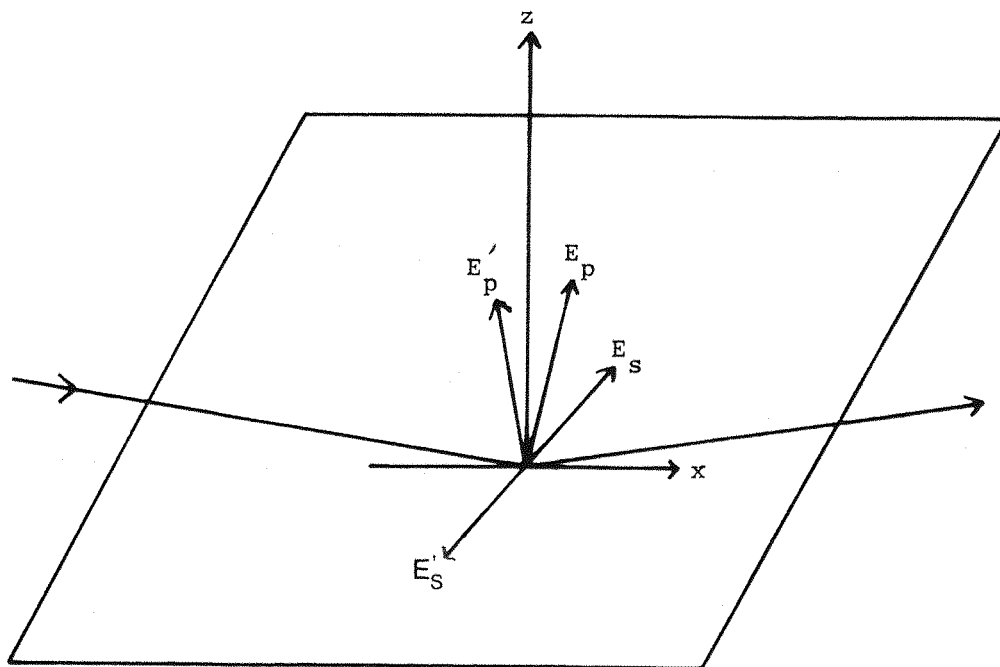


FIGURE II.4 — The incident,  $E$ , and reflected,  $E'$ , electric vectors of the p- and s-polarised components of the radiation at a metal surface. The plane of incidence is the xz plane.

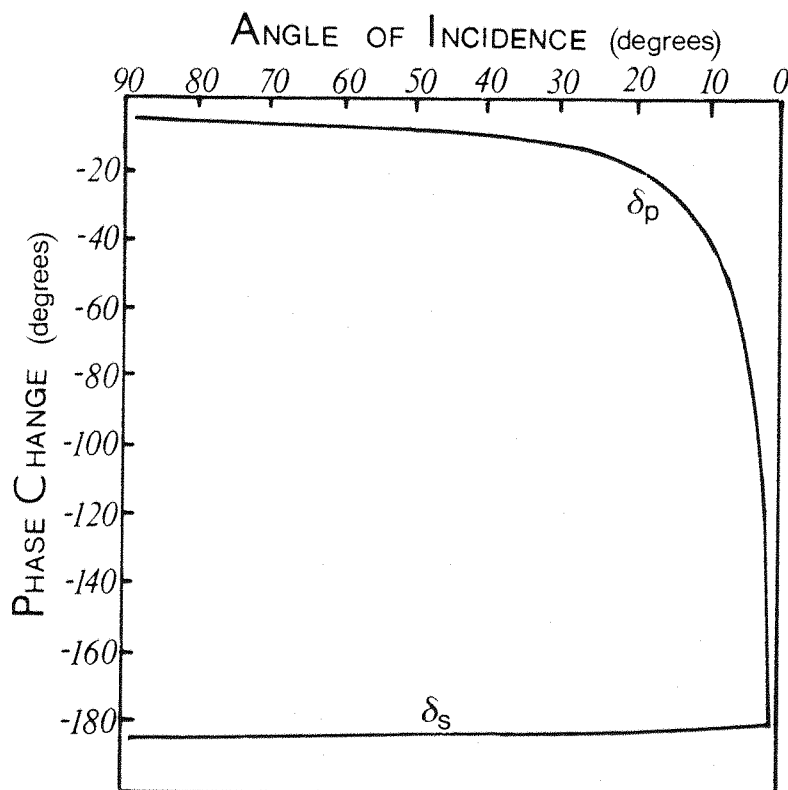


FIGURE II.5 — The phase change on reflection from a typical metal for the parallel,  $\delta_p$ , and perpendicular,  $\delta_s$ , components of the incident light as a function of angle of incidence.

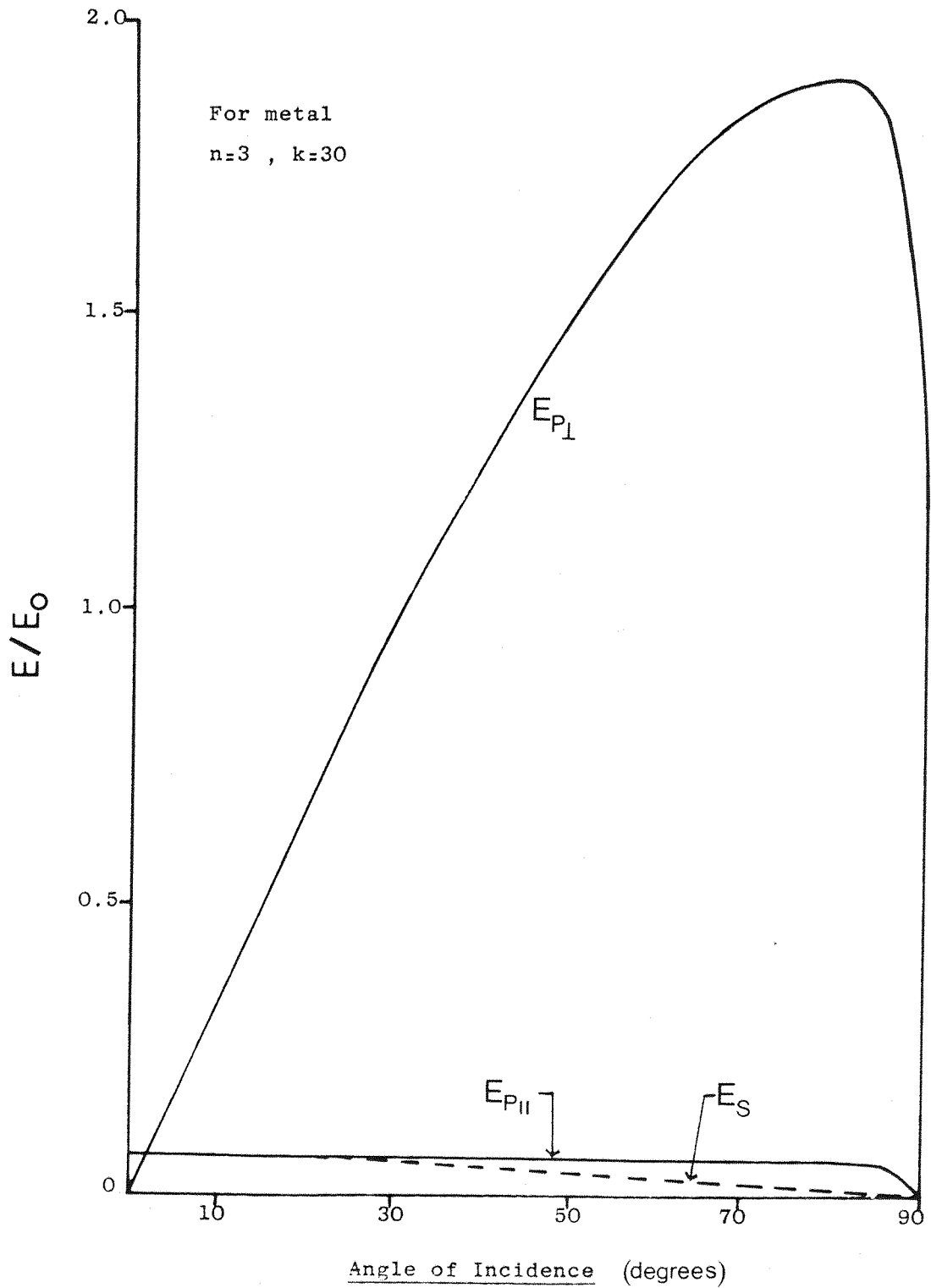


FIGURE II.6 — Angular dependence of the resultant amplitude of the electric field components at a bare metal surface relative to  $E_0$ , the amplitude in the incident ray.

### 2.4.3 Electrochemically Modulated Infra Red Spectroscopy (EMIRS)

#### 2.4.3.1 Description of the EMIRS technique

Electrochemically Modulated Infra Red Spectroscopy (EMIRS) is a direct successful extension into the infra red spectral region of the MSRS technique previously used only with UV-visible radiation, (sections 1.2.3 and 2.4.1). In these methods, the radiation is specularly reflected from a polished electrode surface while the electrode potential is modulated with a square waveform.

The design and performance of the spectroelectrochemical system for EMIRS: cell, spectrometer, detector and instrumentation to modulate the electrode potential and to amplify, average and display the detector output, will be fully described in the next chapter.

The signal observed in an EMIRS experiment is proportional to the difference in intensities of the radiation reaching the detector at the two potential limits defined by the square wave modulation applied to the electrode. In EMIRS spectra this intensity difference is represented as a reflectivity difference  $\Delta R$  which can be defined as,

$$\Delta R = R_A - R_C \quad (2.20)$$

where  $R_A$  and  $R_C$  are respectively the total cell reflectivities at the more positive potential and the more negative potential of the square waveform modulation. These total cell reflectivities may depend upon several sources including the reflectivity of the metal surface (electroreflectance effect) as well as the absorption of radiation by adsorbed species and solvent molecules in the inner region of the electrical double layer (section 2.2).

At this stage it is useful to note for the comprehension, that only the component of the optical signal in-phase with the potential modulation will be amplified by the signal recovery system, i.e. only optical changes related to this modulation will be analysed. Thus a very good sensitivity is achieved, and enable the detection of infra red band of submonolayer quantities

of adsorbates in the electrochemical systems studied.

Since there is a strong wavenumber dependence of the equipment response and the atmospheric transmission, EMIRS spectra are presented in terms of  $\Delta R/R$ , the relative change of reflectivity, vs. wavenumber. It should be noted that dividing  $\Delta R$  by  $R$  normalises  $\Delta R$  for the intensity of the radiation actually reaching the detector at each wavelength; thus  $\Delta R/R$  is directly proportional to the absorbance change produced at the electrode surface if  $\Delta R/R$  is sufficiently small to allow the exponential Beer's absorption law to be assumed linear.  $R$ , the normalising factor, is measured before each experiment for the particular system studied and the wavenumber range of interest.

An example of  $R$  measurement is shown in Figure II.7 and can be explained with the help of Figure II.8. Figure II.7 shows the intensity of the radiation received by the detector over the wavenumber region 1900-2500  $\text{cm}^{-1}$ . The upper curve (a) is for the total radiation which is composed of two major contributions, one being radiation reflected from the window surfaces ((I) in Figure II.8) and the other being that transmitted by the window and reflected from the electrode surface ((i) in Figure II.8). The latter contribution is eliminated in curve (b) which was obtained after pulling the electrode back out of reach of the radiation. Thus, the difference between curves (a) and (b) gives the intensity of the "active" radiation, i.e. the p-polarised radiation which has been reflected from the electrode, the major part of the other component being rejected by means of a polariser placed parallel to the exit slit of the monochromator and this difference is a measure of the normalising factor  $R$ .

If the electrode has the same reflectivity at the two potential limits of the modulation, as it is likely to be the case in most of the EMIRS studies,  $\Delta R/R$  is proportional to the difference of the two adsorbance spectra of species present at the two selected electrode potentials. If the electrode has different reflectivities at the two potential limits, this term appears as an effective absorbance difference which adds to any absorbance difference from the species in the inner region. It is in fact very important to recognise the possible origins for

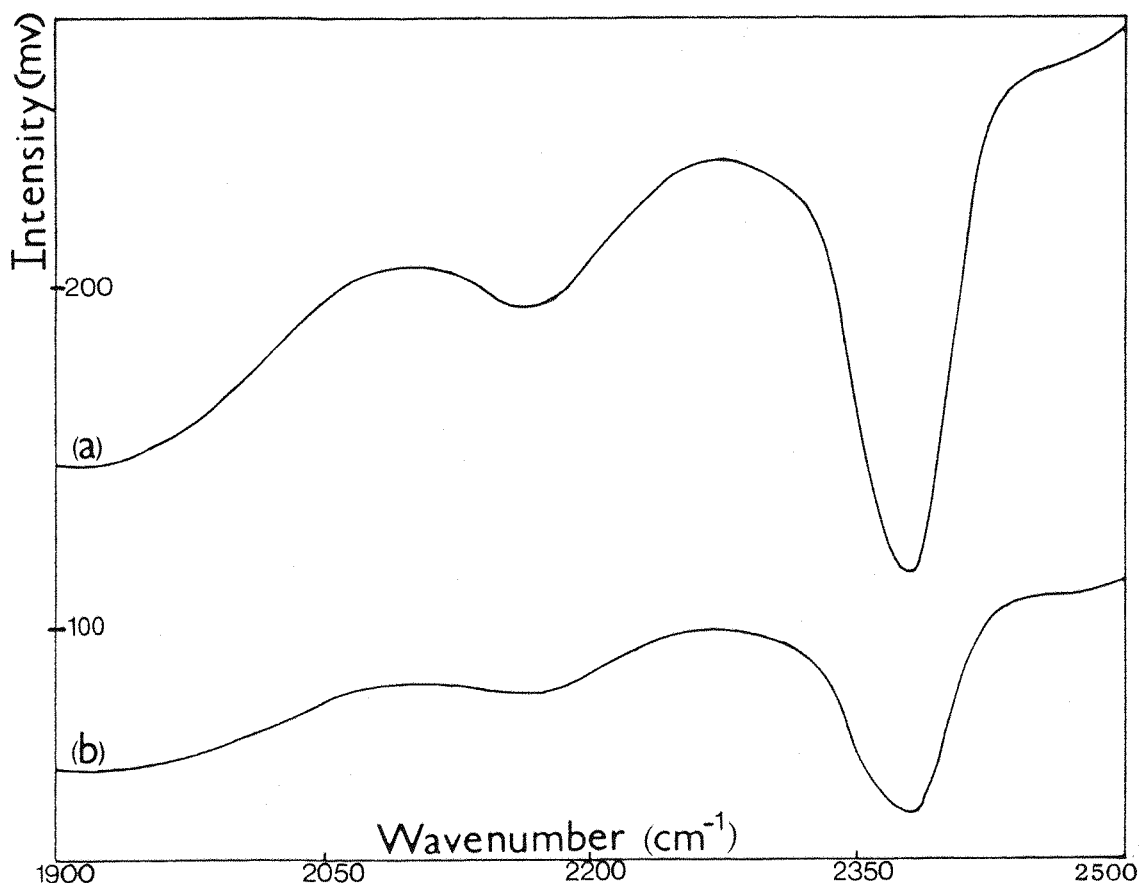


FIGURE II.7 — Intensity of the infra red radiation reaching the detector with the electrode pushed up to the window (a), and away from the window (b).

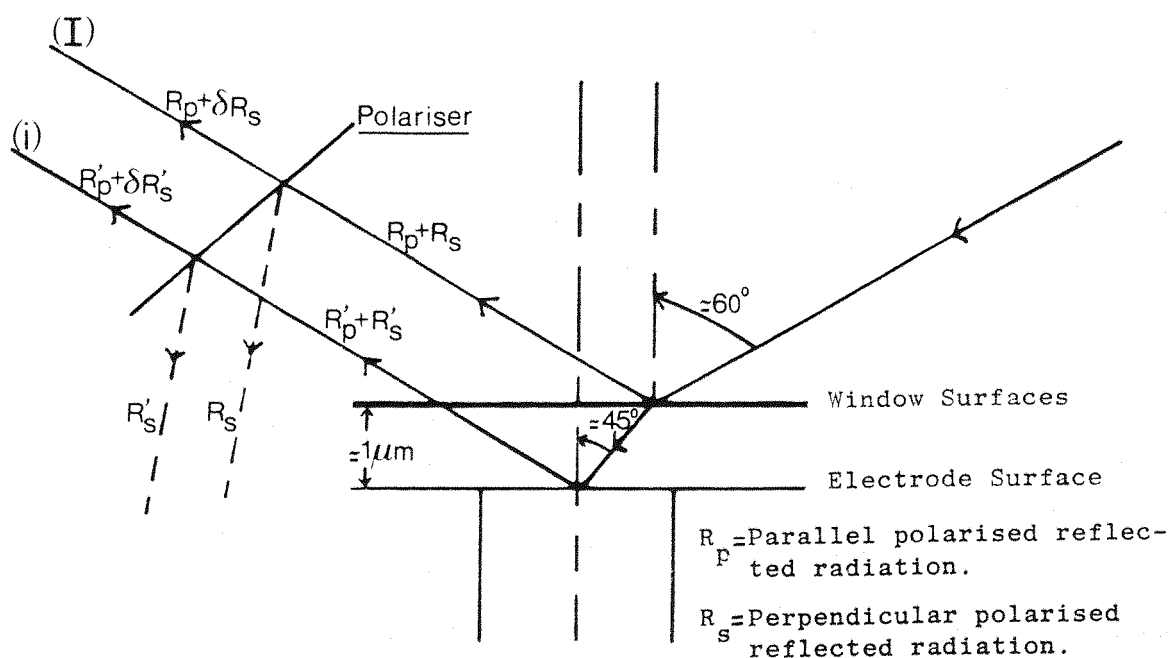


FIGURE II.8 — Optical geometry of the electrochemical cell. Reflected radiation from the window surfaces,  $(R_p + R_s)$ , and from the electrode surface  $(R'_p + R'_s)$ .



various spectral features which may occur and to be aware of the limitations placed upon spectral observations and/or interpretations, since EMIRS results are difference spectra.

$\Delta R$ , being defined as the difference  $R_A - R_C$ , the correspondence between infra red features for species present at these potentials and the EMIRS difference spectrum is shown for the most likely possibilities in Figure II.9:

Figure II.9(a) illustrates how the electrode reflectivity itself could produce a non-zero and possibly non-flat spectral baseline.

In Figure II.9(b) the absorption band for a species present only at one of the two selected electrode potentials is shown as positive or negative depending upon whether the species appears at the negative or the positive potential respectively.

Bisignate EMIRS bands would arise if the band position was potential dependent as in Figure II.9(c) or if the band shape was potential dependent in a way to move intensity from one side to the other as in Figure II.9(d).

Trisignate bands could be possible if a symmetrical change in band shape occurs as in Figure II.9(e).

Figure II.9(f) shows one of the usual cases observed in EMIRS studies where a potential dependence of the intensity of the band is occurring. This dependence may result from a variation of one of these parameters:

- the amount of species present,
- the strength of the infra red oscillator,
- the orientation of the species with respect to the electrode surface.

As seen in the previous section, this third parameter is a direct consequence of the surface selection rule which stated that for the species close to the electrode surface, only the vibrational modes,  $Q_1$ , with non-zero surface normal dipole derivative components,  $\left(\frac{\partial \mu}{\partial Q_1}\right)_\perp$ , will absorb energy from the infra red beam.

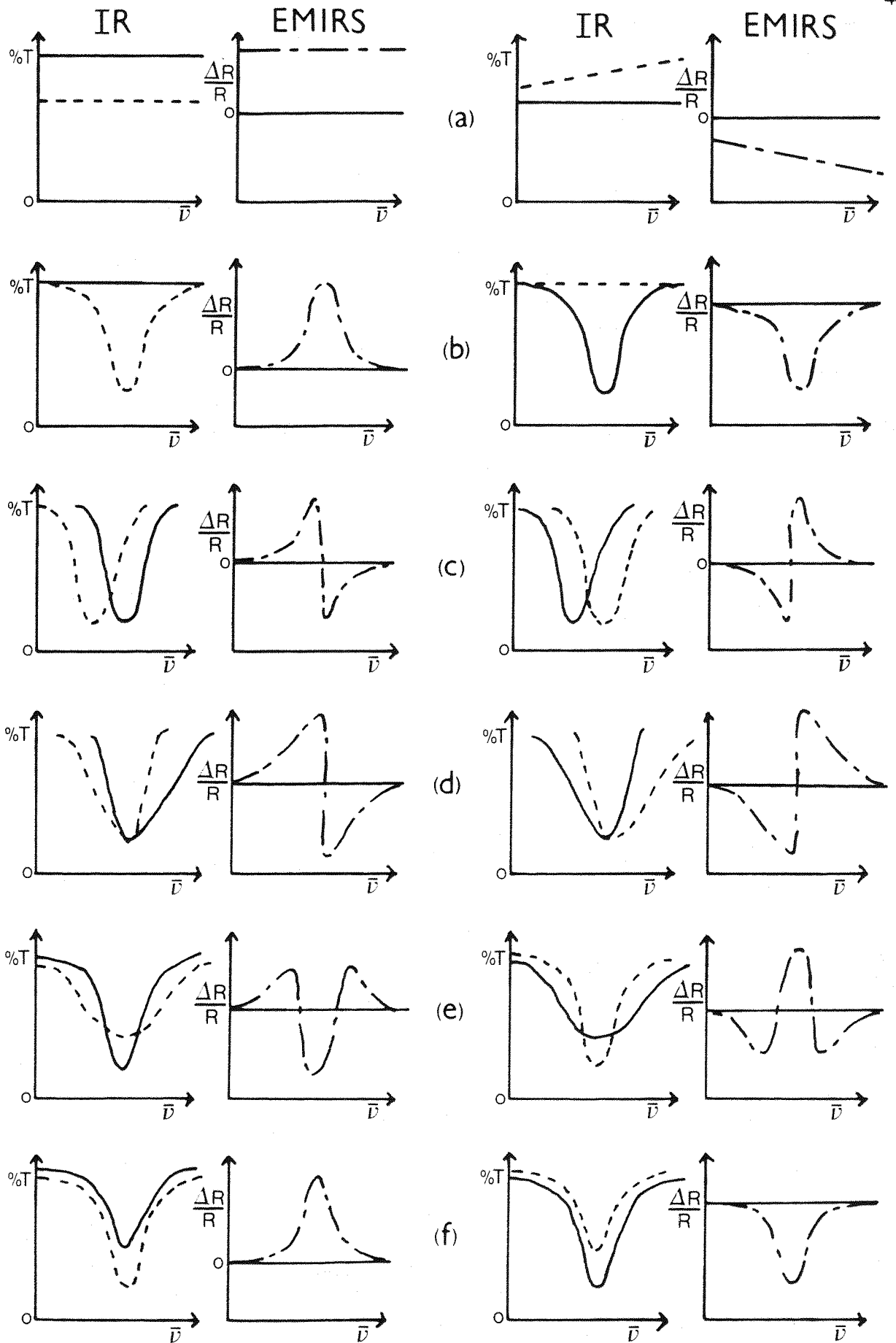


FIGURE II.9 — Correspondence between infra red features for species present at the two potentials of the modulation; (---) for the more negative potential, (—) for the more positive potential; and the EMIRS difference spectra.

Thus, a reorientation of these species with respect to the electrode surface will produce some changes in the magnitude of  $\left(\frac{\partial\mu}{\partial Q_i}\right)_\perp$  and therefore in the intensity of the resulting absorption bands.

As an example of the application of this surface selection rule to difference spectra, it is interesting to consider spectral features to be expected for an aqueous system in which the water layer adjacent to the electrode is reoriented as a function of electrode potential. Assume that the orientation of water molecules at the positive potential limit is as shown in Figure II.10(a) with the orientation at the negative potential limit taking one of the forms shown in Figures II.10(b), II.10(c) and II.10(d). The water molecule has three fundamental vibrational modes as shown in Figure II.11. The symmetric stretching mode,  $\nu_1$ , and bending mode,  $\nu_2$ , produce dipole moment changes along the symmetry axis of the molecule and are called symmetric modes. The asymmetric stretching mode,  $\nu_3$ , produces a dipole moment change perpendicular to the symmetry axis. The symmetric modes of water,  $\nu_1$  and  $\nu_2$ , would absorb IR radiation of the appropriate wavelengths for all four orientations shown in Figure II.10. The asymmetric mode,  $\nu_3$ , would only absorb radiation for the orientation shown in Figure II.10(d) since the other orientations all have  $\left(\frac{\partial\mu}{\partial Q_3}\right)_\perp = 0$ . If at the negative potential limit, water had the orientation shown in Figure II.10(b), no spectral features would appear in  $\Delta R/R$  plots, in this case the magnitudes of  $\left(\frac{\partial\mu}{\partial Q_1}\right)_\perp$  and  $\left(\frac{\partial\mu}{\partial Q_2}\right)_\perp$  being equal for the two different orientations. If Figure II.10(c) represents the orientation at the negative potential, the absorbance at this limit for symmetric modes would be less than at the positive limit since the surface normal component of the dipole derivatives is less for the orientation shown in Figure II.10(c) than the corresponding component for the orientation shown in Figure II.10(a). If the absorbance at the negative potential is less than at the positive potential,  $R_C > R_A$ , the symmetric modes would appear as negative peaks in  $\Delta R/R$  plots. The asymmetric mode,  $\nu_3$ , would not be observed. For orientation II.10(d) at the negative potential, symmetric modes would appear as negative  $\Delta R/R$  peaks and the asymmetric stretch as positive  $\Delta R/R$  peak.

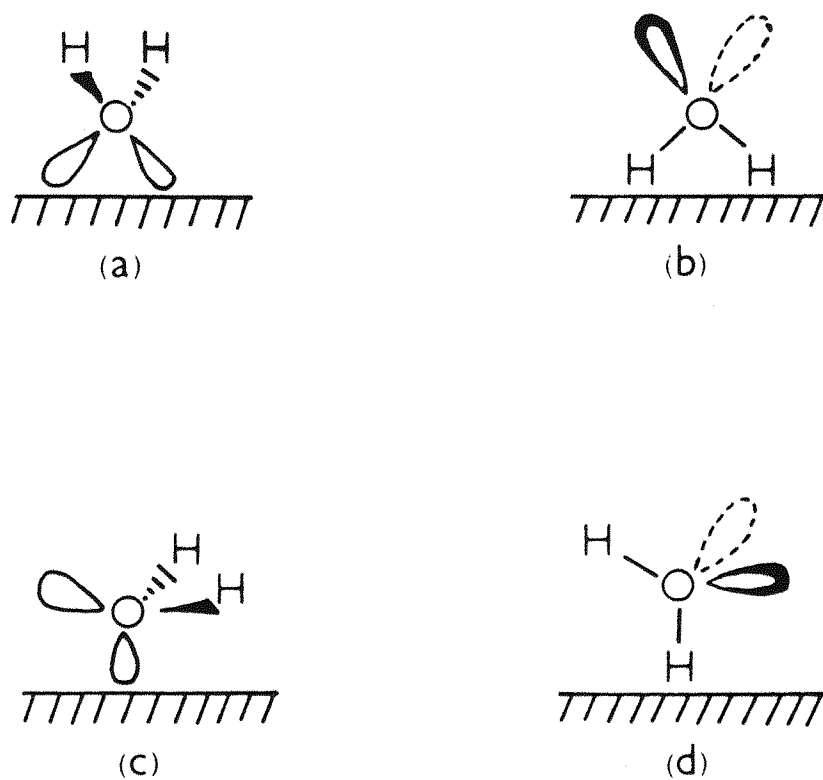


FIGURE II.10 — The four possible orientations of the water molecule with respect to the electrode surface.

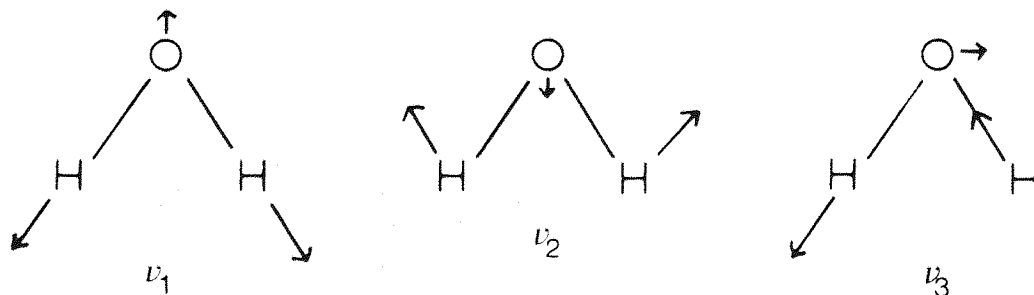


FIGURE II.11 — Normal vibrational modes of the water molecule.

Although the success of EMIRS technique has been established, showing that the detection of submonolayer amounts of adsorbed species could be obtained, the disadvantages of this technique must be pointed out.

- As a difference spectrum method, it can be difficult to be sure of the true origin of an EMIRS band since combinations of the limiting cases described in Figure II.9 may occur. And in some cases the difference might be too small to be detected, even for strong infra red absorption bands.

- Since a thin layer spectroelectrochemical cell, suitable for use with aqueous solution throughout the infra red region, is employed in EMIRS studies, electrochemical complications due to this type of cell may arise, such as the restricted diffusion of species from the bulk solution to the film between the electrode and the window<sup>(134)</sup> or the decrease of the response of the electrode potential as the modulation frequency increases<sup>(141)</sup>.

- The long time normally required by EMIRS experiments could alter the activity of the electrode. In order to maintain this activity it was found possible in some cases<sup>(142)</sup> to interpose a cleaning pulse between successive potential sweeps, but this procedure is not always possible.

In order to estimate the response of the electrode potential, it is good practice to monitor the current/time transients caused by the modulation during an experiment and the activity of the electrode is checked by recording a linear sweep voltammogram of the system before and after each experiment.

#### 2.4.3.2 Earlier work in EMIRS

Since their first successful report<sup>(110)</sup> of the application of the EMIRS technique to structural investigations of the electrode/electrolyte solution interphase both to aqueous and non-aqueous systems, Bewick et al have applied this method to study the molecular structure of the adsorbed intermediates formed:

- in the electrocatalytic evolution of hydrogen on platinum<sup>(142,143)</sup>

- during the electrocatalytic oxidation of organic fuels, such as methanol and formic acid<sup>(144,145)</sup>,
- from the reduction of CO<sub>2</sub> at a platinum electrode<sup>(146)</sup>.
- during the adsorption of carbon monoxide on platinum, rhodium and gold<sup>(109)</sup>.

Valuable information has been obtained from these studies. For example, it was shown<sup>(144,145)</sup> that the strongly chemisorbed species produced by the dissociation of methanol and formic acid molecules at a smooth platinum electrode, the nature of which has been the subject of controversy for years, were CO type species: a linearly bound species, i.e. a CO molecule adsorbed on top of a single platinum atom, and a multi-bonded CO species sitting in a higher coordination site, the former being the predominant one. A recent comparative study<sup>(109)</sup> of the adsorption of carbon monoxide on platinum, rhodium and gold from aqueous perchloric acid saturated with CO has confirmed these assignments of CO species, the spectrum for the Pt/CO system being very similar to those reported for the Pt/CH<sub>3</sub>OH and the Pt/HCOOH cases, Figure II.12. In this study a question of the exact nature of the multi-bonded CO species arises, i.e. whether it is truly bridge-bonded in a two coordinate surface site, or whether it occupies a three or more coordinate site and blocks three or more surface atoms as required by the electrochemical evidence for the strongly adsorbed poison produced in the electrocatalytic oxidation of simple fuels. The spectroscopic data clearly support the conclusion that the strongly bound poison is CO<sub>ad</sub> in a three coordinate surface site. Recent work<sup>(147)</sup> has shown that this species is the first to be removed when small amounts of Pb are adsorbed on the surface under conditions which lead to a strong enhancement of the electrocatalytic oxidation of the fuel. The removal of the linearly bound CO<sub>ad</sub> requires the adsorption of considerably more Pb.

It has been speculated that reduced CO<sub>2</sub> poisons the electrocatalytic oxidation of simple organic fuels<sup>(148)</sup>, the adsorbed species formed from the reduction of CO<sub>2</sub> being for most workers<sup>(149)</sup>

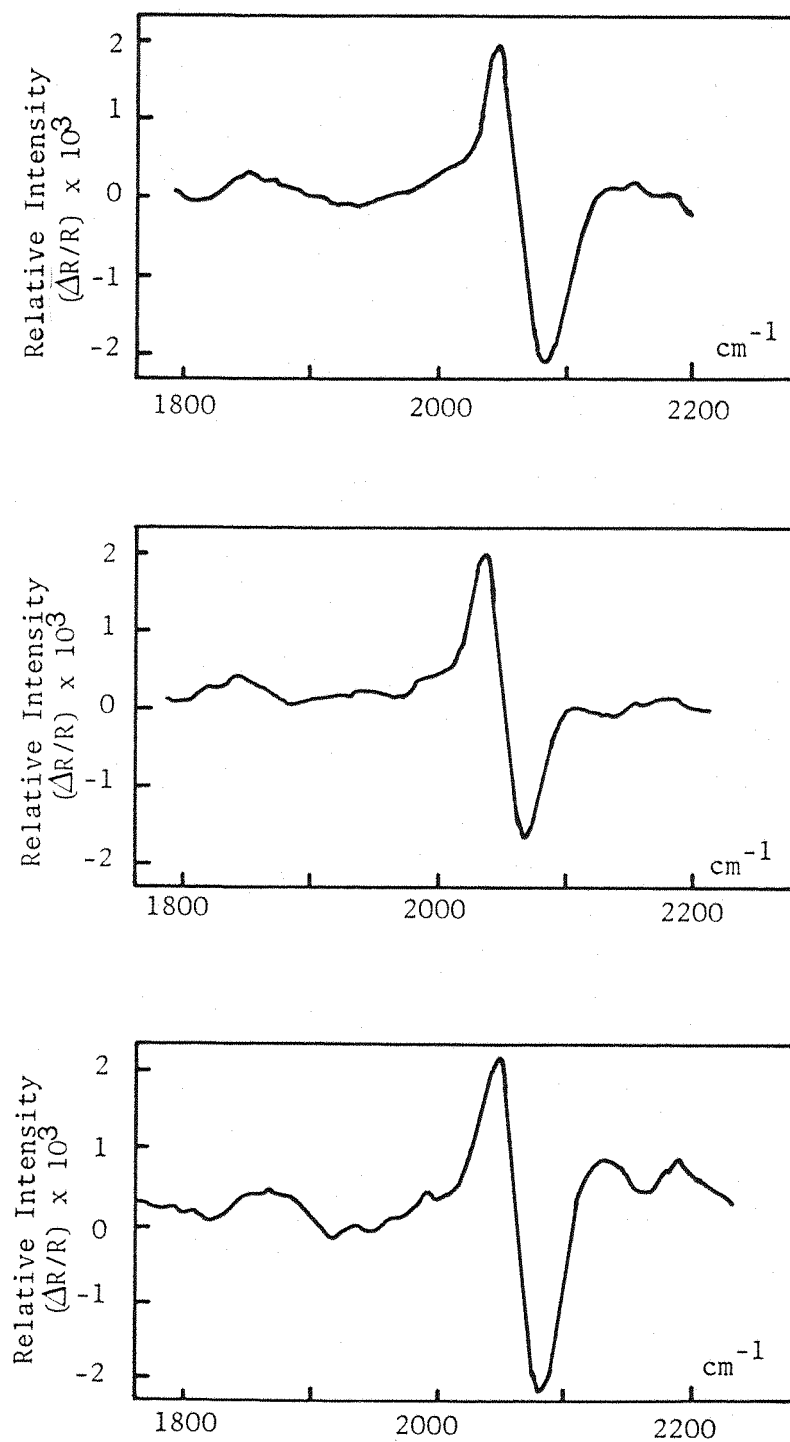


Figure II . 12 — EMIRS spectra from Pt/0.5 M HClO<sub>4</sub> for :

- (a) 0.25 M CH<sub>3</sub>OH. Modulation from 0.05 to 0.40 V (NHE).
- (b) CO saturated solution. Modulation from 0.05 to 0.250 V (NHE).
- (c) 0.3 M HCOOH. Modulation from 0.02 to 0.520 V (NHE).

the same as species formed by adsorption of CO. In order to investigate this reduction reaction by looking for adsorbed species formed at a platinum electrode in aqueous sulphuric acid saturated with CO<sub>2</sub>, the in-situ technique, EMIRS, has been used recently<sup>(146)</sup>. The results obtained lead to the following conclusions:

- (1) The reduction of CO<sub>2</sub> involves reaction with adsorbed hydrogen.
- (2) The adsorbed species formed from reduction of CO<sub>2</sub> resemble, but are not identical with, those formed directly from CO; i.e. the latter gives rise almost exclusively to a linearly bonded adsorbed CO species, whereas reduced CO<sub>2</sub> gives a significant amount of a more highly coordinated adsorbed CO species. This is in agreement with the work of Breiter<sup>(149,150)</sup>.
- (3) The strongly adsorbed species which poisons the electro-catalytic oxidation of many small organic molecules can be formed by reduction of CO<sub>2</sub> and it is probably a CO species in a three-coordinate site on the metal surface, i.e. the species giving the infra red absorption band at 1865 cm<sup>-1</sup>, similar to the one observed for the Pt/CO system.

A comprehensive study on adsorbed hydrogen at a platinum electrode<sup>(143)</sup> demonstrates that detailed information on molecular structure and orientation can be derived from EMIRS measurements. The two types of adsorbed species, which are readily distinguishable by their electrochemical behaviour, were also observed to show distinct optical properties. The shape of the infra red difference spectra obtained from the platinum electrode were found to vary markedly, depending upon the choice of limiting potentials for the square-wave modulation, Figure II.13. All the bands associated with the formation of weakly bound hydrogen may be attributed to vibrations of water molecules and the data obtained from aqueous acid electrolytes, fully deuterated systems and mixed H<sub>2</sub>O/D<sub>2</sub>O systems<sup>(143)</sup> reinforce the earlier conclusions<sup>(142)</sup> that the molecular entity called weakly bound hydrogen on a polycrystalline platinum surface is a hydrogen atom bonded to the surface but also bonded to a distinctly oriented water structure. Several possible



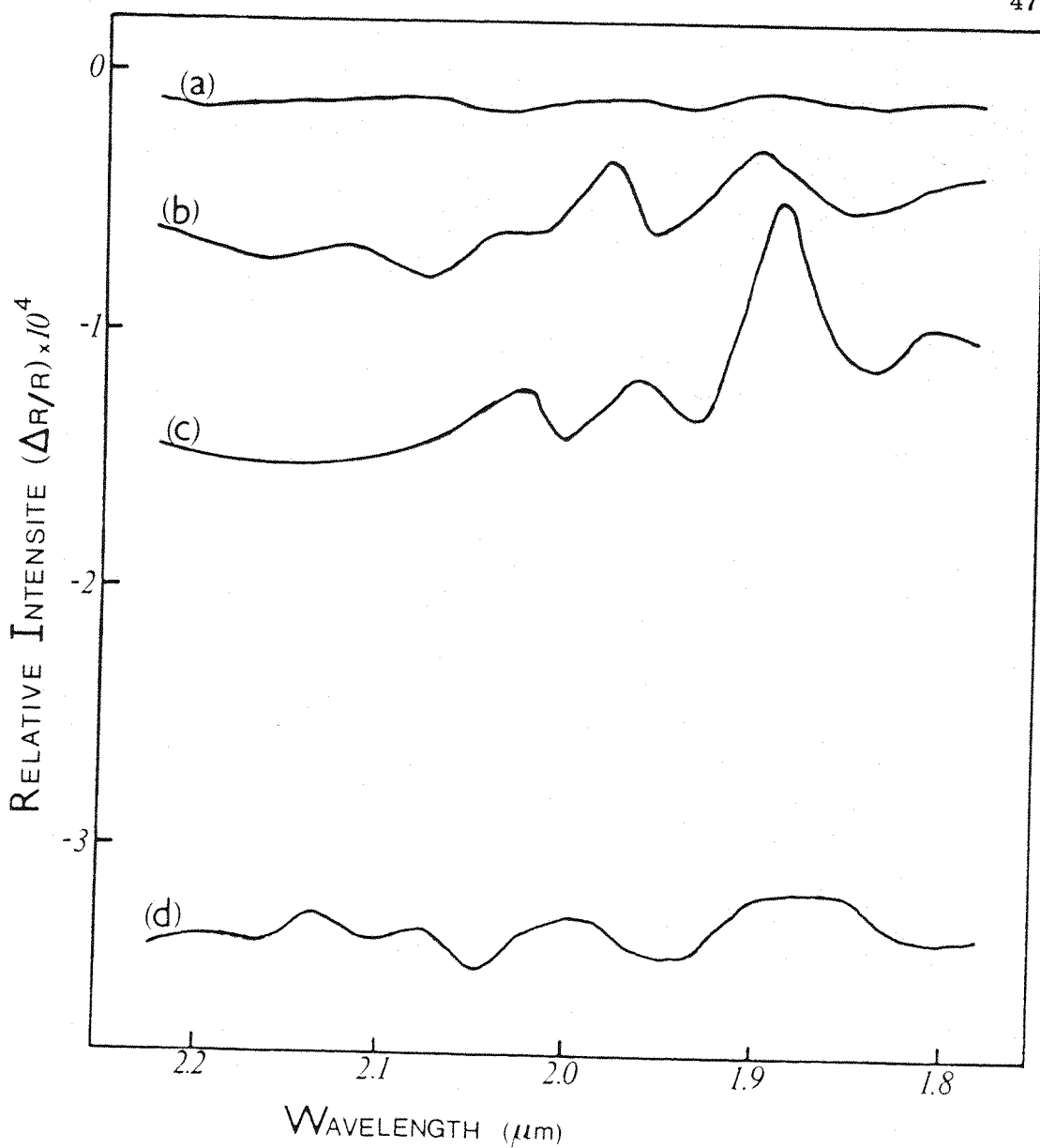


FIGURE II.13 — EMIRS spectra in  $\text{H}_2\text{O } \nu_2 + \nu_3$  region, from Pt electrode in 1 M  $\text{H}_2\text{SO}_4$  using modulation limits :

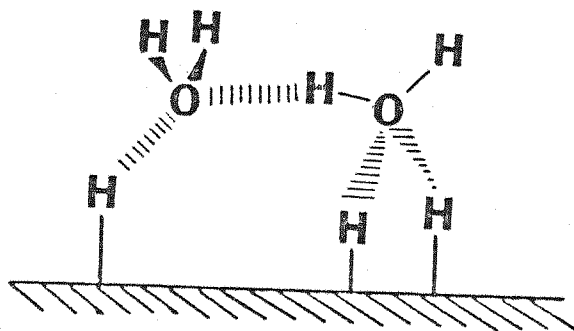
(a) 450 - 570 mV (NHE) : modulation entirely within the double-layer region of potential.

(b) 40 - 110 mV (NHE) : { modulations entirely within  
the weakly bound hydrogen

(c) 50 - 170 mV (NHE) : { region of potential.

(d) 220 - 340 mV (NHE) : modulation entirely within the strongly bound hydrogen region of potential.

models for water molecules associated with weakly bound hydrogen were discussed and in view of all available experimental evidence, the model shown below is considered to be the most suitable one:



In contrast to weakly bound hydrogen, no significant perturbation of the water structure could be seen on formation of strongly bound hydrogen. The view given previously<sup>(68)</sup> that the strongly bound hydrogen involves protons sitting within the electronic surface of the metal and the electrons in the conduction band (s-type adsorption) is therefore reinforced.

#### 2.4.4 Subtractively Normalized Interfacial Fourier Transform Infra Red Spectroscopy (SNIFTIRS)

The principles of the EMIRS technique have been applied successfully to the study of electrode solution interphases using a Fourier-transform infra red spectrometer (FTIR). Pons et al<sup>(131)</sup> have investigated the adsorption of acetonitrile in the double layer at a platinum electrode and the effect of the cation used (lithium or tetrabutylammonium) for the supporting electrolyte. The difference FTIR spectra obtained, indicated that the adsorption phenomena observed is greatly affected by these cations, and a potential dependence of the C≡N stretch vibrational band for lithium perchlorate/acetonitrile solutions was observed.

Since this first successful report further studies have been carried out<sup>(132, )</sup> and although the absolute sensitivity of this technique is for the moment less than the one obtained in EMIRS studies, the advantages of a Fourier-transform spectrometer

over a grating spectrometer<sup>(152)</sup> will make it a very useful tool for the study of electrode-solution interphases. The very much lower data acquisition time required is possibly the greatest advantage because it will minimize electrode degradation during the measurement period.

#### 2.4.5 Infra Red Reflection Absorption Spectroscopy (IRRAS)

Although modulation of the electrode potential is a useful and convenient way to gain the sensitivity required to observe in-situ infra red bands of monolayer quantities of adsorbates in aqueous solution, the EMIRS technique requires a distinct change in the infra red spectrum of the adsorbate between the two potential limits since the signal detected is a measure of the difference spectrum between these two potentials. This difference spectrum corresponds to the true infra red spectrum of an adsorbate at one potential, only if there is no corresponding absorption at the other modulation potential limit. If there is absorption in the spectrum at both modulation potential limits, as appears to be the case in most of the previously reported EMIRS studies, another experimental technique must be used to obtain the true infra red spectrum and to explore its sensitivity to the applied potential.

The technique called polarization-modulated infra red reflection absorption spectroscopy (IRRAS), which has been used for obtaining infra red spectra of adsorbates on metal surfaces in the presence of gas-phase adsorbant<sup>(135)</sup>, has been recently very successfully applied by Russell et al<sup>(133,134)</sup> to the study of electrode surfaces in the presence of an electrolyte and at controlled electrode potentials. IRRAS spectra are obtained using a double modulation technique. Polarization modulation utilizes the surface selection rule to isolate signals from oriented surface species from the unwanted background (Figure II.14). The source radiation is simultaneously modulated with a mechanical chopper to provide a signal which can be used to normalize the polarization modulated signal to compensate for variation in energy throughput of the spectrometer and sampling optics. Simple vibrational spectra are obtained directly by this method which permits the electrode potential to be used independently.

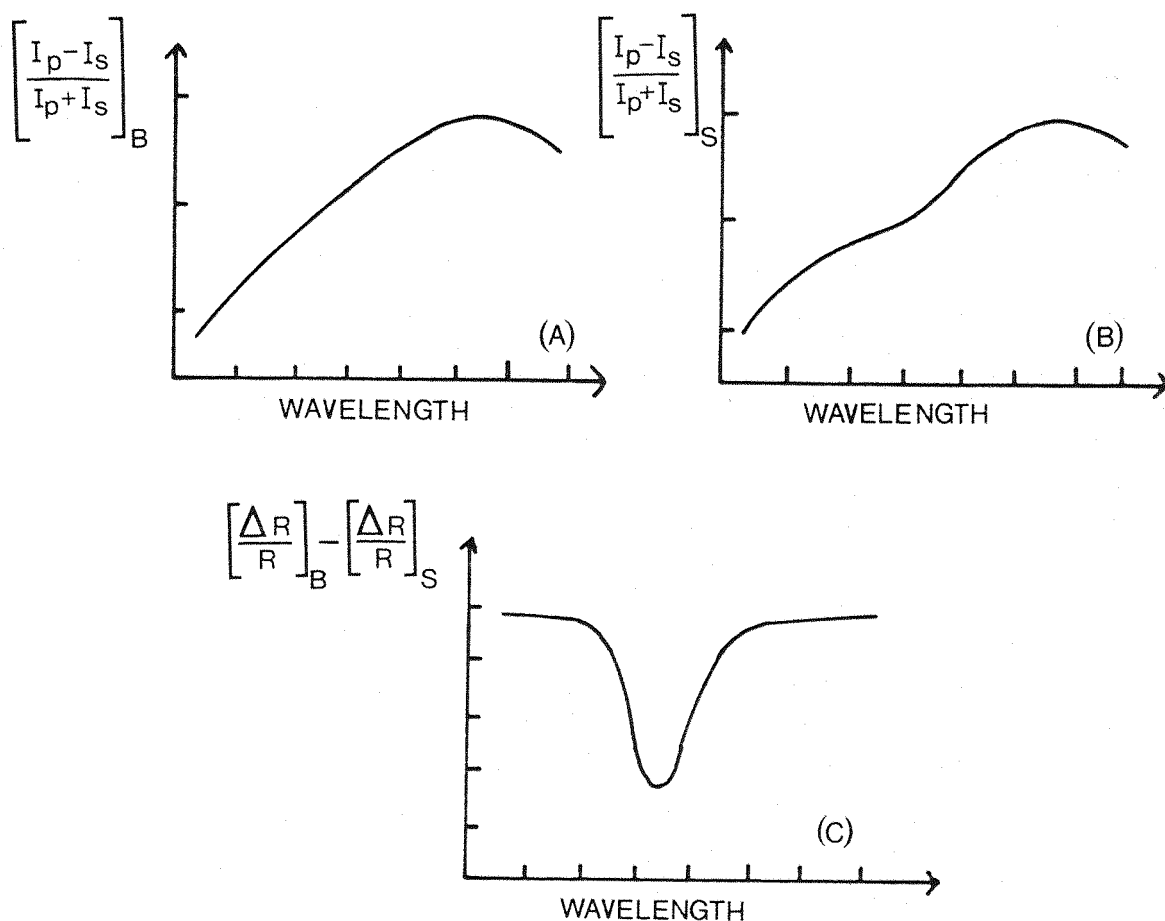


FIGURE II.14 — (A) Schematic representation of the background for "normalized" reflectivity difference between parallel,  $I_p$ , and perpendicular,  $I_s$ , components of light from spectroelectrochemical cell containing solvent and electrolyte.

(B) Schematic representation of sample spectrum for "normalized" reflectivity difference between parallel and perpendicular components of light from spectroelectrochemical cell containing sample, solvent, and electrolyte.

(C) Schematic representation of IRRAS spectrum produced by subtracting sample spectrum (B) from background spectrum (A),  $\Delta R = I_p - I_s$ ,  $R = I_p + I_s$ .

The first application of polarization-modulated IRRAS to investigate electrochemical systems has been reported with a spectrometer developed at the University of Minnesota<sup>(135)</sup> and direct measurement of the infra red band of adsorbed CO on platinum has been obtained. The spectra shown in Figure II.15(a) firmly establishes the dependence of the band wavenumber on electrode potential as the primary source of the unusual bisignate band observed previously using EMIRS<sup>(133)</sup>. For example, the difference spectrum resulting from subtraction of the bands observed for adsorbed CO on Pt when the electrode potential is held constant at 450 mV and 50 mV, cf. Figure II.15(b) is essentially identical to the EMIRS spectrum obtained with modulation between these two potentials, cf. Figure II.15(c). One should note that the EMIRS spectrum might be produced if the infra red spectra at the two potential limits were as shown in Figure II.15(d), but the direct observation of the band at both potential limits definitely eliminated this possibility. Since the spectral resolution of the IRRAS spectrometer used with a fixed slit and circular variable filter monochromator is about  $30\text{ cm}^{-1}$  at  $2100\text{ cm}^{-1}$ , the bands obtained using potential modulation will appear weaker and broader than those obtained at Southampton University using the grating monochromator described in the next chapter, which has a better resolution.

Although this polarization-modulation technique is about ten times less sensitive than the EMIRS technique, the advantage of obtaining direct spectral information instead of difference spectrum, will make it a very useful tool to study the electrode/solution interphase but specially to help in the interpretation of complex EMIRS results.

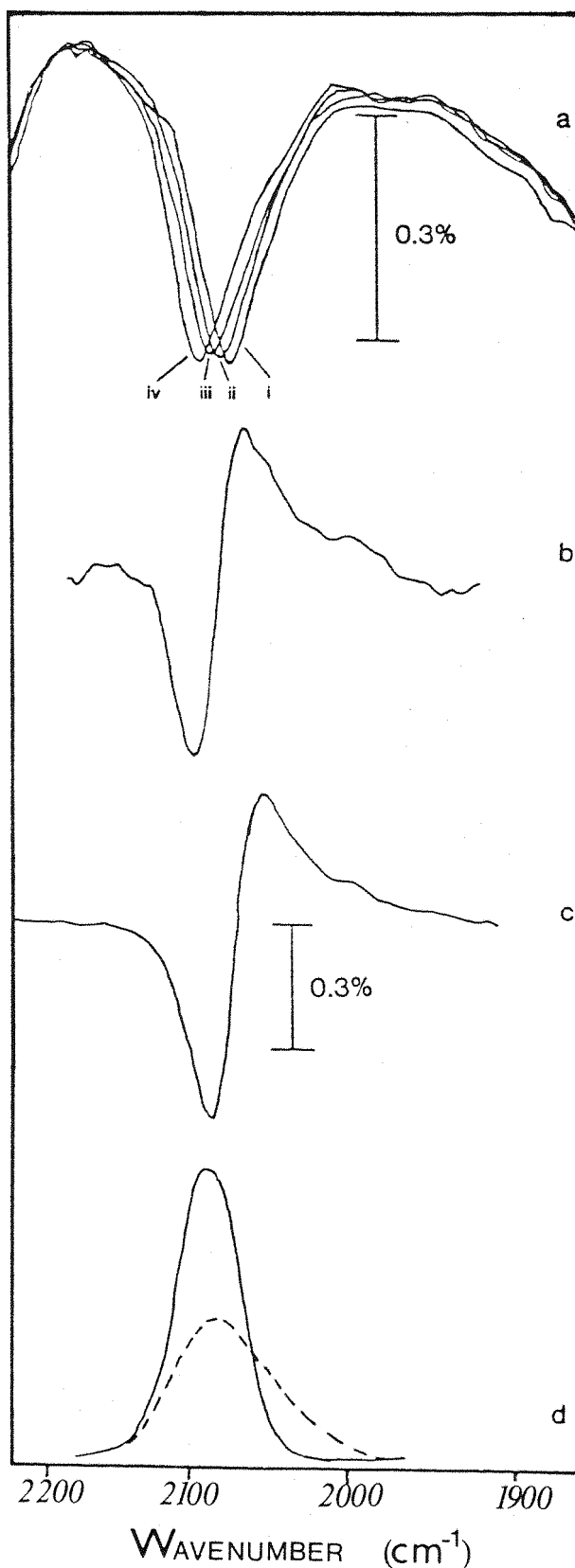


FIGURE II.15 — (a) IRRAS spectra of CO on Pt in 1 M  $\text{HClO}_4$  saturated with CO. The electrode potential is held constant at (i) 50 mV (NHE), (ii) 250 mV, (iii) 450 mV and (iv) 650 mV. (b) Difference spectra resulting from subtraction of IRRAS spectra a(iii) and a(i). (c) EMIRS spectrum from Pt in CO-saturated 1 M  $\text{HClO}_4$  solution, modulated between 50 and 450 mV (NHE). (d) A schematic representation of spectra at two potentials which could produce an EMIRS spectrum similar to that shown in (c).

## CHAPTER THREE

### Experimental

#### 3.1 Infra Red/Electrochemical Cells and Electrodes

##### 3.1.1 Cells

The cell used for the EMIRS experiments is shown in Figure III.1. This two compartment three electrode thin layer cell has been specially designed to meet the electrochemical and optical requirements, e.g. to enable spectroelectrochemical studies of strongly absorbing aqueous solutions throughout the infra red region. The disc working electrodes, Figure III.2, are mounted in a syringe barrel fitting and they were inserted via the barrel entrance of the cell through the platinum wire ring counter electrode fixed near the centre of the cell. The Luggin capillary probe for the reference electrode extends parallel to the working electrode support rod to within one millimeter of the cell window, i.e. one or two millimeters away from the flat metal disc of the working electrode. To provide a low impedance path and reduce high frequency interference, a small platinum wire is mounted between the Luggin and the three way tap which isolates the reference compartment. During an experiment this wire was connected through a 0.1  $\mu\text{F}$  capacitor to the reference electrode.

For the studies reported in this thesis the cell was fitted with a 1.5 mm thick silicon window which is transparent all over the wavenumber range investigated, i.e. from 1300  $\text{cm}^{-1}$  to 2450  $\text{cm}^{-1}$ . This silicon window is sealed in an appropriate water-free silica window which may be used at wave numbers above 2300  $\text{cm}^{-1}$ . Although silicon windows are useful to low wave number (down to around 900  $\text{cm}^{-1}$ ) and are not attacked by dilute acid solutions they have two serious limitations, such as their visible opaqueness and their high reflection losses<sup>(141)</sup>, which are avoided if silica windows can be used. A calcium fluoride ( $\text{CaF}_2$ ) window, transparent to visible, prepared from a 6 mm thick blank glued with epoxy to a glass joint, has been recently used in studies of water absorption bands. The small but finite water

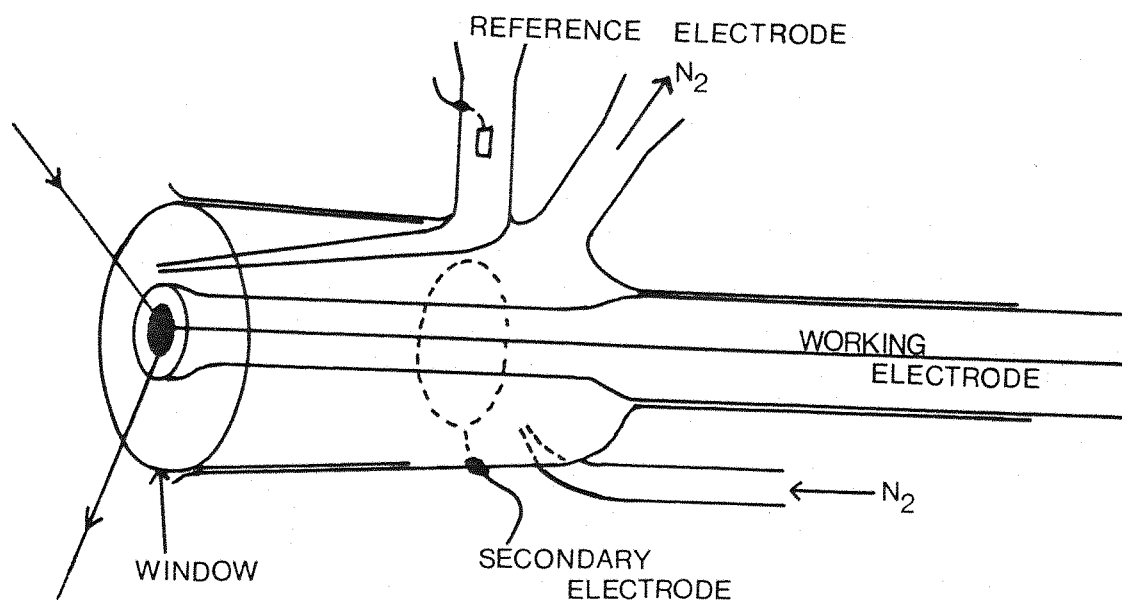
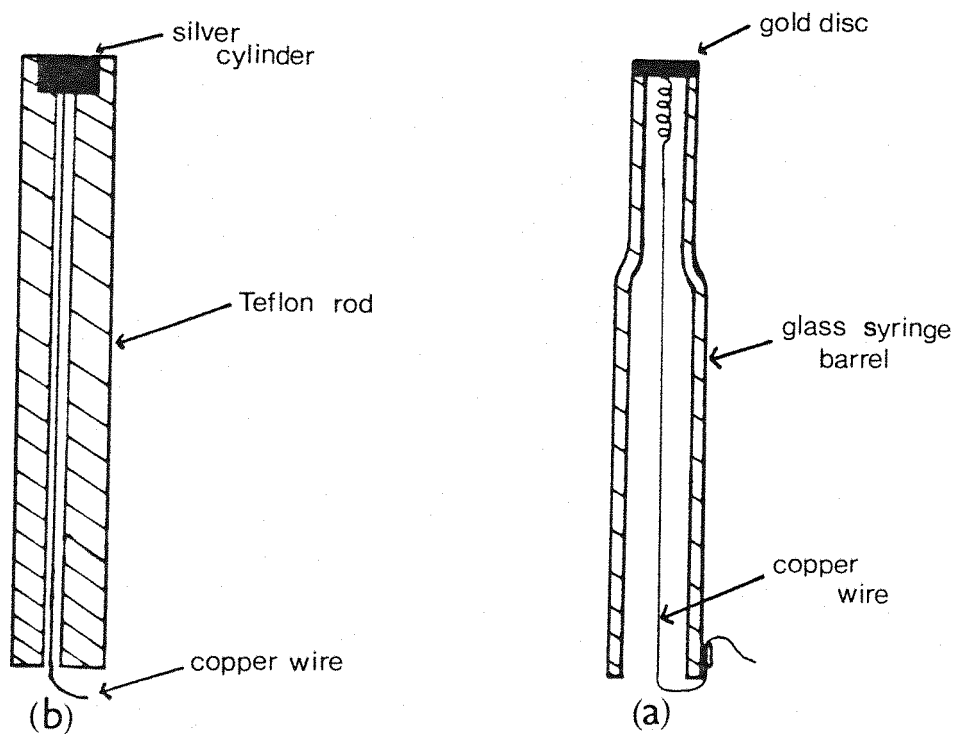


FIGURE III.1 — Schematic diagram of the EMIRS electrochemical infra red cell.

FIGURE III.2 — (a) The gold electrode.  
(b) The silver electrode.





solubility of calcium fluoride and the attack on the epoxy by contact with acidic solutions are the disadvantages of this window.

The cell used for the double layer capacity measurements is shown in Figure III.3. The Luggin capillary is mounted in a syringe barrel to permit it to be adjusted very close to the working electrode before each experiment ( $\sim 1$  mm). The secondary electrode consists of a platinum grid fixed parallel to the working electrode to give an even current distribution at the working electrode. As for the spectroelectrochemical cell the working disc electrodes are mounted in a syringe barrel fitting.

These two cells have inlets and outlets to permit purging. The reference electrode used was a Radiometer type K 401 saturated calomel electrode (SCE) to which all potentials given in this thesis are referred.

### 3.1.2 Electrodes

The gold disc electrodes were constructed from 99.99% pure gold metal (Johnson Matthey Co Ltd) carefully glued with epoxy resin onto the extended nose of a syringe plunger made of Pyrex glass, Figure III.2(a). The electrical contact is made via a copper wire pushed against the back of the gold disc. There was just a size difference between the gold electrode used for the EMIRS experiments ( $0.58 \text{ cm}^2$ ) and the one used for the double layer capacity measurements ( $0.48 \text{ cm}^2$ ).

The silver electrode was made from a 99.99% pure silver metal cylinder (Research Metals Ltd.), 7 mm in diameter, shrink-fitted into a hollow Teflon rod, machined to fit the syringe barrel of the cell, Figure III.2(b). A copper wire, soldered into the back of the metal cylinder, insured the electrical contact.

In all cases, these working electrodes were designed to permit electrical contact with the solution only by the front surface.

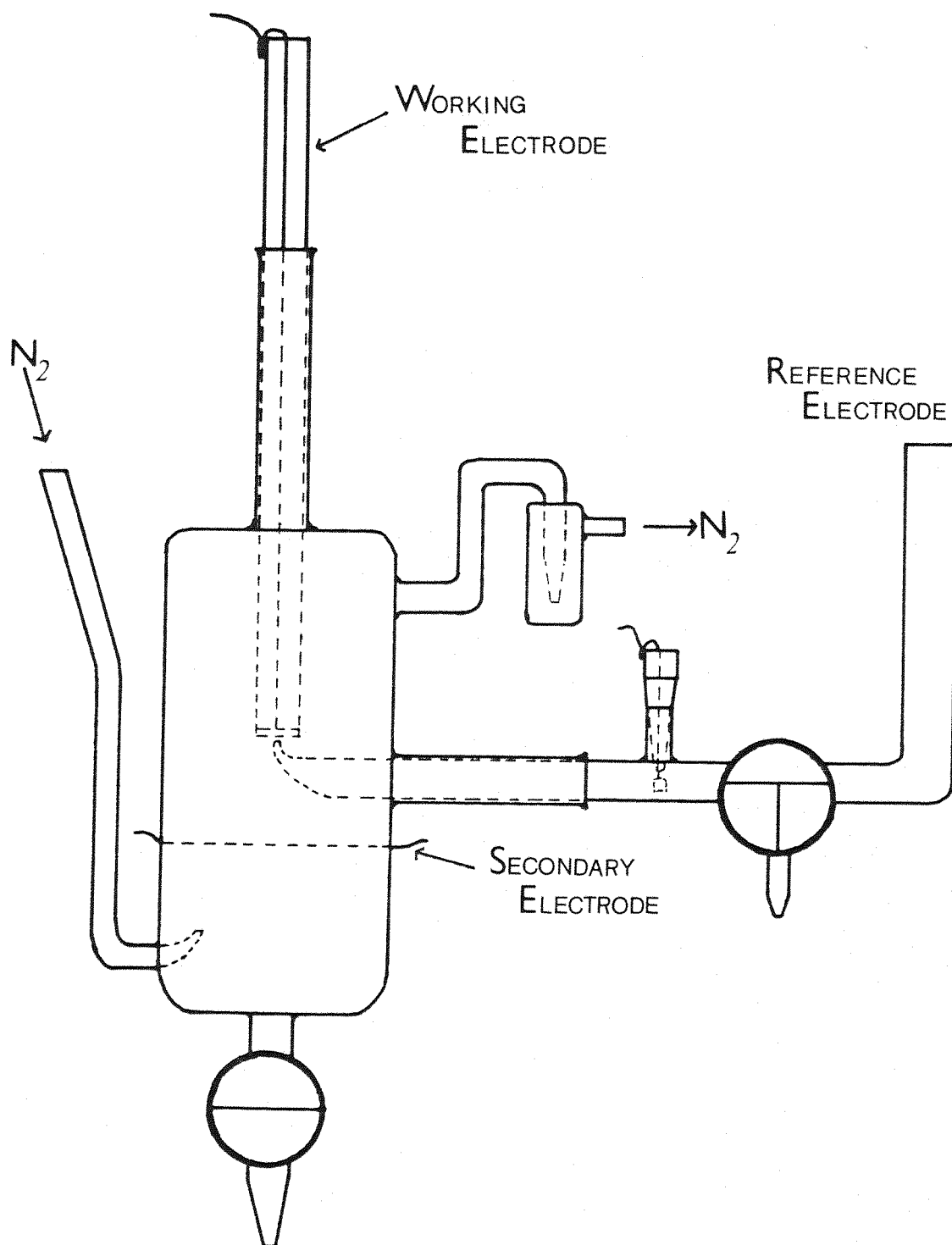


FIGURE III.3 — The double-layer capacitance cell.

### 3.2 Preparation of solutions, glassware and electrodes

In order to eliminate the surface active substances, organic or inorganic, which could later be adsorbed on the electrode surface, important attention was taken in the preparation of the solutions and in the cleaning of cells and glassware.

All solutions were prepared from four times distilled water. Water was first distilled from a glass still, then very slowly from a weakly alkaline dilute solution of potassium permanganate and finally from a solution containing a trace amount of orthophosphoric acid. This water was stored in three litre flasks with non-greased ground glass stoppers, and freshly redistilled before making a solution. During this latter distillation the first and last 50 ml were discarded and the distillate was collected directly into the solution flask.

All glassware including cells was cleaned by prolonged immersion in a mixture of equal volumes of concentrated nitric and sulphuric acids followed by a thorough rinsing with singly distilled water and finally by boiling in triply distilled water for about  $\frac{1}{2}$ -hour.

Analar sodium fluoride was recrystallized from triply distilled water and dried in a vacuum desiccator. Acrylonitrile (BDH) was freshly distilled before use in order to eliminate the small amount of p-methoxy-phenol (0.005%) contained in the commercial product to avoid auto-polymerization. Aristar grade sulphuric acid and analar grade potassium cyanide were used without further purification. All solutions were made just before use and were deaerated in the cell with a nitrogen purge for  $\frac{1}{2}$ -hour before starting any experiment.

In all electrochemical measurements, and in particular in optical ones, in which information is sought about the electrode/solution interphase, it is important to be able to produce an electrode surface smooth, highly reflecting and reproducible. This was achieved by polishing to a mirror finish the gold and the silver electrode surfaces with polishing alumina of decreasing grades (0.3  $\mu\text{m}$ , 0.1  $\mu\text{m}$ , 0.05  $\mu\text{m}$ ) on a polishing cloth

lubricated with triply distilled water. The electrodes were then rinsed with running water to remove residual alumina, immersed a few times in sulphuric-nitric acid mixture to wash them, and finally thoroughly rinsed with triply distilled water before being transferred to the cell. The final conditioning of the gold electrode was carried out in the spectroelectrochemical cell filled with 1M  $\text{H}_2\text{SO}_4$  solution by cycling the potential at  $50 \text{ mV s}^{-1}$  between  $-0.235$  and  $+1.45\text{V}$  (SCE) and observing the current-potential characteristic, Figure IV.1(a).

### 3.3 EMIRS Experimental Apparatus

A block diagram of the apparatus is shown in Figure III.4. The optical and electronic components are considered separately in the following sections.

#### 3.3.1 The Optical Equipment

EMIRS spectra have been obtained at Southampton using two different spectrometers. Part of the results presented in this thesis were obtained on a  $\frac{1}{4}$  meter  $\frac{8}{8}$  grating spectrometer, Figure III.5, which was originally used to demonstrate the feasibility of obtaining useful infra red spectra from electrochemical systems (110,151). This spectrometer required considerable manual control as it was not controlled through a programmable micro-processor system, and the  $\Delta R/R$  spectra had to be calculated manually using point by point time consuming calculations.

The currently used spectrometer was designed once the success of EMIRS had been established and was optimized for this technique. The major objective determining the design of this spectrometer and spectroelectrochemical cell was to achieve the best possible detectivity in terms of  $\Delta R/R$ . This means aiming for the highest possible throughput of energy which has been reflected from the electrode surface. Since bands of less than  $10 \text{ cm}^{-1}$  half width are quite unlikely to be encountered, the resolution was not a major problem and therefore a spectrometer of relatively short focal length has been chosen. It was assembled by Anaspec Ltd., utilizing a  $\frac{1}{2}$  meter  $f/4$  monochromator with a Czerny-Turner optical system, one of the most frequently

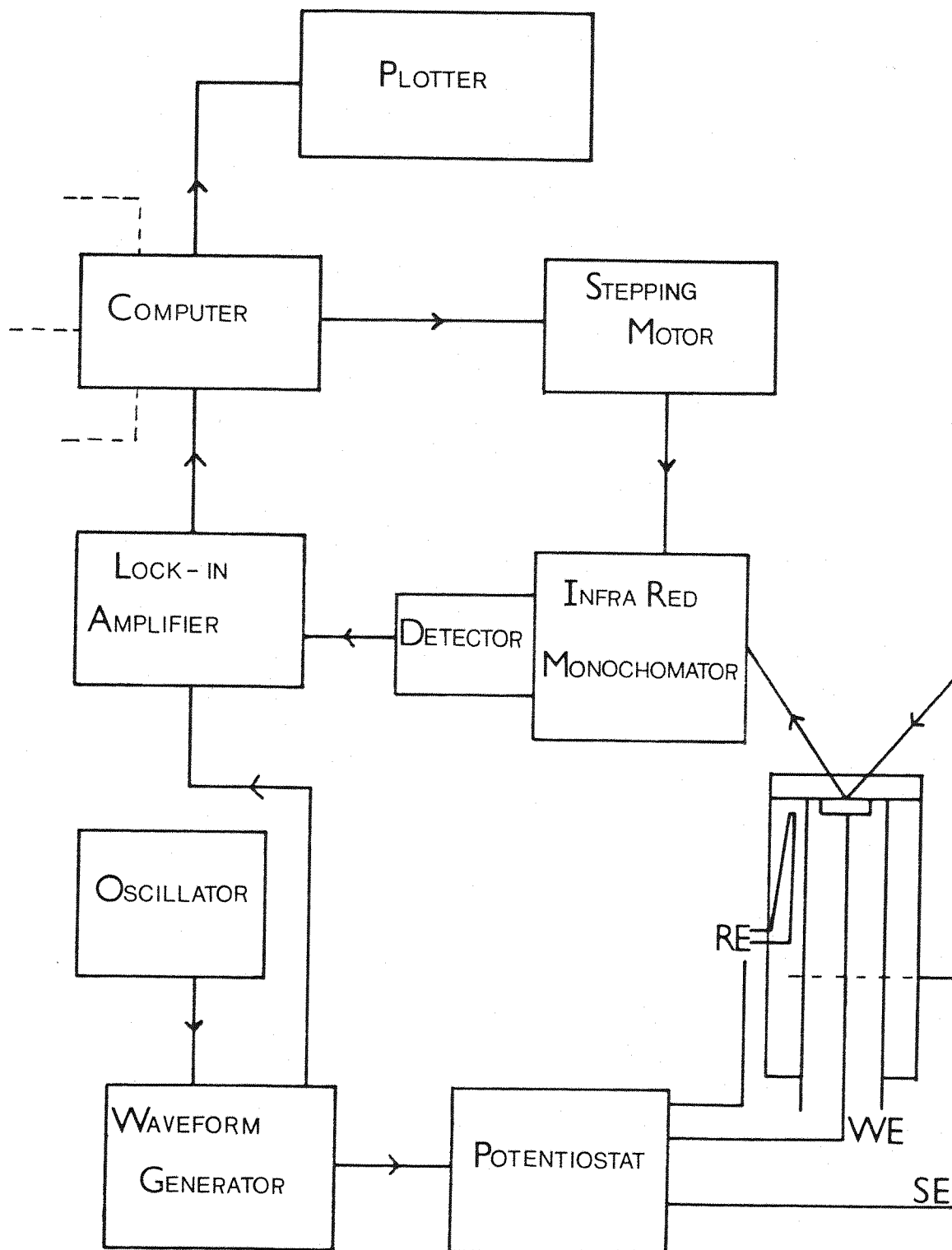


FIGURE III.4 — A block diagram of the EMIRS apparatus. (SE) secondary electrode; (WE) working electrode; (RE) reference electrode.

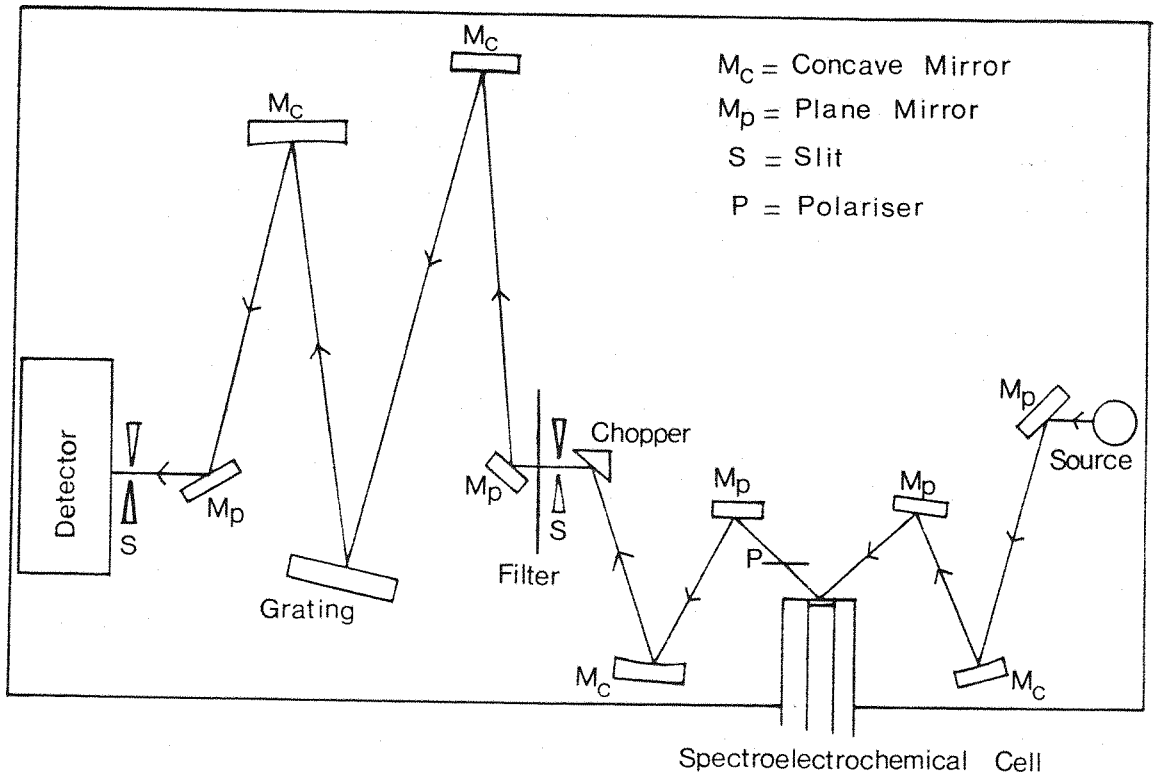


FIGURE III.5 — Schematic diagram of the spectrometer originally used to demonstrate the feasibility of extending the simple technique, modulated specular reflectance spectroscopy, into the true vibrational infra red range.

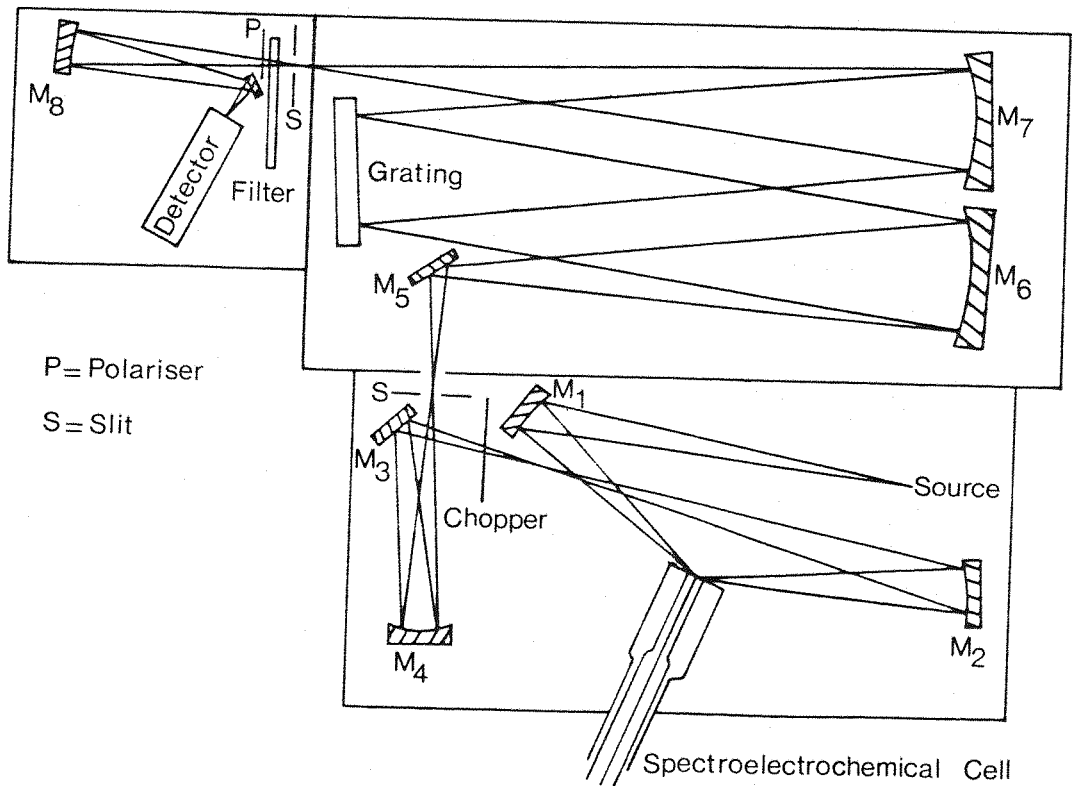


FIGURE III.6 — Schematic diagram of the currently used spectrometer for EMIRS experiments.

employed for grating spectrometers<sup>(152)</sup>.

The optical layout of the sampling chamber, monochromator and detector chambers of this spectrometer is shown in Figure III.6. The light source, a Nernst filament, operated at about 2300°C, was usually overrun to give a higher output energy at the expense of lifetime. All the spherical mirrors ( $M_1$ ,  $M_2$  and  $M_4$ ) are used at low off-axis angles to minimize aberrations while the two plane mirrors  $M_3$  and  $M_5$  are used at large angles of incidence. The fore-optics design shown in Figure III.6 does not collimate the infra red beam and typically it was adjusted to give an angle of incidence of 60°, for a cone of radiation with a spread of  $\pm 12^\circ$ , for the air/window-cell interface. The radiation transmitted through the entrance slit of the monochromator is collimated and directed towards the diffraction grating by two collimating mirrors ( $M_5$  and  $M_6$ ). The diffraction grating disperses the incident radiation and part of the dispersed radiation falls on to a focussing mirror ( $M_7$ ) which directs and focuses a spectrum to and at the exit slit. An IR 50 (Pye Unicam), Golay-type pneumatic detector, was employed and a Pfund mirror design is used to image the exit slit of the monochromator on the detector window.

The monochromator has a two position grating mount equipped with  $\surd$  84 x 84 mm Jarrell-Ash echelette diffraction gratings with the following specifications of grooves / mm and blaze positions: 150/mm ( $1300\text{ cm}^{-1}$ ), 50/mm ( $500\text{ cm}^{-1}$ ). The  $1300\text{ cm}^{-1}$  grating was used in first order from  $1350\text{ cm}^{-1}$  to  $3300\text{ cm}^{-1}$  and may be used in second order from  $3200\text{ cm}^{-1}$  to  $6200\text{ cm}^{-1}$ , useful range for the observation of combination and overtone bands<sup>(143)</sup>. The  $500\text{ cm}^{-1}$  grating was used in first order from  $1000\text{ cm}^{-1}$  to  $1600\text{ cm}^{-1}$ .

A blazed grating is a grating from which the majority of the incident radiation would be diffracted into a single order, almost invariably in the first order. Such a grating will have a very high efficiency for a wavelength  $\lambda$  which obeys the relationship:

$$n\lambda = 2d\sin\theta_B$$

where  $n$  is the order number,  $\theta_B$  is the blaze angle and  $d$  is the grating constant (inversely proportional to the number of lines per mm). The disadvantage of a blazed grating is its high efficiency for unwanted shorter wavelengths. For example, a grating blazed in the first order for one chosen wavelength ( $\lambda$ ), will also be blazed in higher orders for wavelengths which are exact sub-multiples of the chosen wavelength,  $\lambda/2$ ,  $\lambda/3$ ,  $\lambda/4$ ....,  $\lambda/n$ . It is therefore necessary when using a blazed grating of the first order to remove all wavelengths up to and including half the chosen wavelength. This could be achieved by means of a small prism or filters. In our case an eight position filter wheel (F) was employed for order sorting. Actually, four different filters may be used:

Filter 1 can be used in first order from  $850 \text{ cm}^{-1}$  to  $1550 \text{ cm}^{-1}$  and below  $850 \text{ cm}^{-1}$  in second order.

Filter 2 can be used in first order from  $1550 \text{ cm}^{-1}$  to  $2800 \text{ cm}^{-1}$ .

Filter 3 can be used in first order from  $2700 \text{ cm}^{-1}$  to  $5200 \text{ cm}^{-1}$  and in second order from  $3300 \text{ cm}^{-1}$  to  $5000 \text{ cm}^{-1}$  using the silica window as the cell window to filter out the first order.

Filter 4 can be used in second order from  $3800 \text{ cm}^{-1}$  to  $6200 \text{ cm}^{-1}$ .

Filters 1 and 2 are long-pass filters and filters 3 and 4 are short-pass filters. Due to the low energy throughput of the present spectrometer above  $3300 \text{ cm}^{-1}$ , it is better to look at the second order using the silica window and filter 3, if this spectral region has to be investigated.

A silicon plate (P) acting as a simple reflective polariser is placed parallel to the exit slit of the monochromator, to reject that "inactive" unwanted part of the radiation reflected from the cell window and from the electrode surface which had the electric vector perpendicular to the plane of incidence (see section 2.4.2.2). The chopper (C) is used to produce an 8.5 Hz signal for background, R, spectra but is positioned on an open



quadrant when potential modulated,  $\Delta R$ , spectra are being measured. The chopper frequency and the potential modulation frequency were adjusted to 8.5 Hz which is the frequency for which the maximum signal to noise ratio is obtained using the Pye IR50 Golay detector.

The main monochromator chamber and detector chamber are kept under constant purge by a slow stream of dry air. When spectral regions containing strong atmospheric absorptions are studied the sample chamber can also be purged. The alignment procedure for the cell and fore-optics is given in section 3.4 where the EMIRS experimental procedures are described. It is interesting to note that the single beam spectrometer used acts as a nearly perfect pseudo-double beam spectrometer since the identical optical path is followed by "beams" separated temporally but not spatially at the modulation frequency. The spectral resolution of this instrument, at the usual width slit (2 mm), is about 10 to 15  $\text{cm}^{-1}$ . The calibration of the spectrometer was carried out using bands from polystyrene film, atmospheric  $\text{CO}_2$  and residual water in a quartz window.

### 3.3.2 The Electrode Potential Modulation Equipment

A square pulse train, with a mark space ratio of unity, was applied to the working electrode via the potentiostat (Hi-Tek DT 2101), to modulate its potential. This pulse train was obtained from the waveform generator (Hi-Tek PP1), the frequency being set by external triggering with a square wave signal from an oscillator (Levell TG 200 DM) and the pulse length being adjusted on the waveform generator to give a signal in-phase with the triggering one. The height or amplitude of the potential step of this pulse was set on the waveform generator and added to the base potential set on the potentiostat. Using the sign conventions of Figure II.9, the more negative potential was set on the potentiostat and the potential step required to give the more positive potential was set on the waveform generator. These two potential limits were chosen according to the cyclic voltammogram or to the double layer capacity measurement for each particular system.

### 3.3.3 The Signal Recovery and Processing Systems

As has been mentioned already EMIRS is a potential modulation technique, and this modulation is used as a means of perturbing the reflected light intensity thus enabling correlation signal recovery techniques to be used. These very useful techniques can be used to make accurate measurements of a.c. signals obscured by high noise levels or, alternatively, to measure very small signals in the presence of lower noise levels with an accuracy higher than with other signal recovery methods. Two such techniques, phase sensitive detection and signal averaging are used in EMIRS to measure and amplify only the component of the optical signal in-phase with the potential modulation and thus to enhance the sensitivity to the level adequate for detection of infra red bands of submonolayer quantities of adsorbates, i.e. to enable relative reflectivity changes as small as  $1 \times 10^{-6}$  to be detected.

As the lock-in amplifier (LIA), the Brookdeal 401A used as a part of the EMIRS apparatus, contains a phase sensitive detector (psd) which is effectively a frequency selective a.c. voltmeter, also sensitive to the phase of the signal. The phase-sensitive detector works simply as the principle of the synchronous switch, the reference signal, which is synchronous with the signal to be measured, switches alternatively the signal, or its inverse, into an averaging circuit (low-pass filter), as shown in Figure III.7. The effect of such a psd on both synchronous and asynchronous (noise) input signals is shown in Figure III.8, from which two important features are readily seen:

- (a) When the a.c. signal and the reference input have the same frequency and are in-phase, the lock-in output will give a d.c. voltage proportional to the average amplitude of the input signal. A phase difference between the signal and reference will affect the output voltage as given by,

$$V_{\text{out}} \propto V_{\text{in}} \cos\beta$$

where  $V_{\text{out}}$  is the average output voltage,  $V_{\text{in}}$  is the signal voltage and  $\beta$  is the phase angle between the signal and the reference. For instance, a phase difference of  $26^\circ$  will cause a decrease of approximately

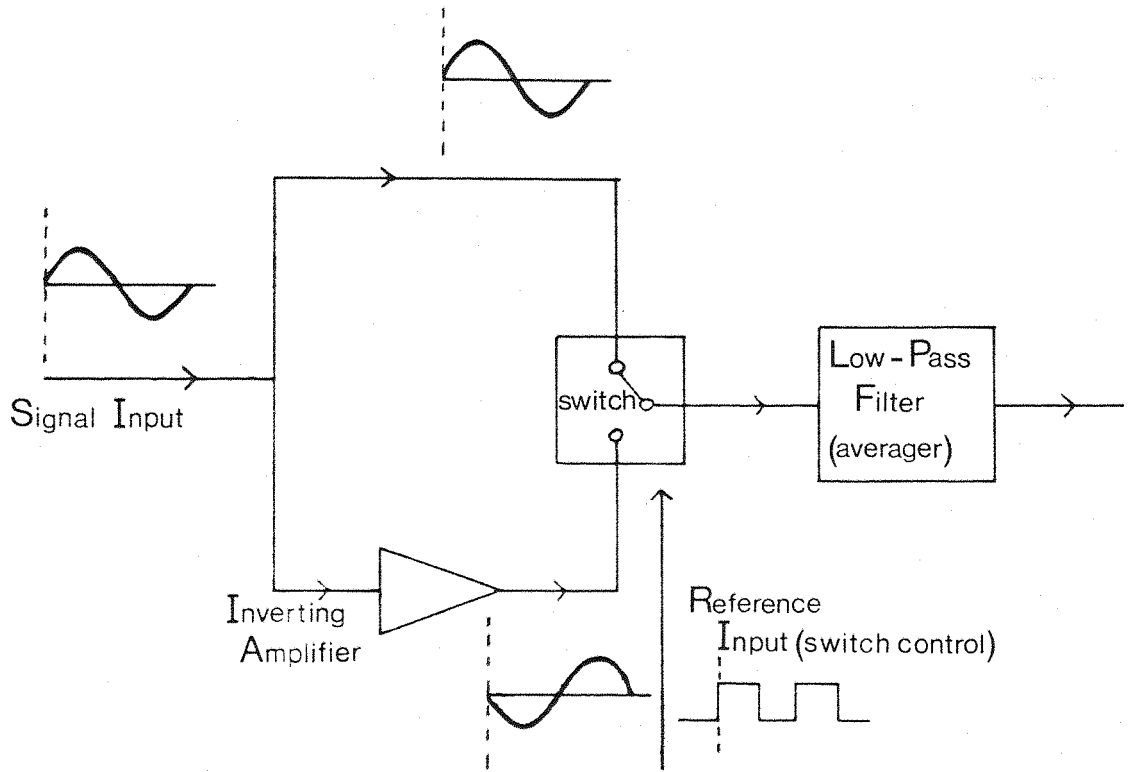


FIGURE III.7 — A block diagram of a phase-sensitive detector.

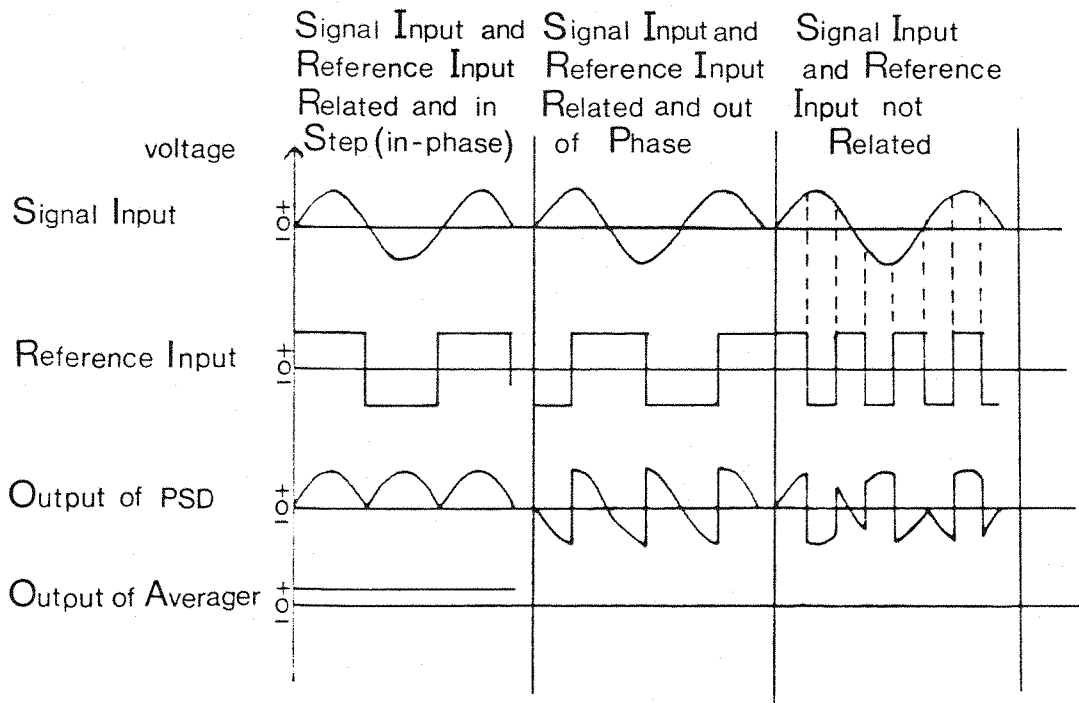


FIGURE III.8 — Description of the effect of a lock-in amplifier on both synchronous and asynchronous (noise) input signals.

10% in the output. To counteract any such phase shifts caused in an experiment by the electronic equipment, a phase shift facility is included in a lock-in system.

- (b) When the signal and reference inputs are not at the same frequency, the average value of the output will be zero, providing a sufficiently long time is taken to establish the average, i.e. the time constant of the low-pass filter must be appropriate .

The lock-in has therefore the overall effect of filtering out voltage fluctuations which are not at the reference frequency, i.e. it rejects noise and passes the wanted signal. Signal-to-noise ratios can be enhanced by factors as large as  $10^5$ , but at the expense of the direct time information, the output being an average over all the period of one cycle of the signal.

As the detector output was fed directly to a Brookdeal LIA type 401A described above, its output signal was fed directly to an analog-to-digital convertor and was digitally averaged for a certain number of scans over the chosen spectral region, until an adequate signal-to-noise ratio was achieved. As a signal averager would have done the controlling computer samples the output signal of the LIA at constant preset time intervals, the sampled voltages are then converted into digital form by an analog-to-digital convertor, and each information is stored in a computer memory location. The sampling process is repeated a preset number of times,  $n$ , and each new sample is added algebraically to the value already accumulated in its memory location so that the final value stored at each location is equal to  $n$  multiplied by the average value of the sample taken at that point. Noise being random, its average value will approach zero as  $n$  increases, and the signal being normally constant its contribution to the value stored will increase linearly with  $n$ . The controlling computer program was written to permit display of the  $\Delta R$  spectrum on the computer screen when the preset number of scans is completed, this spectrum is therefore the average value of the output of the LIA, over the chosen spectral region, calculated in mV/cm by the computer.

The detailed configuration of the Commodore computer system used in EMIRS is shown in Figure III.9. A Commodore Pet, range of microcomputer is used (CBM 3032) as the programmable controller, heart of the system. Additional peripherals have been added to the CBM which totally control them. Analog signals derived from the monitored system are connected into the analog-to-digital convertor where they are internally conditioned. On the digital side the convertor is connected into the system by the IEEE-488 instrumentation bus. The selected diffraction grating is rotated by the stepping motor drive under the control of the bus interface. A plotter (HP 7225A) a printer (Commodore 3022) and a dual drive floppy disk (Commodore 3040) all controllable over the IEEE-488 bus are connected into the system and they added a great deal of versatility and convenience to the use of the Commodore 3032 computer. The controlling computer program was written essentially to enable the  $\Delta R$  spectrum to be ratioed by the memorized R spectrum to give a  $\Delta R/R$  spectral plot. When an adequate signal-to-noise ratio has been achieved the  $\Delta R$  spectrum, expressed by the computer in the same units as the related R spectrum already in memory, may be divided by this background spectrum to give a  $\Delta R/R$  spectrum which is therefore a dimensionless quantity.

#### 3.4 Experimental Procedures

The procedures for cleaning the cell, polishing the electrode, and preparing samples have been described previously (section 3.2).

Once the electrode had been prepared and the cell filled the electrochemistry is checked by observing a cyclic voltammogram and if satisfactory the cell is then aligned correctly in the light beam (Figure III.6), i.e. the cell is positioned such that the source image, demagnified by a factor of two by mirror  $M_1$ , is focussed upon the surface of the electrode. Vertical adjustments are made to position the circular electrode in the centre of the source image. Tilt adjustments are made in order to collect all the light reflected from the cell on mirror  $M_2$  which forms a remagnified 1:1 image of the source at the chopper

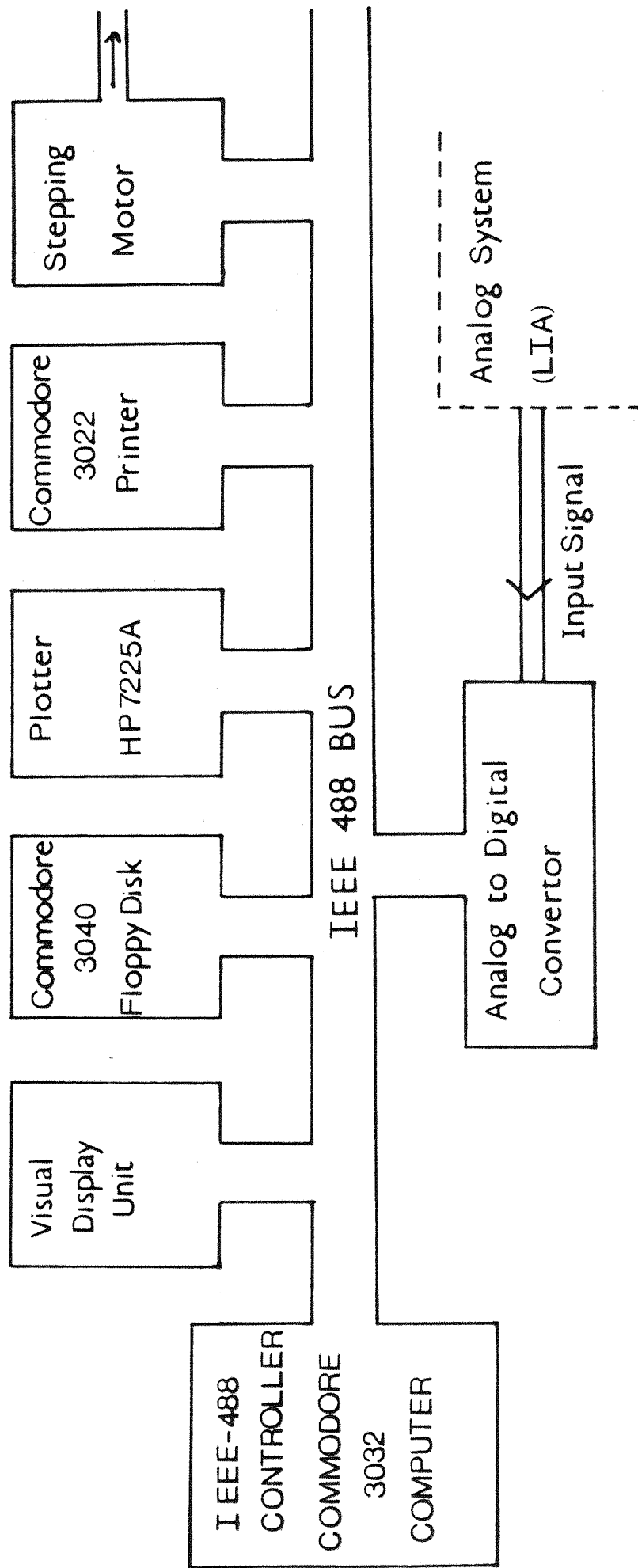


Figure III.9 - A block diagram of the processing control system of the EMIRS apparatus.

position. With the image from the electrode at the vertical centre of the entrance slit of the monochromator and all cell radiation collected by mirror  $M_2$ , the rotation of mirror  $M_2$  about its vertical axis is adjusted to produce a maximum signal at the detector from the electrode with the chopper on.

The proper grating for the spectral region of interest is selected using the manual grating switching control and the appropriate transmission filter positioned after the exit slit. The spectral region to be scanned and the number of data points to be used to cover this region are set on the computer.

Two background scans were run to determine the electrode reflectivity curve,  $R$  (Figure II.7). During the first scan the electrode is withdrawn from the window and during the second positioned against the window. The difference in energy between these two scans is the background  $R$  curve for the IR radiation reflected from the electrode for the chosen spectral range. During the background scans the chopper is on and the electrode can be held at any potential or even modulated since the  $\Delta R$  curves produced during potential modulation are orders of magnitude weaker than the  $R$  curve. For background and sample scans the monochromator is moved by uniform wavenumber increments by the computer giving the grating drive stepping motor the appropriate number of pulses. After each increment a delay of between one half and one second, as set on the computer, occurs before a reading is made of the output signal of the lock-in amplifier to permit damping out of noise produced by stepping the grating. Data are recorded during monochromator movement to both higher and lower wavenumbers with appropriate corrections made upon each grating direction reversal to compensate for backlash in the gears. For background scans the lock-in reference signal may either be taken from a photocell mounted opposite a visible lamp at a position cut by the chopper blades or by using the preamplifier output for both signal and reference inputs.

Sample ( $\Delta R$ ) scans over the chosen spectral region are made with the chopper positioned in the open position and the desired potential modulation applied to the electrode. For such scans the lock-in reference is taken from the waveform

generator and is phase adjusted for delays produced by detector response (Figure III.10). The a.c. signal from the IR detector, produced by the square wave modulation of the electrode potential, presents a constant phase shift with respect to the modulation waveform whenever the radiation intensity reaching the detector from the electrode differs at the two limiting potentials. The controlling computer program was written to permit display of the  $\Delta R$  spectrum on the computer screen after a preset number of scans. Data for each spectral element *are* collected in one computer memory location as the sum of the detector signals for that element from all scans. If an adequate signal-to-noise ratio has been achieved, the  $\Delta R$  spectrum may be ratioed by the R spectrum to give a  $\Delta R/R$  spectral plot. If the  $\Delta R$  signal-to-noise ratio is still low, additional scans may be taken before displaying again on the computer screen. R,  $\Delta R$ , and/or  $\Delta R/R$  plots may all be plotted on the hard copy plotter and/or stored on a floppy disk.

It is interesting to note that the detectivity of the EMIRS system described depends, of course, on the chosen wavelength range and on the nature of the electrolyte. In regions of good energy throughput, bands with  $\Delta R/R$  values as low as  $10^{-6}$  can be detected.

### 3.5 Electrode Capacitance Measurements

Capacitance measurements were made on electrodes prepared as for the optical measurements with the cell shown in Figure III.3. A small sine wave voltage (5 mV peak to peak) from the oscillator was superimposed on a very slow ramp ( $10 \text{ mV s}^{-1}$ ) from the waveform generator and the result applied to the electrode via a potentiostat. A lock-in amplifier was used to analyse the in-phase and quadrature components of the a.c. current response of the working electrode, the reference signal of the LIA being taken from the oscillator. These two components were plotted directly on a X-Y recorder. Figure III.11 shows a diagram of the experimental set up. Phase adjustments and calibrations were made using known capacitance dummy cell, and as explained in section 2.3, the electrode capacitance plots



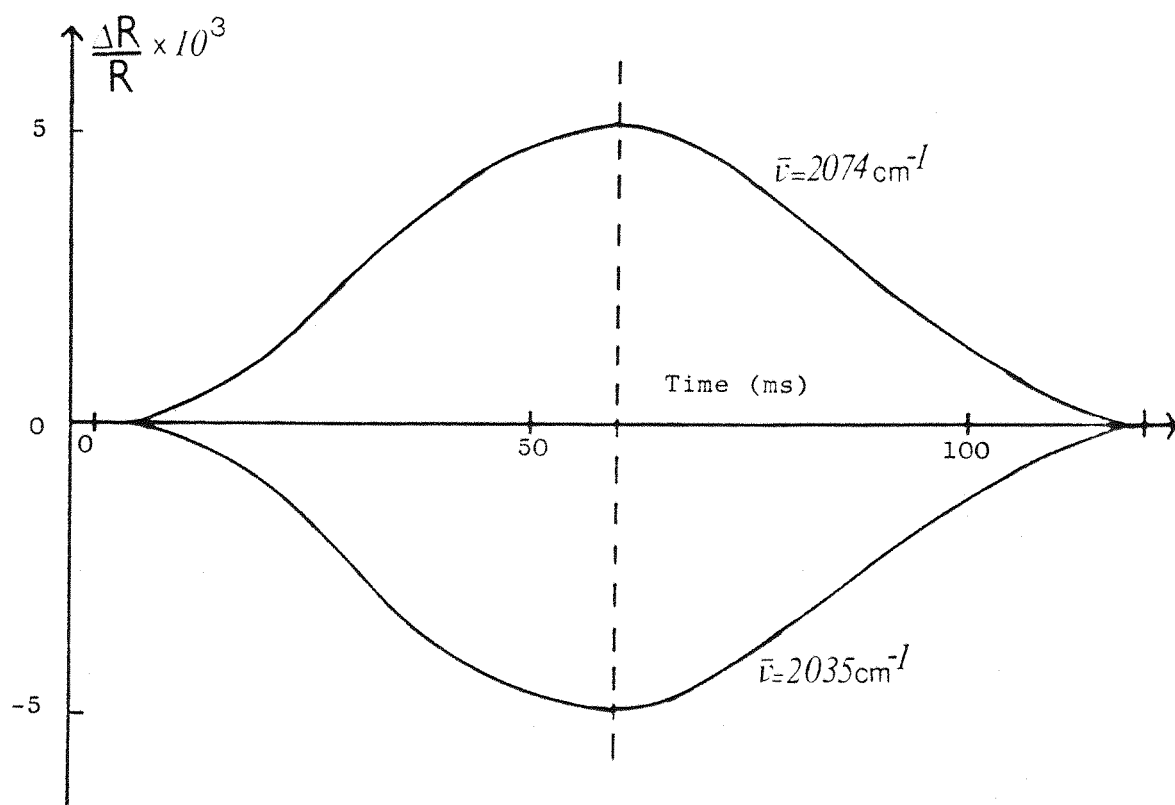


Figure III . 10 — Detector response to modulation between 50 mV and 800 mV (NHE) at 8.5 Hz for 0.5 M methanol in 1 M  $\text{H}_2\text{SO}_4$ . Shape of response curve is due to time constants of detector (Golay type cell).

were calculated from the in-phase and quadrature components of the current and the constant determined from the calibration applying equation (2.19).

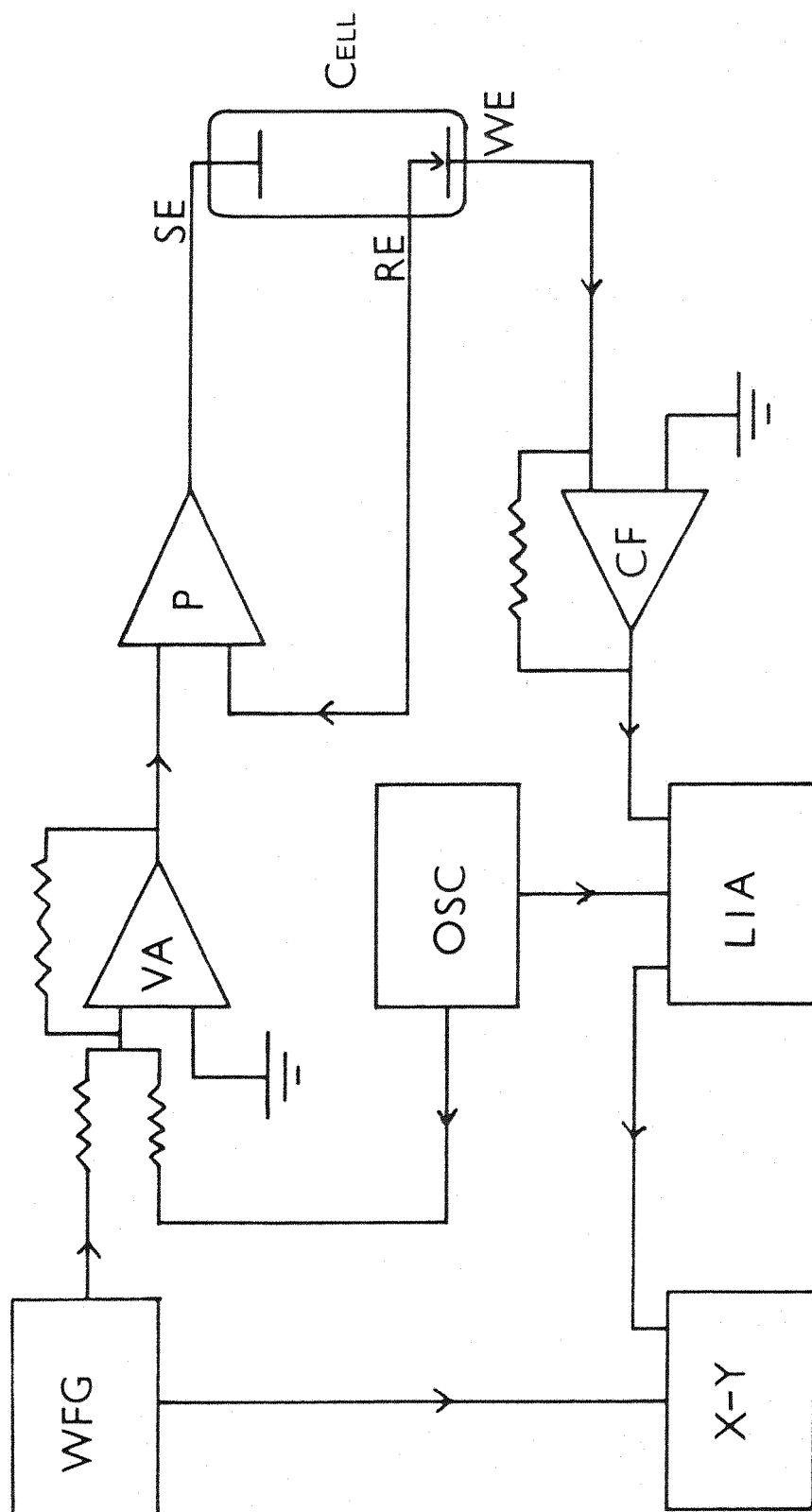


FIGURE III.11 — A block diagram of the capacitance apparatus. (WFG) waveform generator; (VA) voltage adder; (P) basic potentiostat; (SE) secondary electrode; (RE) reference electrode; (WE) working electrode; (CF) current follower; (LIA) lock-in amplifier; (OSC) oscillator; (X-Y) x-y recorder.

## CHAPTER FOUR

### Acrylonitrile Adsorption on a Gold Electrode

#### 4.1 Introduction

Information on the adsorption behaviour of organic substances at catalytic metals is of primary importance in several areas of electrochemistry.

The behaviour of nitriles, e.g.  $\text{CH}_3\text{CN}$ ,  $\text{C}_6\text{H}_5\text{CN}$ , etc., is of interest in regard to: (a) their use as electrochemically "inactive" aprotic solvents; (b) their involvement in organic oxidation processes where nitrilium ions, and subsequently amides, can be formed and (c) in reductive dimerisation. Since, some twenty years ago, M. Baizer of Monsanto<sup>(153)</sup> showed that adiponitrile, a key intermediate in the preparation of Nylon 6.6, could be synthesised via acrylonitrile by a direct electrochemical reaction, research in this field and in organic electrochemistry in general has increased substantially.

The bonding and geometry of the acrylonitrile molecule are also particularly interesting with regard to the further development of EMIRS. It possesses a conjugated  $\pi$ -orbital system incorporating two IR active vibrational modes which are well within the range of frequency covered by the present EMIRS instrumentation. It is therefore well suited to investigations of the orientation of an adsorbed molecule and to the perturbation of the vibrational frequencies caused by bonding to the electrode surface. In the present work we have investigated the adsorption behaviour of acrylonitrile at a polycrystalline gold electrode by means of double layer capacity measurements followed by EMIRS studies.

#### 4.2 Double Layer Capacity Measurements

This study was carried out as a preliminary investigation on the adsorption characteristics of acrylonitrile on a gold electrode.

Before every experiment, the electrochemistry was checked

by observing cyclic voltammograms. The shape of those shown in Figure IV.1 display a suppression of the oxygen region in the presence of acrylonitrile. This behaviour is usually typical of an adsorption phenomenon<sup>(14,154)</sup>.

The theoretical aspects and the experimental procedures related to the electrode capacitance measurements were described respectively in sections 2.3 and 3.5.

The differential capacitance curves obtained for a polycrystalline gold electrode in sulphuric acid solution (1 M) and sulphuric acid/acrylonitrile solutions (1M/0.05M), for a very slow sweep rate (10 mV/s) and a small a.c. modulation (5 mV peak to peak), are shown in Figures IV.2, IV.3 and IV.4. These measurements were carried out at three different frequencies of the small sinusoidal modulation which were respectively 8.5 Hz, 70 Hz and 280 Hz.

The measurement made in sulphuric acid alone (1M) at 8.5 Hz, which is the modulation frequency used for the EMIRS study, shows two different peaks around +0.580V to +0.850V (vs. SCE). Although the latter tends to disappear when the same measurement is made with acrylonitrile (0.05M) the former peak seems to keep the same relative intensity. This first peak is probably due to the adsorption of bisulphate ( $\text{HSO}_4^-$ ) anions on the electrode. An overall reduction of the double layer capacity is observed for the measurement carried out in the presence of the uncharged surfactant (acrylonitrile). This feature suggests that this compound is adsorbed over the whole range of potentials, from 0.0V to +1.0V (SCE) but this adsorption is probably weakened by a competitive adsorption of  $\text{HSO}_4^-$  anions.

The decrease of the electrode capacitance for the high concentration solutions, Figure IV.5, could be due either to the slow formation of a polymer film on the gold surface, or to the slow establishment of the adsorption equilibrium. According to an internal reflectance spectroscopic study of a polyacrylonitrile film formation on a germanium electrode by Trifonov *et al*<sup>(44)</sup>, the polymerisation process was accompanied

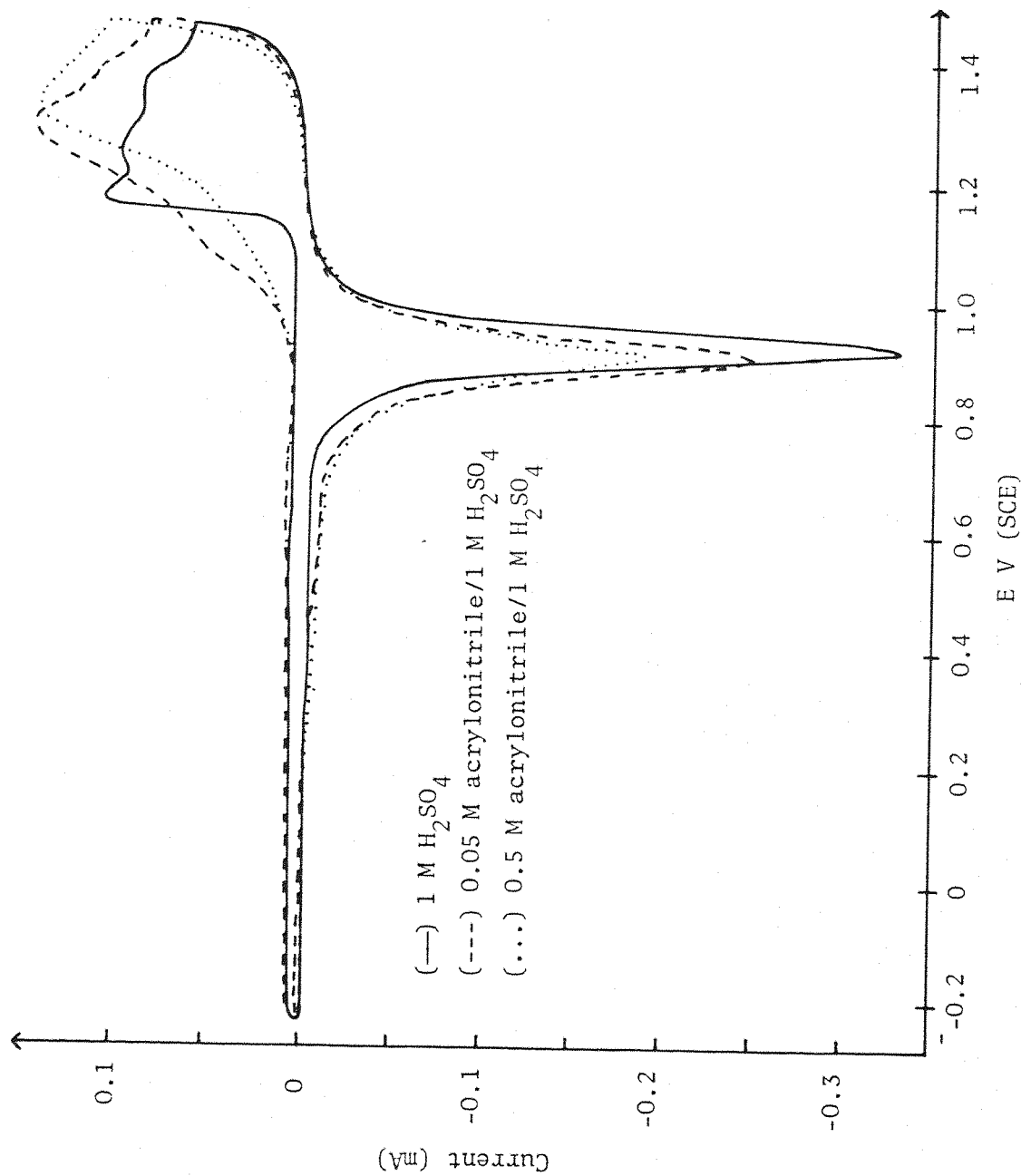


Figure IV . 1 — Cyclic voltammograms for Au electrode in different solutions.

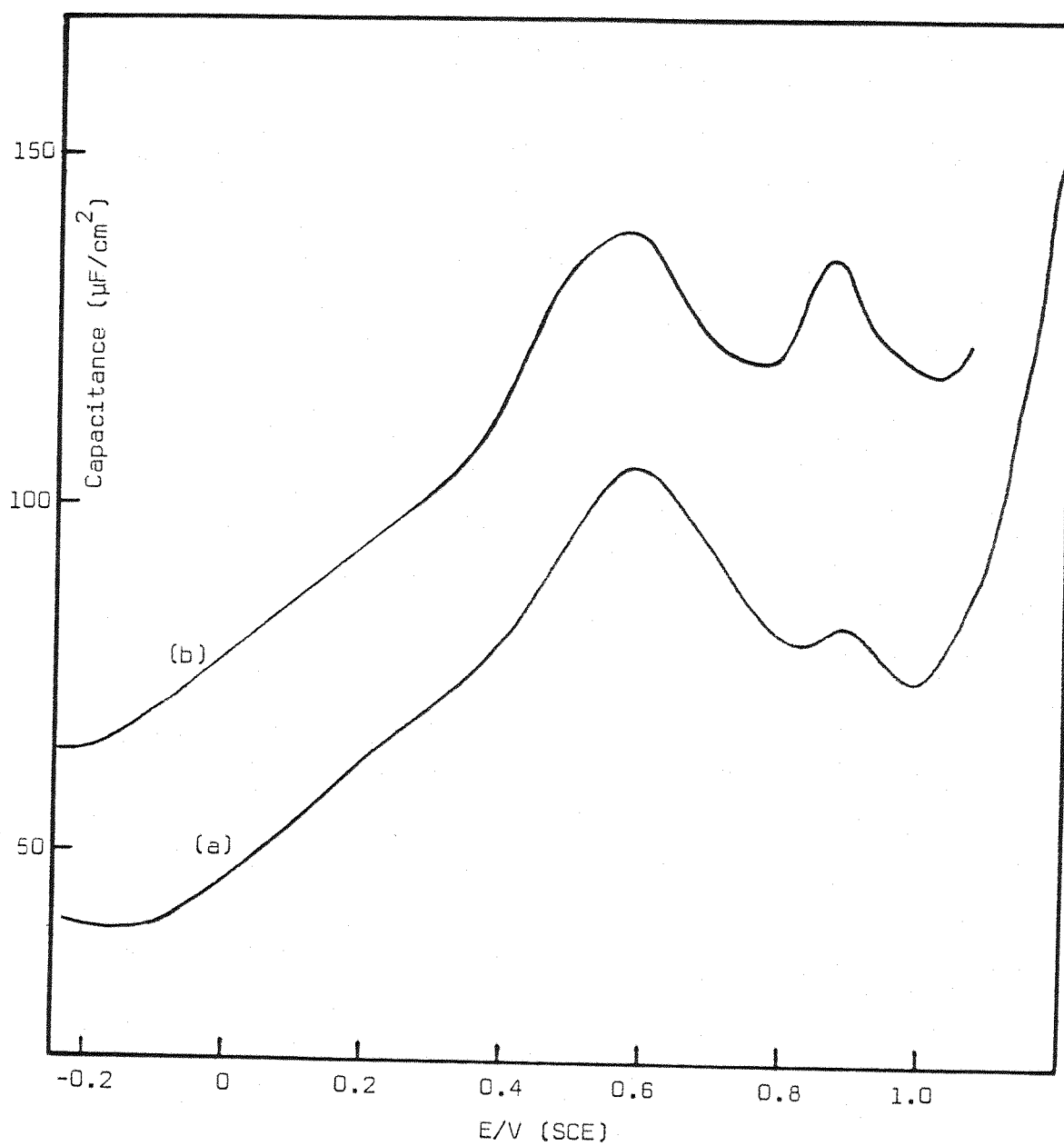


FIGURE IV. 2 — Differential capacitance curves of a gold electrode  
in :  
(a) 1 M  $\text{H}_2\text{SO}_4$  / 0.05 M acrylonitrile solution  
(b) 1 M  $\text{H}_2\text{SO}_4$  solution

A.C. modulation : 8.5 Hz, 5 mV peak to peak  
Slow ramp :  $10 \text{ mV s}^{-1}$

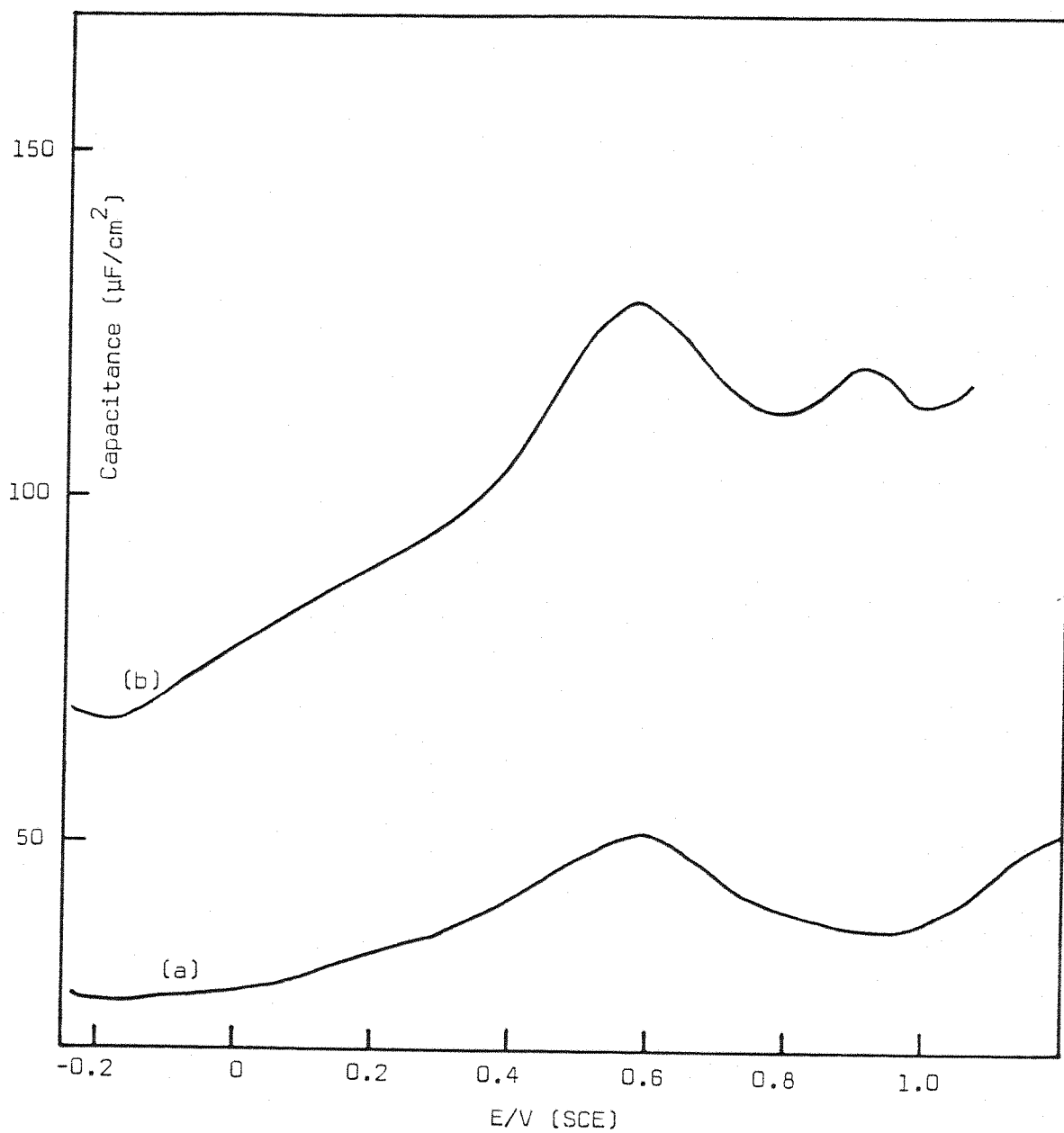


FIGURE IV.3 — Differential capacitance curves of a gold electrode in :  
(a) 1 M  $\text{H}_2\text{SO}_4$  / 0.05 M acrylonitrile solution  
(b) 1 M  $\text{H}_2\text{SO}_4$  solution

A.C. modulation : 70 Hz, 5 mV peak to peak  
Slow ramp :  $10 \text{ mV s}^{-1}$

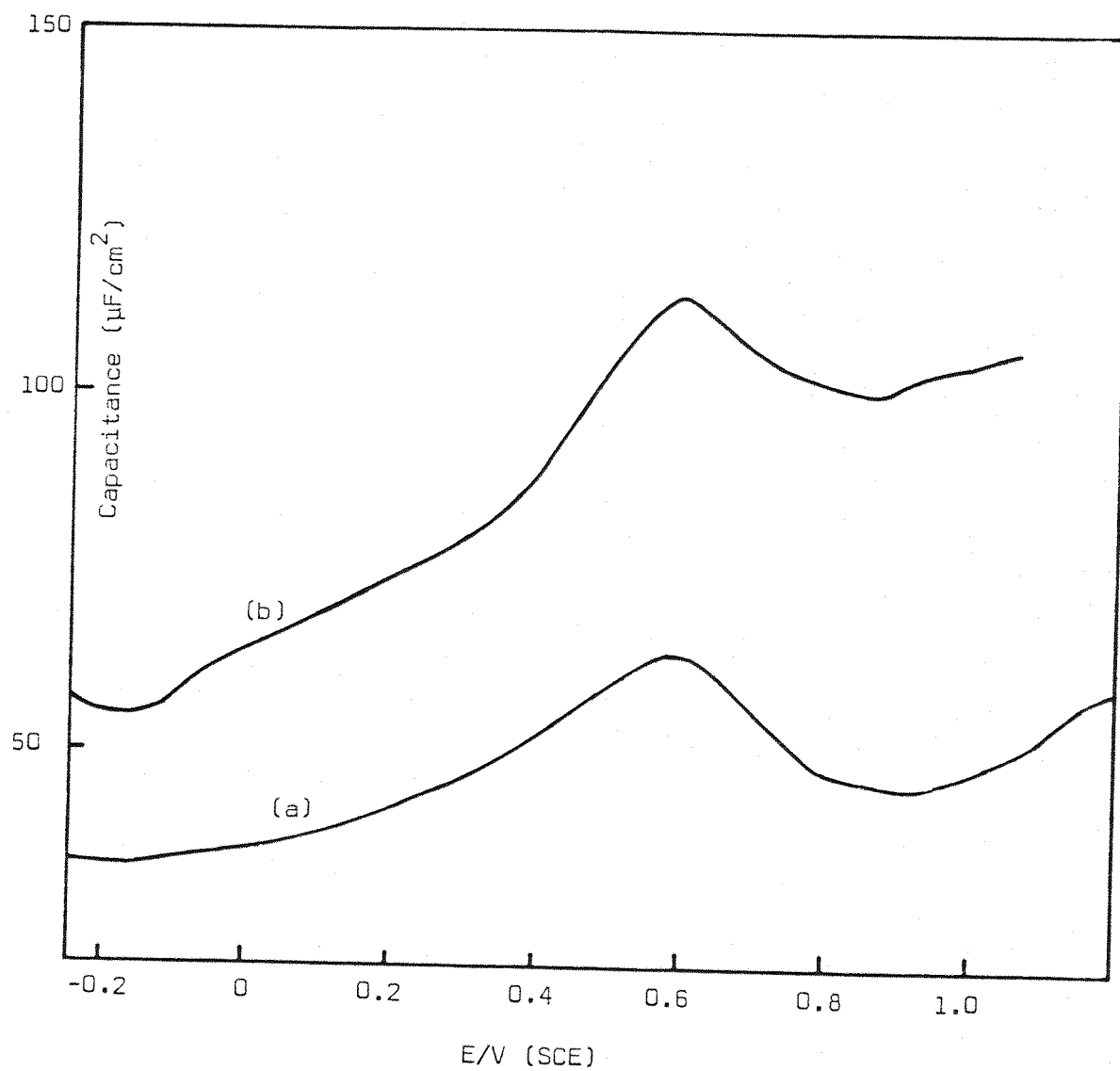


FIGURE IV. 4 — Differential capacitance curves of a gold electrode in :

(a) 1 M  $\text{H}_2\text{SO}_4$  / 0.05 M acrylonitrile solution

(b) 1 M  $\text{H}_2\text{SO}_4$  solution

A.C. modulation : 280 Hz, 5 mV peak to peak  
Slow ramp :  $10 \text{ mV s}^{-1}$



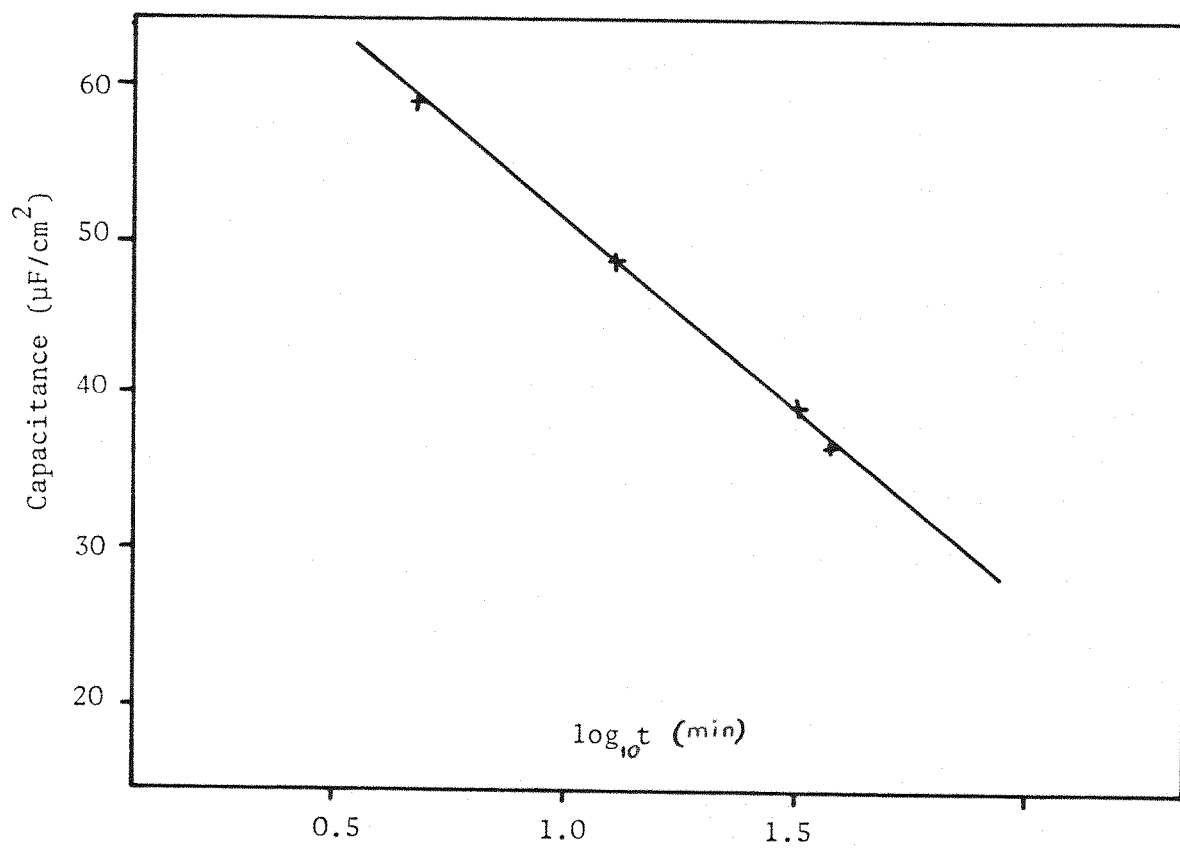


Figure IV . 5 — Capacitance decay at 0.580 V (SCE) for a gold electrode in 0.4 M acrylonitrile/1 M  $\text{H}_2\text{SO}_4$  solution.

by the appearance of two new absorption bands at 2115 and 2165  $\text{cm}^{-1}$  in the infra red spectrum; these were not observed in the EMIRS study of this system (next section). We can therefore conclude that no polymer film is formed at the surface and that a slow adsorption process occurs at the electrode.

Unfortunately, it was impossible to determine from these capacitance results two potential values which would alternately define an electrode surface free from acrylonitrile and one with an appreciable coverage of adsorbed molecules. Two such potentials would have been particularly useful for the limits of the square wave modulation for the EMIRS study. This simple condition was possible in a previous study of the adsorption of indole at a Pt electrode in  $\text{CH}_3\text{CN}$  (125).

#### 4.3 EMIRS Experiments

##### 4.3.1 Experimental

Preparation of the sulphuric acid/acrylonitrile solutions and the gold electrode are described in section 3.2. The experimental procedures used to obtain spectra by the electrochemically modulated infra red reflectance spectroscopy technique (EMIRS) are given in detail in section 3.4.

##### 4.3.2 Results and Discussion

Figure IV.6 shows the spectrum obtained over the range 1950  $\text{cm}^{-1}$  to 2450  $\text{cm}^{-1}$  for the Au/acrylonitrile system investigated by modulating the electrode potential between -0.195V and +0.750V (SCE), with a square wave at 8.5 Hz, and using the set of apparatus without processor control. An absorption band assigned to the  $\text{C}\equiv\text{N}$  stretching vibration mode of adsorbed acrylonitrile molecules can be seen at 2131  $\text{cm}^{-1}$ , which corresponds to a 100  $\text{cm}^{-1}$  shift towards lower energy compared with acrylonitrile free in solution. The large amplitude noise between 2300  $\text{cm}^{-1}$  and 2400  $\text{cm}^{-1}$  is due to the residual absorption by atmospheric  $\text{CO}_2$ .

The main band ( $\nu\text{C}\equiv\text{N}$ ) is approximately ten times weaker than those observed for adsorbed CO species from methanol (144),

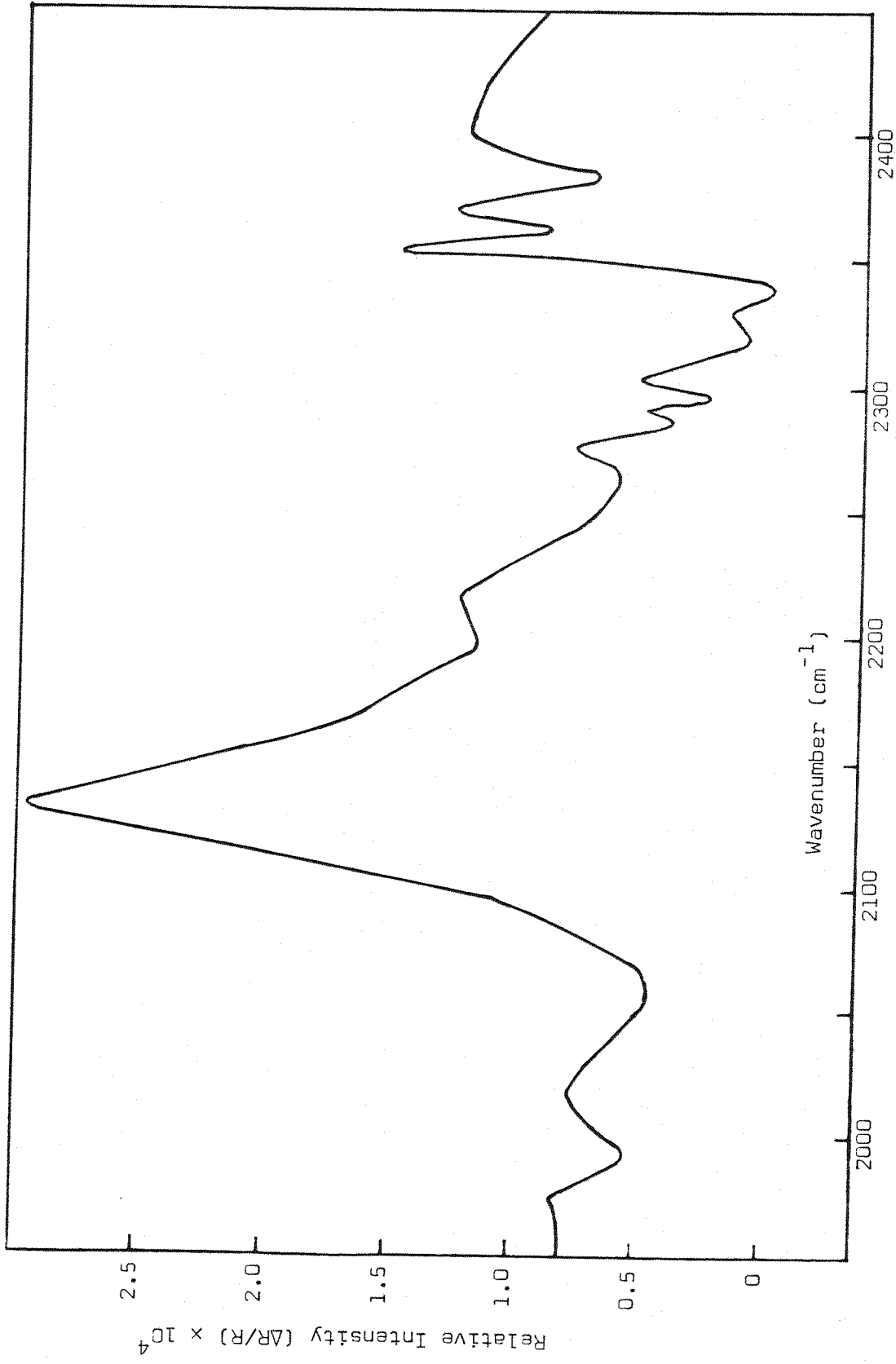


FIGURE IV.6 — EMIRS spectrum from Au electrode in 1 M  $\text{H}_2\text{SO}_4$  / 0.05 M acrylonitrile solution. Modulation from -0.195 to +0.750 V (SCE).

formic acid <sup>(145)</sup> and carbon monoxide <sup>(109)</sup> in previous EMIRS studies. The potential dependence of the band maximum and the band intensity are given respectively in Figures IV.7 and IV.8. These results are from absorption spectra for modulation from a fixed potential of -0.195V to various more positive values, Figures IV.9 to IV.13. Figure IV.7 shows a shift of the band maximum to higher wavenumber with increasing positive potential, towards a limit value (around  $2134\text{ cm}^{-1}$ ). Figure IV.8 shows clearly the increasing intensity of the band with increasing pulse amplitude, beyond +0.75V the intensity of the band decreases probably because of the onset of acrylonitrile oxidation.

Figures IV.14 and IV.15 show the spectra obtained over the ranges  $2000\text{ cm}^{-1}$  to  $2225\text{ cm}^{-1}$  and  $1325\text{ cm}^{-1}$  to  $1675\text{ cm}^{-1}$ , for the same system, by modulating the electrode potential between -0.200V and +0.750V (SCE), and using the new spectrometer equipped with a processor control. An absorption band assigned to the C=C stretching vibration mode of adsorbed acrylonitrile molecules can be seen at  $1520\text{ cm}^{-1}$  (Figure IV.14). It is interesting to note that this band is shifted by exactly the same amount as the C≡N stretching mode (Figure IV.15), i.e.  $100\text{ cm}^{-1}$  towards lower energy, compared with solution free acrylonitrile. The fine structure on the C=C band at  $1520\text{ cm}^{-1}$  is believed to be noise resulting from the much lower signal-to-noise ratio in this region of strong water absorption.

The positive sign of  $\Delta R/R$  for the two bands indicates stronger infra red absorption at the less positive potential. Since acrylonitrile is thought to be adsorbed on gold at both potentials, as seen in the previous section, this change in intensity of infra red absorption may be an example of a change in oscillator strength produced by a change in electrode potential.

The fact that both the C=C and C≡N stretching modes are strongly shifted towards lower wavenumbers from their respective values found in dilute solution spectra indicates the involvement of the entire molecule in the bonding with the surface. It must be concluded, therefore, that the bonding to the gold surface is via the delocalised  $\pi$  orbitals arising from the conjugation

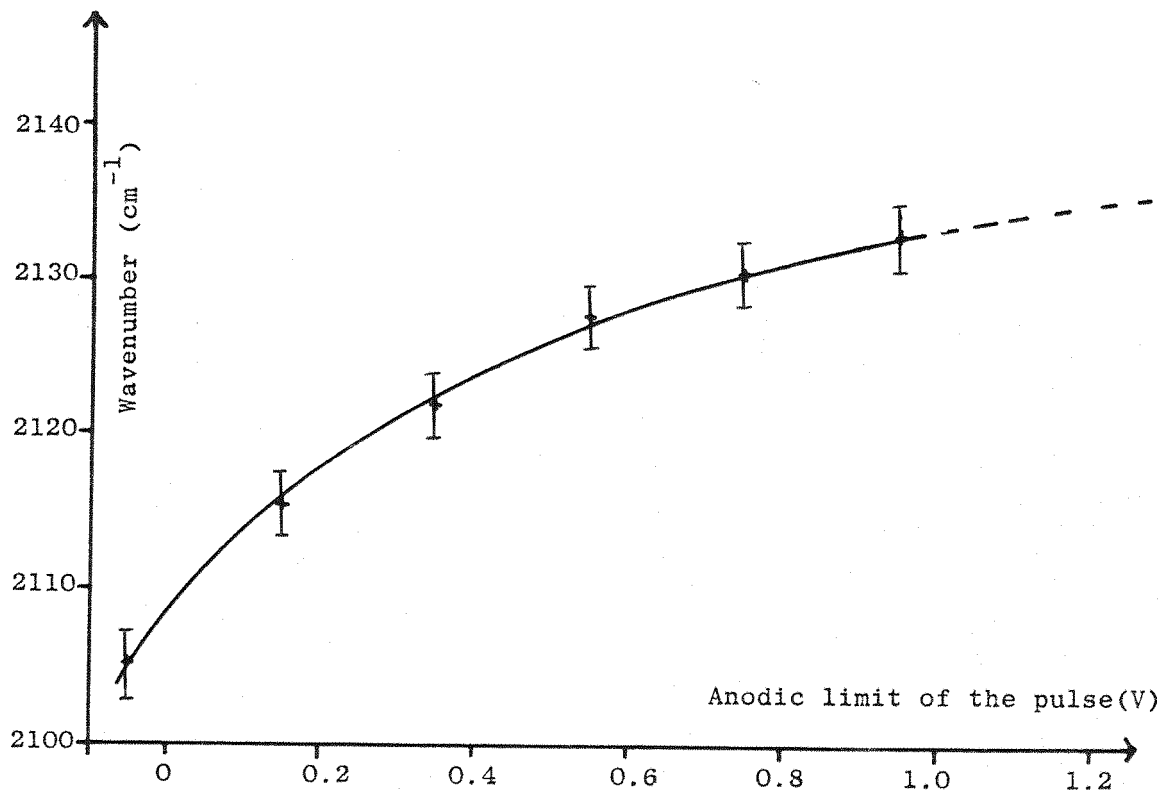


Figure IV . 7 — Potential dependence of the  $\nu_{\text{C}\equiv\text{N}}$  absorption band position for the gold/acrylonitrile system.

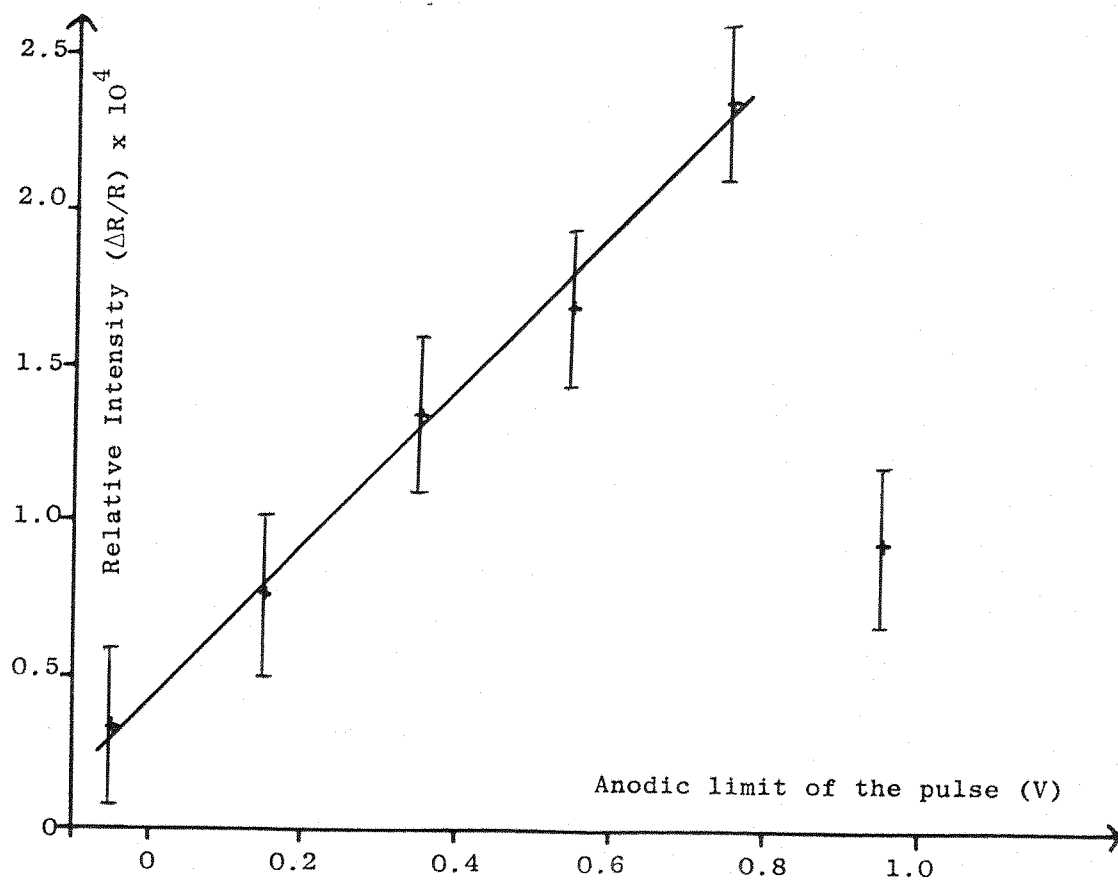


Figure IV . 8 — Potential dependence of the  $\nu_{\text{C}\equiv\text{N}}$  absorption band intensity for the gold/acrylonitrile system.

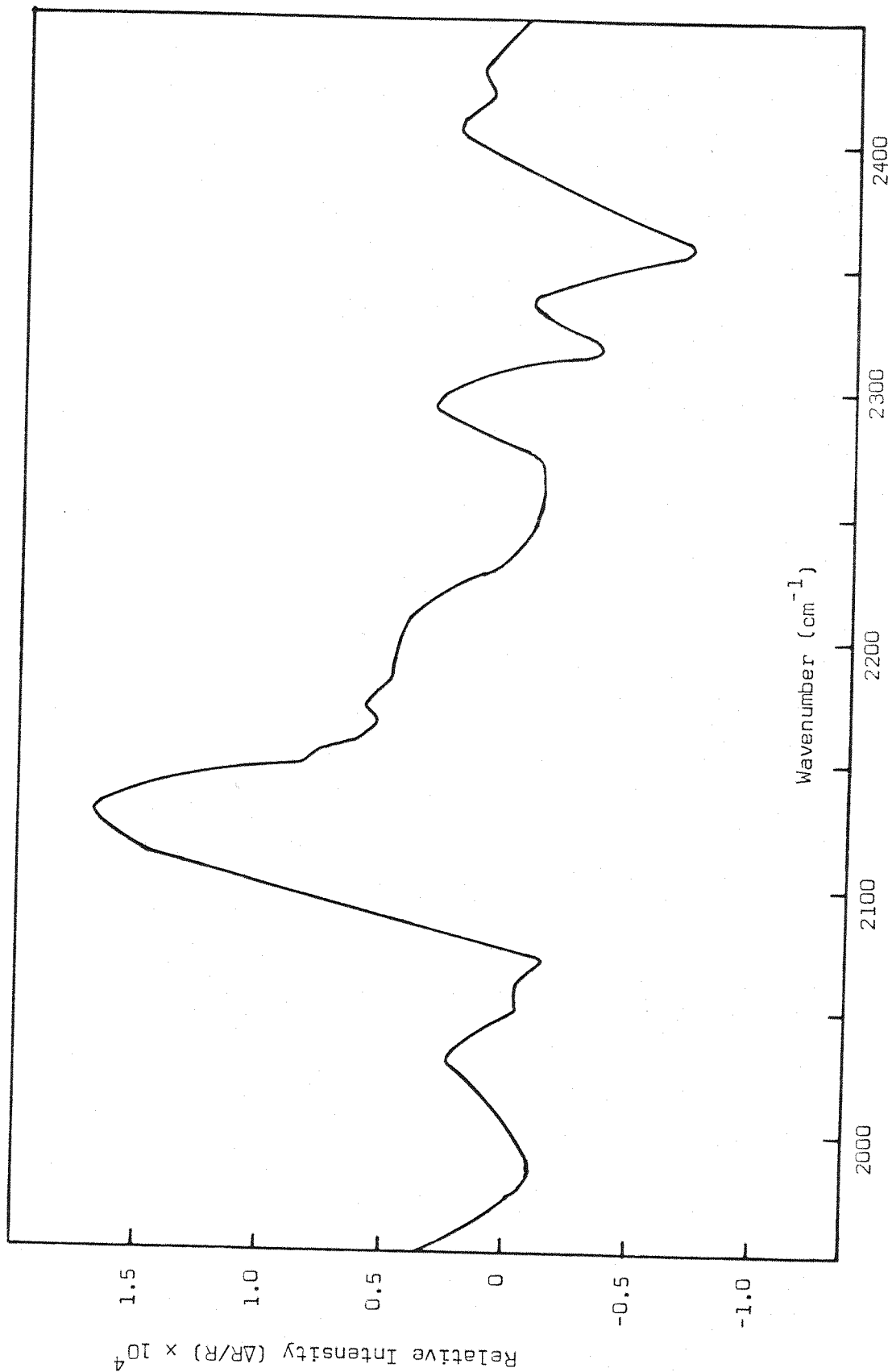


FIGURE IV.9 — EMIRS spectrum from Au electrode in 1 M  $\text{H}_2\text{SO}_4$  / 0.05 M acrylonitrile solution. Modulation from -0.195 to +0.550 V (SCE).

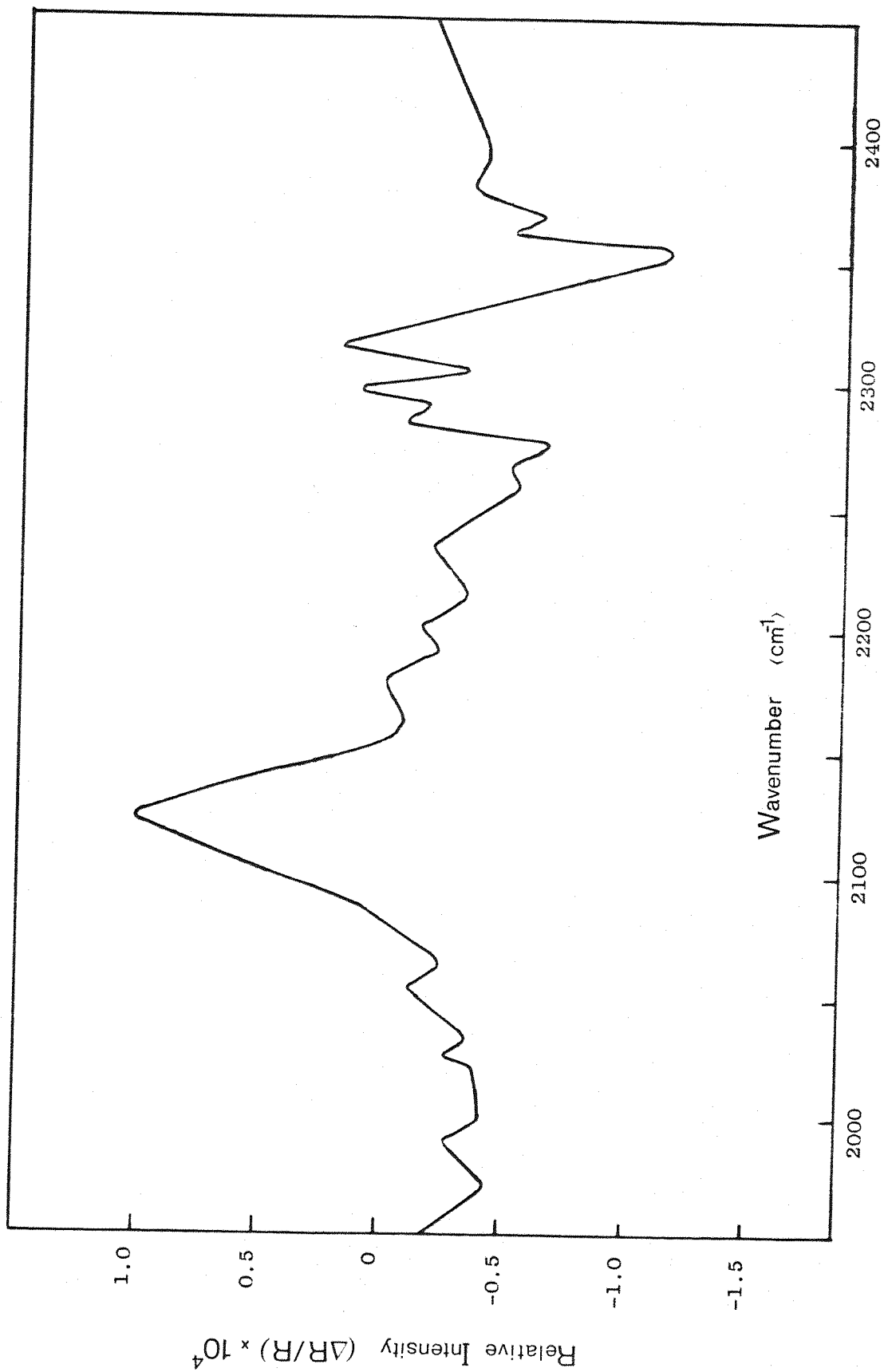


Figure IV.10 — EMIRS spectrum from Au electrode in 1 M  $\text{H}_2\text{SO}_4$  / 0.05 M acrylonitrile solution. Modulation from -0.195 to +0.350 V (SCE).

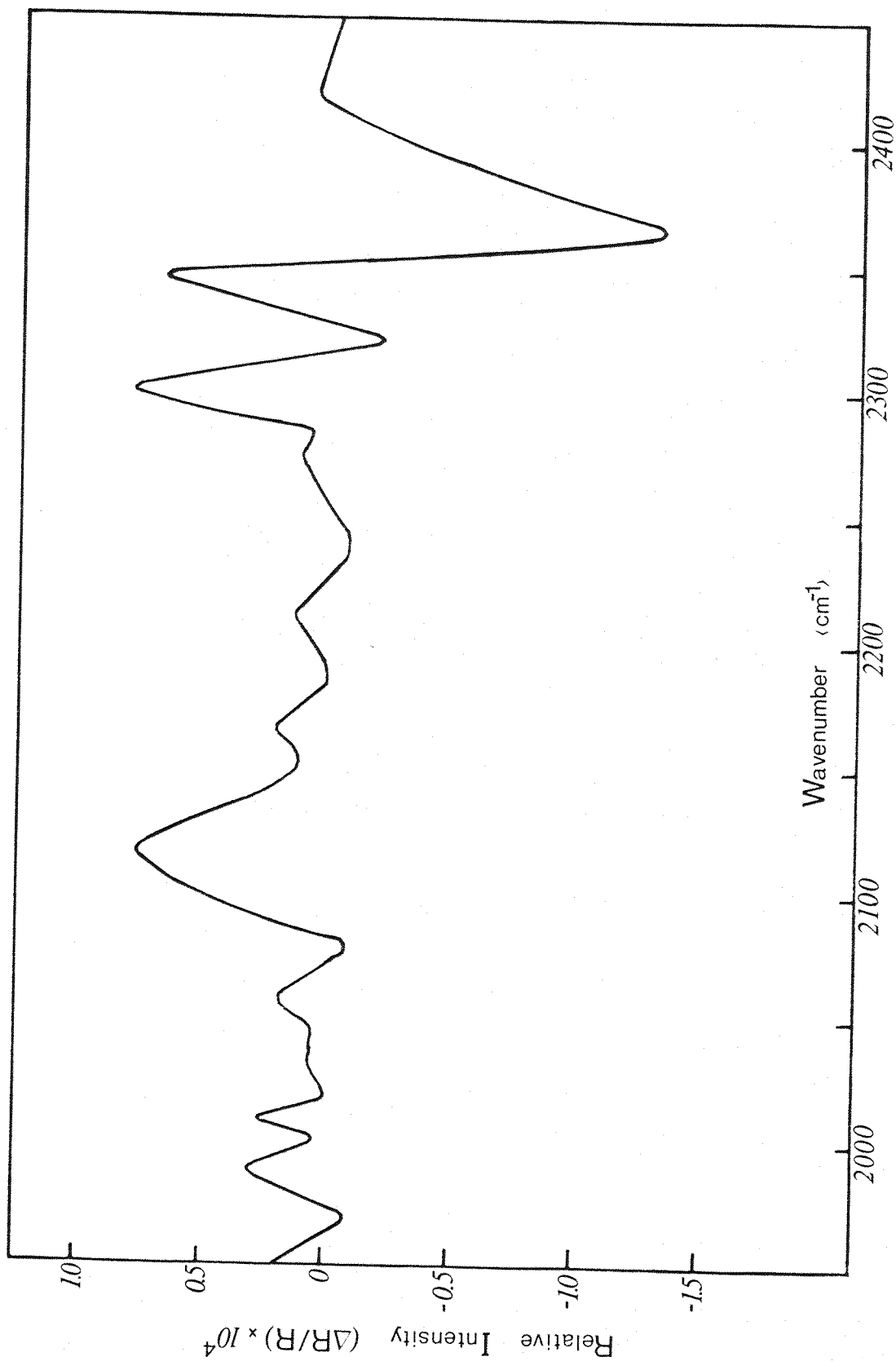


Figure IV.11 - EMIRS spectrum from Au electrode in 1 M  $\text{H}_2\text{SO}_4$  / 0.05 M acrylonitrile solution. Modulation from -0.195 to +0.150 V (SCE).



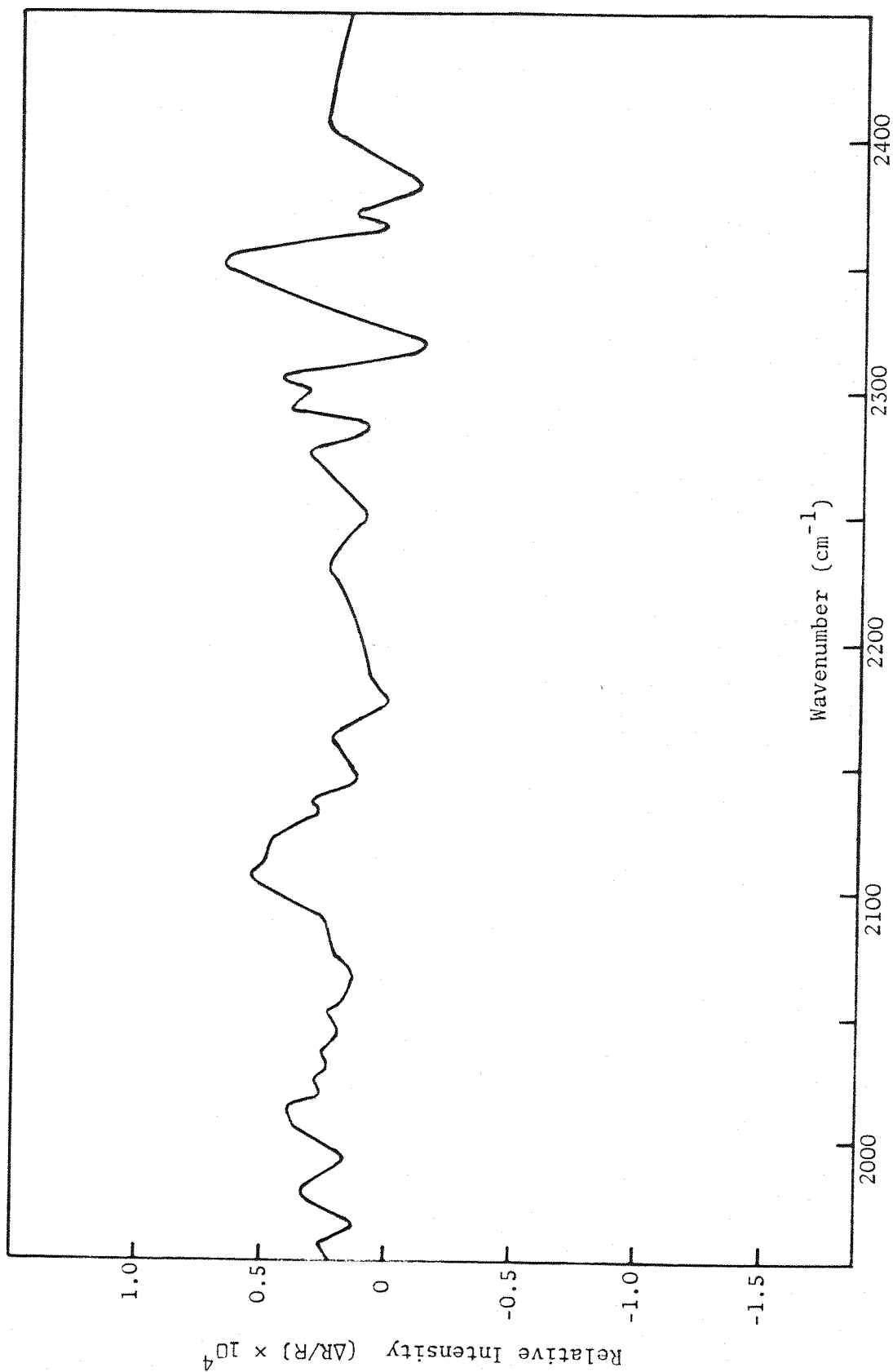


FIGURE IV.12 — EMIRS spectrum from Au electrode in 1 M H<sub>2</sub>SO<sub>4</sub>/ 0.05 M acrylonitrile solution. Modulation from -0.195 to -0.050 V (SCE).

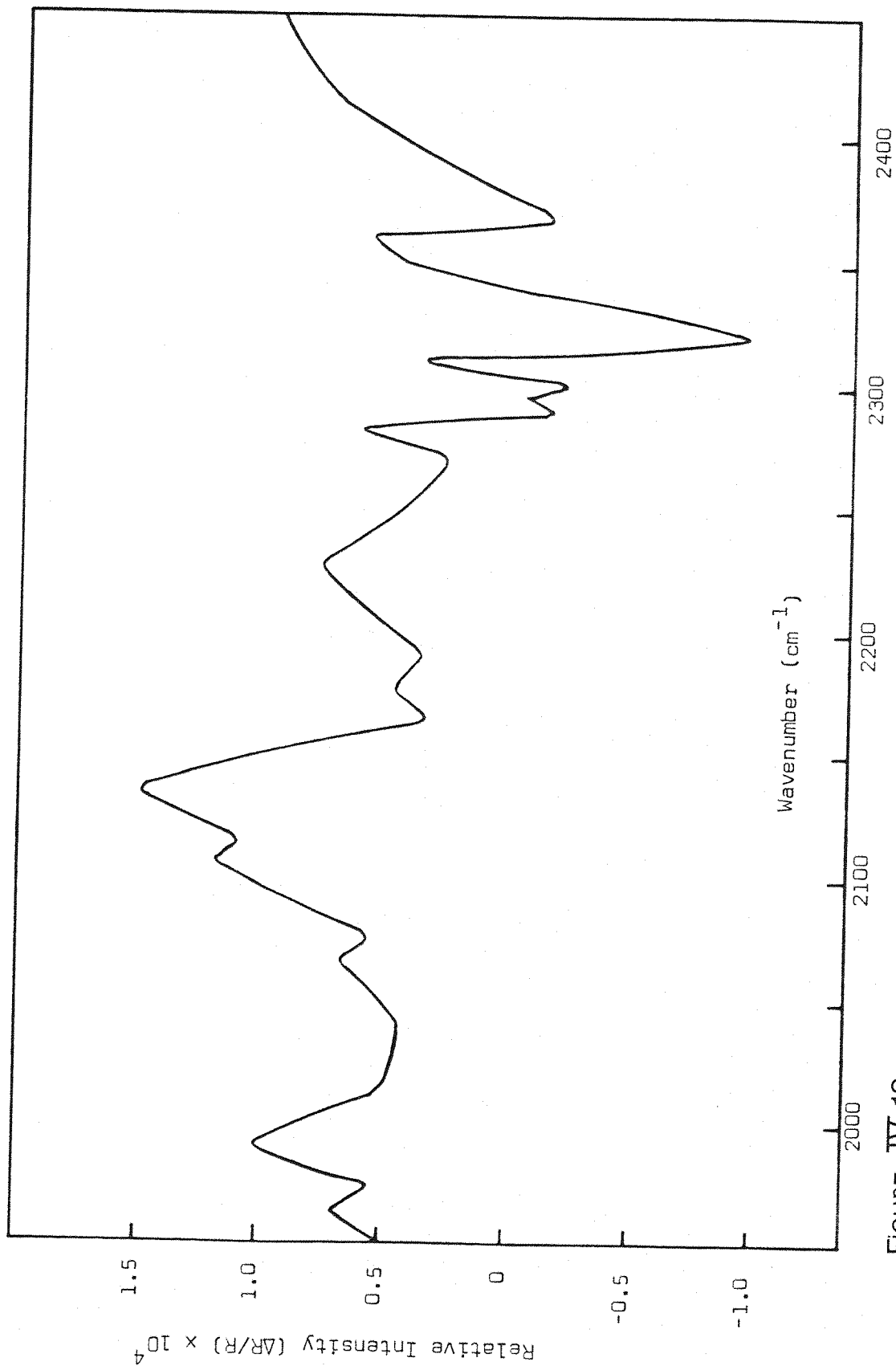


FIGURE IV.13 — EMIRS spectrum from Au electrode in 1 M  $\text{H}_2\text{SO}_4$  / 0.05 M acrylonitrile solution. Modulation from -0.195 to +0.950 V (SCE).

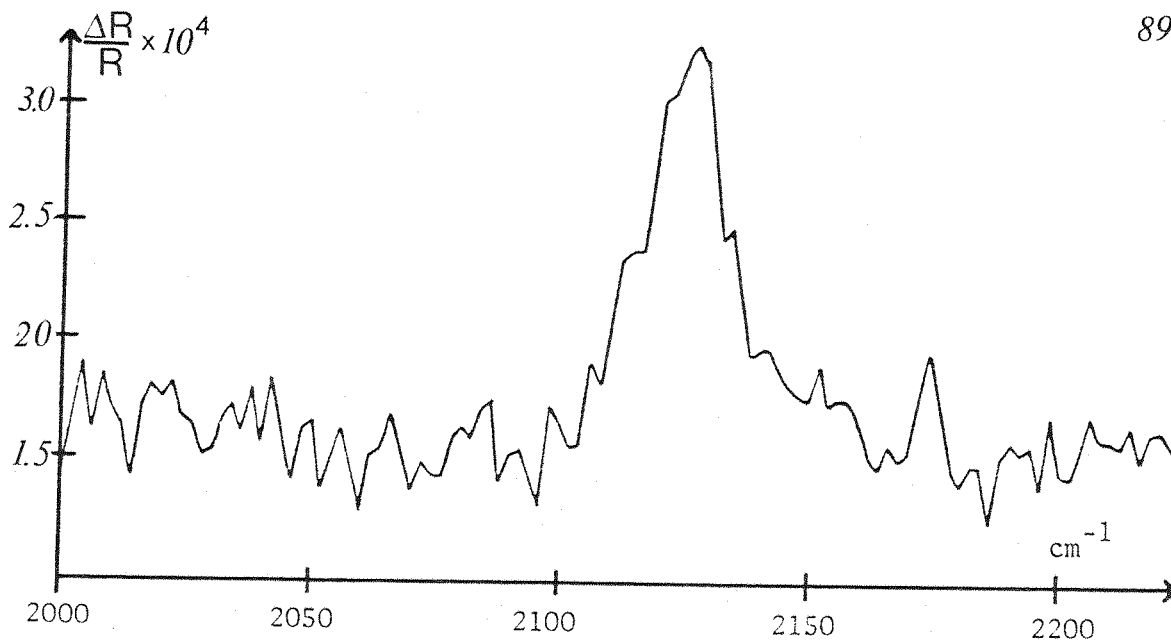


Figure IV . 14 — EMIRS spectrum from Au electrode in 1 M  $\text{H}_2\text{SO}_4$  / 0.05 M acrylonitrile solution. Modulation from -0.195 to +0.750 V (SCE).

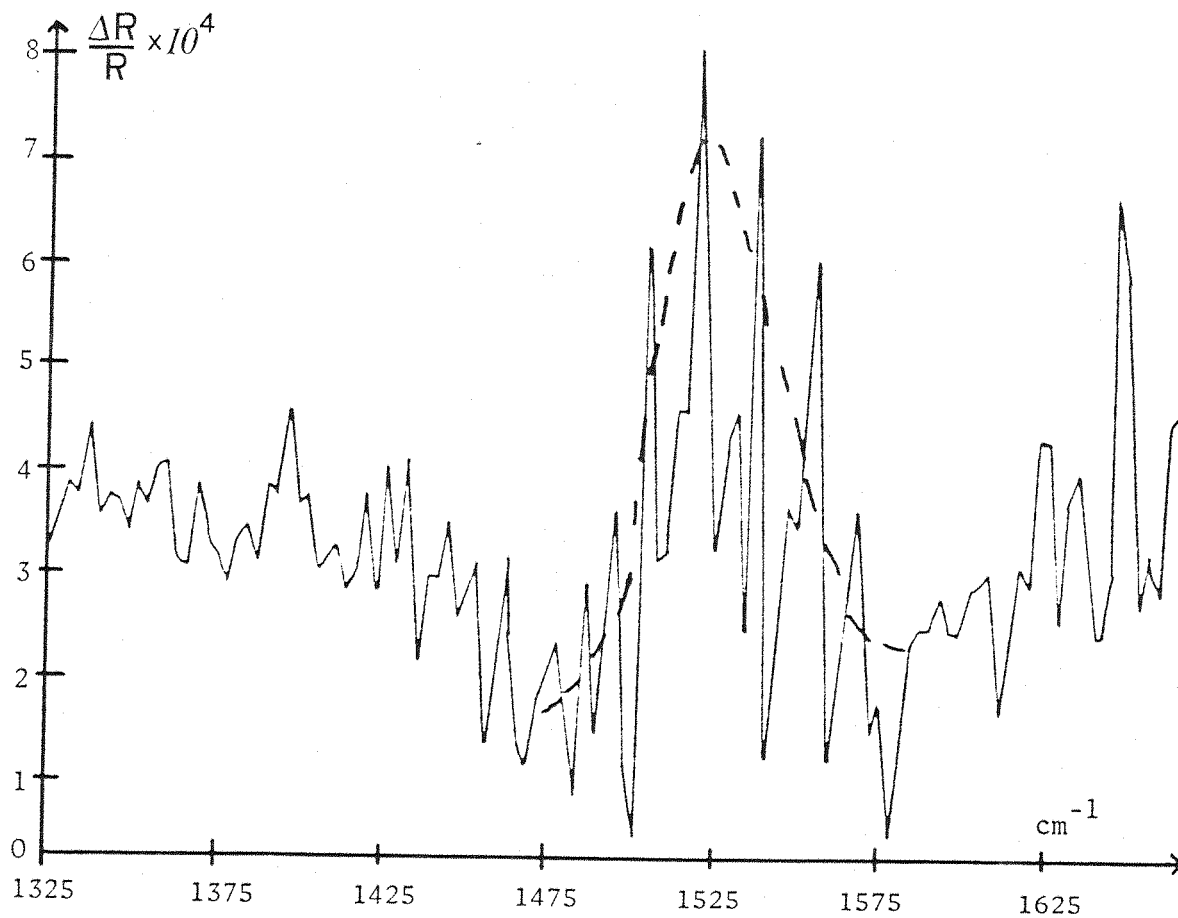


Figure IV . 15 — EMIRS spectrum from Au electrode in 1 M  $\text{H}_2\text{SO}_4$  / 0.05 M acrylonitrile solution. Modulation from -0.195 to +0.750 V (SCE).

effect occurring between the double bond and the C≡N group in acrylonitrile molecules. Since the acrylonitrile molecule is planar, the only possibility is that the molecule is lying flat on the surface during the adsorption. This is the type of interaction usually observed for aromatic and strongly conjugated planar molecules on electrode surfaces<sup>(155,175)</sup>.

The absence of absorption bands at the positions corresponding to the vibrational modes of acrylonitrile molecule free in solution ( $2231\text{ cm}^{-1}$  and  $1621\text{ cm}^{-1}$ ) is particularly interesting. The usual spectrum corresponding to an adsorption/desorption process would have absorption bands from the non-adsorbed species, present in the thin solution layer between the window and electrode, together with bands of opposite sign from the adsorbed species, these being shifted due to the perturbation of the molecular bonding caused by adsorption. The absence of the former bands in the present case implies that the acrylonitrile molecule is adsorbed at approximately constant coverage over the whole range of potential studied.

If the adsorbed molecule is considered to be parallel to the electrode surface, the vibrational stretching modes will produce only dipole moment changes in the plane of the molecule, i.e. parallel to the electrode surface. Therefore all the vibrational modes of the molecules will have a zero surface normal dipole derivative,  $\left(\frac{\partial\mu}{\partial Q}\right)_\perp$ , and theoretically they cannot absorb energy from an incident or reflected beam according to the surface selection rule<sup>(140)</sup>. The fact that absorption bands have been observed in spite of the parallel position of the acrylonitrile molecules, is an apparent violation of the surface selection rule and has to be explained by a novel mechanism. Two alternative explanations can be postulated.

The first one is related to the presence of a very large electric field at the electrode surface. This field which is perpendicular to the surface of the electrode can easily interact with the parallel vibrational modes of the molecules via a change in polarizability of the molecule during these vibrations. This interaction will induce a resulting dipole moment with a

component oscillating perpendicularly to the surface. This phenomenon is similar in some respects to that observed in the study of adsorbates which participate in a charge-transfer interaction with the metal surface<sup>(156)</sup>.

The other explanation involves the bonding of the molecules to the surface. The bonding of the acrylonitrile molecules to the metal surface produces a complex with a lower symmetry than that of the free molecules. In general the complex will not have the same normal modes of vibration as the free acrylonitrile molecule, i.e. the normal motions of the atoms will be different for acrylonitrile in the adsorbed state. The C=C and C≡N vibrations will involve some motions of these atoms perpendicular to the surface and thus the dipole changes due to these stretching vibrational modes of the bonded molecule will have a non-zero, although probably rather small, perpendicular component and therefore will be observable in EMIRS experiments.

As these two explanations each provide mechanisms for the formation of a dipole derivative component perpendicular to the electrode surface, they both fit the EMIRS results obtained. It is possible, tentatively, to decide which of these explanations is likely to be correct.

The observed spectra are not consistent with the second explanation for an adsorbed layer which keeps approximately constant coverage over the range of the modulation of potential. Apart from second order effects, e.g. due to changes in bonding with potential, this layer could be detected in these experiments only if there was a shift in the band position with potential (as in fact observed) but this would necessarily mean that the observed bands must be bipolar and not single sided.

The first explanation would lead to the observation of single sided bands in experiments in which the modulation of electrode potential was between a state of lower electrical field strength and a state of much higher field strength. This condition could easily apply in the present case although the sign of the bands observed (positive values of  $\Delta R/R$ ) requires that the higher electrical field strength is imposed upon the acrylonitrile

molecule at the more negative potential, i.e. the positive sign of  $\Delta R/R$  indicating a stronger infra red absorption at the more negative potential of the modulation. This explanation could also account for the observation of a nearly two times more intense band for the C=C stretching vibrational mode than for the C≡N stretching mode (Figures IV.14 and IV.15), the former band being normally two times smaller than the latter band in pure acrylonitrile spectra<sup>(157)</sup>. The fact that the C=C band is bigger in EMIRS experiments than the C≡N band would be explained by a difference of polarizability of the two bonds.

In these experiments a shift of the  $\nu_{C\equiv N}$  absorption band to higher energy as the electrode potential is made more positive, is observed, Figure IV.7. This effect must be due to changes in the extent of electron donation from the metal to the  $\pi^*$  antibonding orbital of the C=C and C≡N conjugated bonds as the effective electronegativity of the metal is varied, the metal orbitals and the empty antibonding  $\pi^*$  orbitals of the acrylonitrile molecules being overlapping. Therefore, when the surface is becoming more cathodic, more electrons from the metal will fill the  $\pi^*$  orbital, i.e. the bonding between the metal and the molecule will become stronger while the  $\pi$  conjugated orbital of the molecule will become weaker and therefore a shift towards lower energy for more negative potentials will occur.

One factor in the explanation of the results needs further comment. The spectroscopic observations require that the measurements were made under conditions such that the extent of adsorption of acrylonitrile was approximately constant at the two potentials of the square wave modulation. This is unlikely to be the case if the adsorption was at equilibrium. It is very likely, however, that the changes in adsorption are sufficiently slow in this system to allow little response at a frequency of 8.5 Hz. On the other hand, the sweep through the potential range during the capacitance measurements was at a slow rate ( $10 \text{ mV s}^{-1}$ ), and the coverage would always have been closer to the equilibrium value for these measurements.

#### 4.4. Conclusion

This study has shown that the data obtained from the EMIRS

technique enables the orientation of adsorbed infra red active molecules at the electrode to be determined. This type of information is of great value for the understanding of the processes occurring in studies of organic electrochemistry. It is clear that the study of the adsorption behaviour of many other organic molecules in aqueous or non-aqueous solutions will therefore be possible.

## CHAPTER FIVE

Cyanide Adsorption on Silver and Gold Electrodes5.1 Introduction - Earlier work in Raman (83,84,166)

The Raman spectra of cyanide chemisorbed on an Ag surface have been investigated extensively at the metal-electrolyte interphase<sup>(161-166)</sup> as well as at the metal-air interphase<sup>(158-160,170)</sup>.

The behaviour of  $\text{CN}^-$  ions at a silver electrode surface is of considerable interest in electrochemistry: firstly, because silver is known to be corroded in cyanide solutions and, secondly, this corrosion reaction is often utilised in order to produce planar silver surfaces<sup>(82)</sup>. It is believed that such surfaces are obtained as a result of the preferential dissolution of silver atoms located at surface irregularities, via the formation of labile  $[\text{Ag}(\text{CN})_n]^{(n-1)-}$  complexes. As with many corrosion reactions, the mechanism by which such species are formed is not well understood.

Interest in the behaviour of such systems has developed since the observation that under certain conditions, cyanide molecules adsorbed on silver electrode surfaces exhibit surface-enhanced Raman scattering (SERS), cf. section 1.2.4.3, comparable to that from pyridine adsorbates at Ag electrode-electrolyte interphases<sup>(177)</sup>.

The first SERS spectra of cyanide at a silver electrode were reported by Otto<sup>(159)</sup> and Furtak<sup>(161)</sup>. In these initial experiments it was found that as in the pyridine/silver systems, if a silver electrode was subjected to a short oxidation/reduction cycle in aqueous cyanide solution the resulting surface exhibited intense Raman spectra which were attributed to adsorbed  $\text{CN}^-$  ions. The Raman scattering cross-section of these adsorbed species are of the order of  $10^5 - 10^6$  times that of  $\text{CN}^-$  in solution<sup>(162)</sup>, as deduced by the intensities of the SERS bands.

Although the mechanism by which SERS is produced is still uncertain, most of the researchers active in the field agree that



some kind of roughness of the electrode surface is important<sup>(167)</sup>. In all previous work on Raman scattering from silver electrodes, the enhanced Raman signal was only found when the silver surface was either reformed by one or several anodic oxidation-reduction cycles as an electrochemical activation<sup>(162)</sup> or pretreated by a mechanical polishing (600  $\mu\text{m}$  abrasive) followed by a water rinse and a peroxide etch ( $\text{H}_2\text{O}_2:\text{NH}_3\text{OH}$ , 3:5)<sup>(168)</sup>.

The SERS spectra observed by both Otto et al<sup>(162)</sup> and Furtak and coworkers<sup>(161)</sup> from a polycrystalline silver electrode at -1.0V and -0.8V (vs SCE) respectively, in 0.1M  $\text{Na}_2\text{SO}_4/0.01\text{M}$  KCN aqueous electrolyte, after switching for 5s to +0.5V, are almost identical. The spectral bands observed are listed in Table V.1, together with their proposed assignments. The two strong bands at  $2114\text{ cm}^{-1}$  and  $226\text{ cm}^{-1}$  were assigned by Furtak to the two stretching modes of AgCN single units of monolayer coverage. In contrast, by comparison with the frequencies of the CN stretching modes in the complex ions in aqueous solution, presented in Table V.2, Otto has concluded that the surface adsorbates are probably  $\text{Ag}(\text{CN})_3^{2-}$  units, each pyramidal complex being constructed around a silver adatom<sup>(162)</sup>.

Dornhaus and coworkers<sup>(163,165)</sup> used an optical multi-channel analyzer (OMA) system to relate the SERS of cyanide on Ag with the voltammogram shown in Figure V.3. During the second oxidation cycle a band appeared at  $2110\text{ cm}^{-1}$  and -0.9 V (SCE) which shifted to  $2140\text{ cm}^{-1}$  by -0.06V. This shift, by comparison with the data presented in Table V.2, was interpreted as a change in coordination from 3 or 4 to 2 cyano groups respectively for the  $\text{Ag}(\text{CN})_n^{(n-1)-}$  complexes detected.

One cannot simply compare frequencies of the SERS bands with those of the solution species because of the potential dependence of the SERS bands<sup>(164,172,178)</sup>, and also because of the large difference in the metal-C stretching frequencies between typical metal-cyanide complexes and SERS data<sup>(165)</sup>.

In a very recent study by Fleischmann et al<sup>(164)</sup> additional spectroscopic data concerning  $^{13}\text{CN}$  and also coadsorbed water have been reported :

Work of Otto <sup>(162)</sup> band frequency $\text{cm}^{-1}$	Work of Furtak <sup>(161)</sup> band frequency $\text{cm}^{-1}$	Assignment
2113	2114	$\nu(\text{C}\equiv\text{N})_{\text{sym.}}$
312	315	
230	226	$\nu(\text{Ag}-\text{C})_{\text{sym.}}$
	150	
(a)	(b)	

Table V.1 Raman spectral bands from a polycrystalline silver electrode at: (a) -1.0V, (b) -0.8V in 0.1M  $\text{Na}_2\text{SO}_4$ , 0.01M KCN aqueous electrolyte after switching for 5s to +0.5V.

	Infra red	Raman
(CN) <sup>-</sup> aqueous	2080	
AgCN solid	2164	2165
Ag(CN) <sub>4</sub> <sup>3-</sup> aqueous	2092	2097 (ν <sub>sym.</sub> , ν <sub>anti</sub> )
Ag(CN) <sub>3</sub> <sup>2-</sup> aqueous	2105	2108 (ν <sub>sym.</sub> , ν <sub>anti</sub> )
Ag(CN) <sub>2</sub> <sup>-</sup> aqueous	2135 (ν <sub>anti</sub> )	2141 (ν <sub>sym.</sub> )
AuCN solid	2239	
Au(CN) <sub>4</sub> <sup>-</sup>	2189	
Au(CN) <sub>2</sub> <sup>-</sup>	2147	

Table V.2 Frequencies and assignment of CN stretching vibrations, with ν<sub>sym.</sub> = totally symmetric mode and ν<sub>anti</sub> = non-totally symmetric mode. The data for the silver complexes are from reference [162] and references therein, and the data for the gold complexes are from reference [179] and references therein.

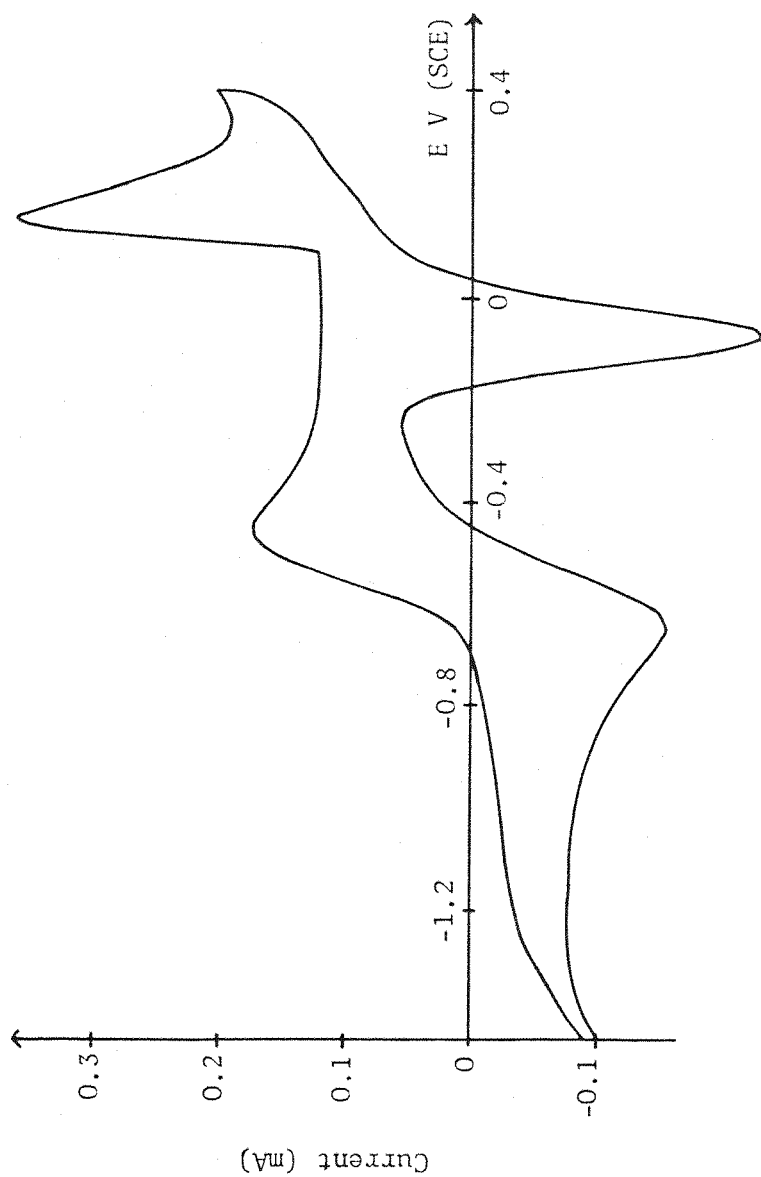


Figure V . 3 — Cyclic voltammogram for Ag electrode in 0.01 M KCN / 0.1 M Na<sub>2</sub>SO<sub>4</sub> solution. Sweep rate 50 mV/s.

- (i) An intense SERS spectrum of the cyanide species adsorbed at the surface of the silver electrode, from the 0.5 M KCN aqueous solution used as electrolyte, was obtained. Raman bands at -1.0 V were detected at 2108, 306, 226,  $\approx 154$  and  $\approx 104 \text{ cm}^{-1}$ , similar to those reported by Furtak<sup>(161)</sup>, a band was seen at  $8 \text{ cm}^{-1}$ , and an additional band was detected at  $3521 \text{ cm}^{-1}$  (cf. Table V.4). The band detected near  $8 \text{ cm}^{-1}$  is believed to be analogous to that observed by Weitz and Genack<sup>(180)</sup> which they assign to a libration of adsorbed  $\text{CN}^-$ . The strong band detected at  $3521 \text{ cm}^{-1}$  was assigned to coadsorbed water (OH stretching mode) as confirmed by the use of  $\text{D}_2\text{O}$  as solvent.
- (ii) Apart from the weak shoulders  $\approx 154$  and  $\approx 104 \text{ cm}^{-1}$ , which could not accurately be measured, all bands were observed to shift appreciably over the potential range of investigation (from -1.0 to -1.5V) as seen in Table V.4. Both the  $2108 \text{ cm}^{-1}$  and  $3521 \text{ cm}^{-1}$  bands shift in a roughly linear fashion over this potential range (cf. Figure V.5), so the cyanide stretching frequency would appear to reflect the strength of the metal-cyanide interaction rather than the formation of different complexes.
- (iii) The SERS spectrum obtained using  $0.5\text{M K}^{13}\text{CN}$  as electrolyte has shown that, apart from those bands known to arise from water, all the  $^{12}\text{CN}$  bands have shifted to lower frequency, confirming that they arise from cyanide or cyanide-related species. The use of  $^{13}\text{CN}$  enabled Fleischmann *et al* to establish the existence of a complex involving more than one cyanide group by using isotopic mixtures.
- (iv) From a general comparison of the cyanide surface spectrum with the Raman spectra of the di-, tri- and tetra-cyanoargentate complexes in solution, cf. Table V.2, they have shown that the SERS spectrum of cyanide resembles the Raman spectrum of  $[\text{Ag}(\text{CN})_2]^-$  in terms of relative peak heights and relative peak positions, but not frequencies. They assigned the surface complex to di-cyanoargentate (I) entity having  $\text{C}_{2v}$  symmetry; with all bands shifted to lower frequency under the influence of the applied potential.

Potential/V vs SCE	$\nu_s(\text{OH})$ ( $\Delta\bar{\nu} / \text{cm}^{-1}$ )	SERS of $^{12}\text{CN}$ ( $\Delta\bar{\nu}/\text{cm}^{-1}$ )
-1.0	3521	2108    2.063.5    306    226
-1.1	3503	2105    2061    300    224
-1.2	3488	2102.5    2058.5    294    221
-1.3	3459	2099.5    2055.5    288    220
-1.4	3449	2097    2052    286    218
-1.5	3431	2093    2049    281    215
Assignment	$\nu_s(\text{OH})$	$\nu_s(\text{CN})$ $\nu_s(\text{CN})$ $\nu_s(\text{AgC})$ $\delta_s(\text{AgC})$

Table V.4: Potential dependence of the major bands observed by Fleischmann et al (164) in the SERS spectra of cyanide species adsorbed on silver electrodes from 0.5M aqueous cyanide.

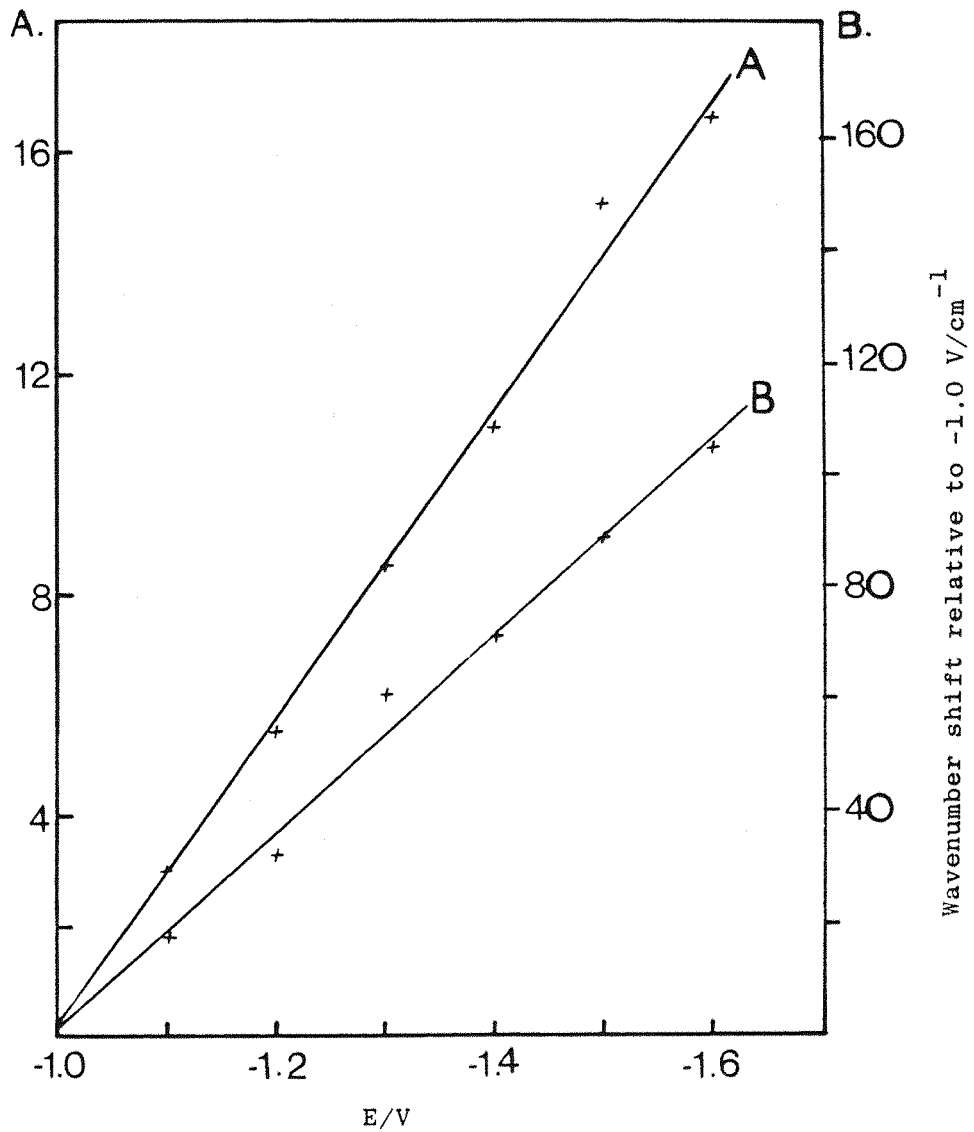


Figure V.5 - Frequency shifts of observed SERS bands with potential

A - (CN) stretching mode;

B - OH symmetric stretching mode.

Taken from reference (164).

- (v) An interesting new finding in this study has been the spectrum of what appears to be the reduced form of the surface complex at very negative potentials. Three new bands appeared at -1.2V and increase in intensity up to -1.5V. At -1.5V these bands are located at 1995,  $\sim$  400 and 352  $\text{cm}^{-1}$ . The positions of these bands are consistent with the reduction of formally  $\text{Ag}^{\text{I}}(\text{CN}^-)_x \longrightarrow \text{Ag}^{\text{0}}(\text{CN}^-)_x$ . These zero valent silver reduced species are probably  $[\text{Ag}(\text{CN})_2]^{2-}$  and coexist with the formally  $\text{Ag}^{\text{I}}$  species at the surface.

In the following section, the results of an examination of this Ag/cyanide system in infra red using electrochemically modulated infra red spectroscopy (EMIRS) are presented and discussed in the light of the previous Raman work on this system. An investigation of the Au/cyanide system is also reported. This latter system was of special interest in respect of the particular behaviour shown by gold in the few Raman investigations performed with this metal as substrate. Up to now the surface enhanced Raman effect has been observed on gold electrodes only from adsorbed pyridine molecules and under different conditions than those which produce the giant effect on silver. Pettinger et al <sup>(173,176)</sup> have reported SERS from pyridine adsorbed on a slightly rough gold electrode only when the red line (647 nm) of the krypton laser was used, i.e. they did not observe any SERS with an excitation at shorter wavelengths. However, enhanced Raman scattering from adsorbed pyridine molecules has been observed with 514.5 nm incident radiation by Furtak et al <sup>(168,174)</sup> onto Au substrates prepared by the controlled deposition of submonolayer quantities of Ag. They conclude from this result that a particular chemical bond between the molecule and the substrate is the most important prerequisite to the occurrence of surface enhanced Raman scattering.

## 5.2 EMIRS Experiments

### 5.2.1 Experimental

Knowing that supporting electrolyte anions also give rise to structures on a silver electrode surface <sup>(166)</sup>, 0.5M KCN alone



was used as electrolyte throughout this work, rather than 0.1M  $\text{Na}_2\text{SO}_4$ /0.01M KCN which has been used by most workers. The solutions were prepared as described in section 3.2.

The silver and gold electrodes were polished to a mirror finish as described in section 3.2 and the experimental procedures are given in detail in section 3.4.

## 5.2.2 Results and Discussion

### 5.2.2.1 The silver/cyanide system

Figure V.6 shows the EMIRS spectrum obtained for the silver/cyanide system (Ag/ 0.5M KCN aqueous) over the range 1900 to 2200  $\text{cm}^{-1}$  by modulating the electrode potential between -1.4V and -1.0V (SCE) with a square wave at 8.5 Hz. A strong bipolar absorption band centred at 2101  $\text{cm}^{-1}$ , which is assigned to the CEN stretching vibration mode of adsorbed cyanide species, can be seen.

The absorption spectra obtained for modulation from a fixed potential of -1.4V to various more positive values are given in Figures V.6 to V.9. These data showed the absorption band to shift in a roughly linear fashion to higher wavenumbers, whilst retaining almost constant intensity and shape, as the electrode potential is made more positive.

The frequency shifts of the band with potential are plotted in Figure V.10. As confirmed recently<sup>(133)</sup>, bipolar bands observed in EMIRS experiments would arise from the shift with potential of a simple single-sided absorption band, due to the effects of electrode potential on the bonding of the adsorbed species. The shift of the crossing point of a bipolar band is therefore approximately half the shift which would be observed by a direct measurement of the infra red band at the two potentials of the modulation. In our case the shift observed for the crossing point of the bipolar band is about 16  $\text{cm}^{-1}$  per volt (cf. Figure V.10) which is in a reasonable agreement with the shift of 28  $\text{cm}^{-1}$  per volt reported by Fleischmann et al<sup>(164)</sup> (cf. Figure V.5) and Yeager et al<sup>(177)</sup> in similar Raman studies.

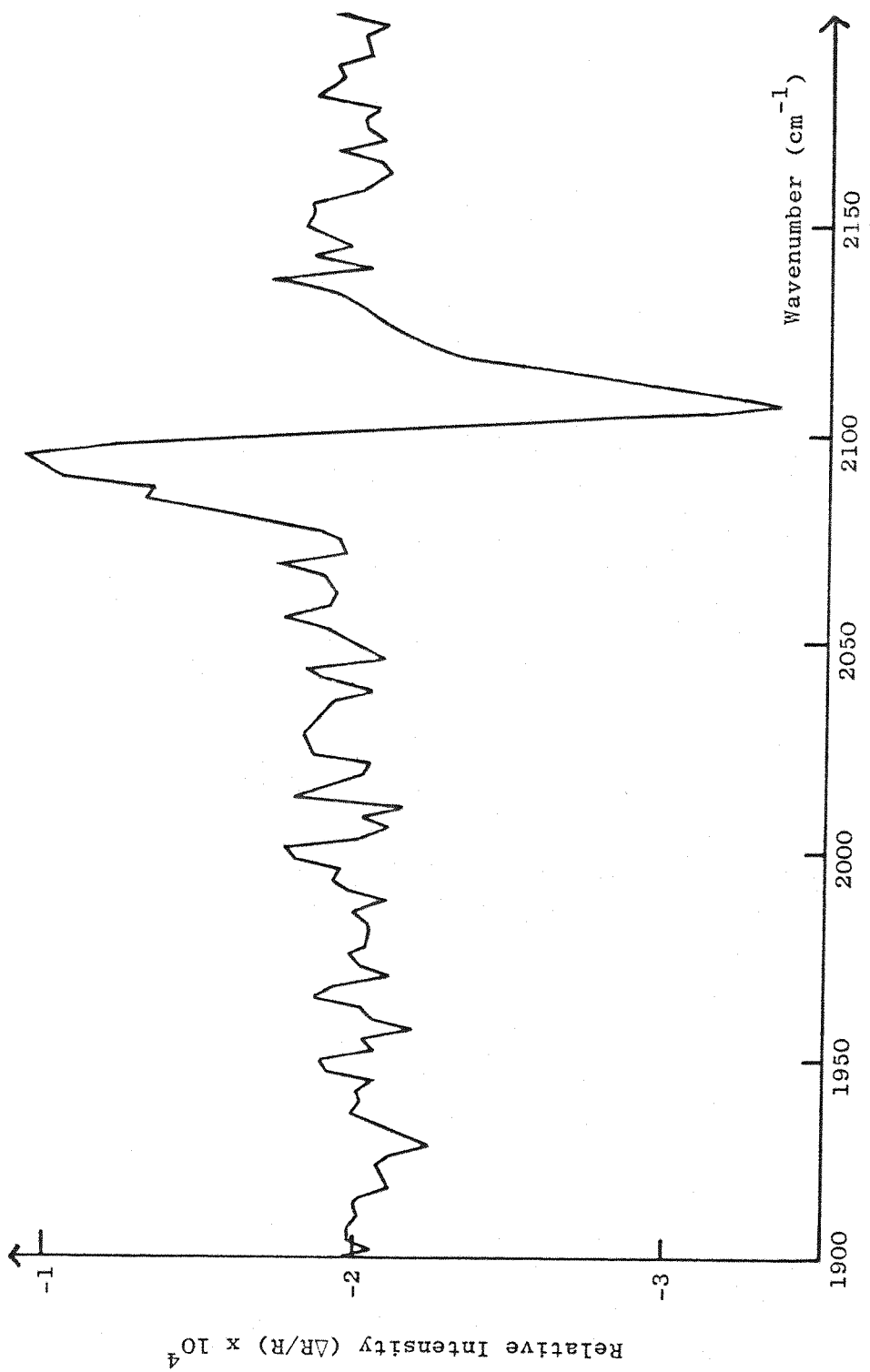
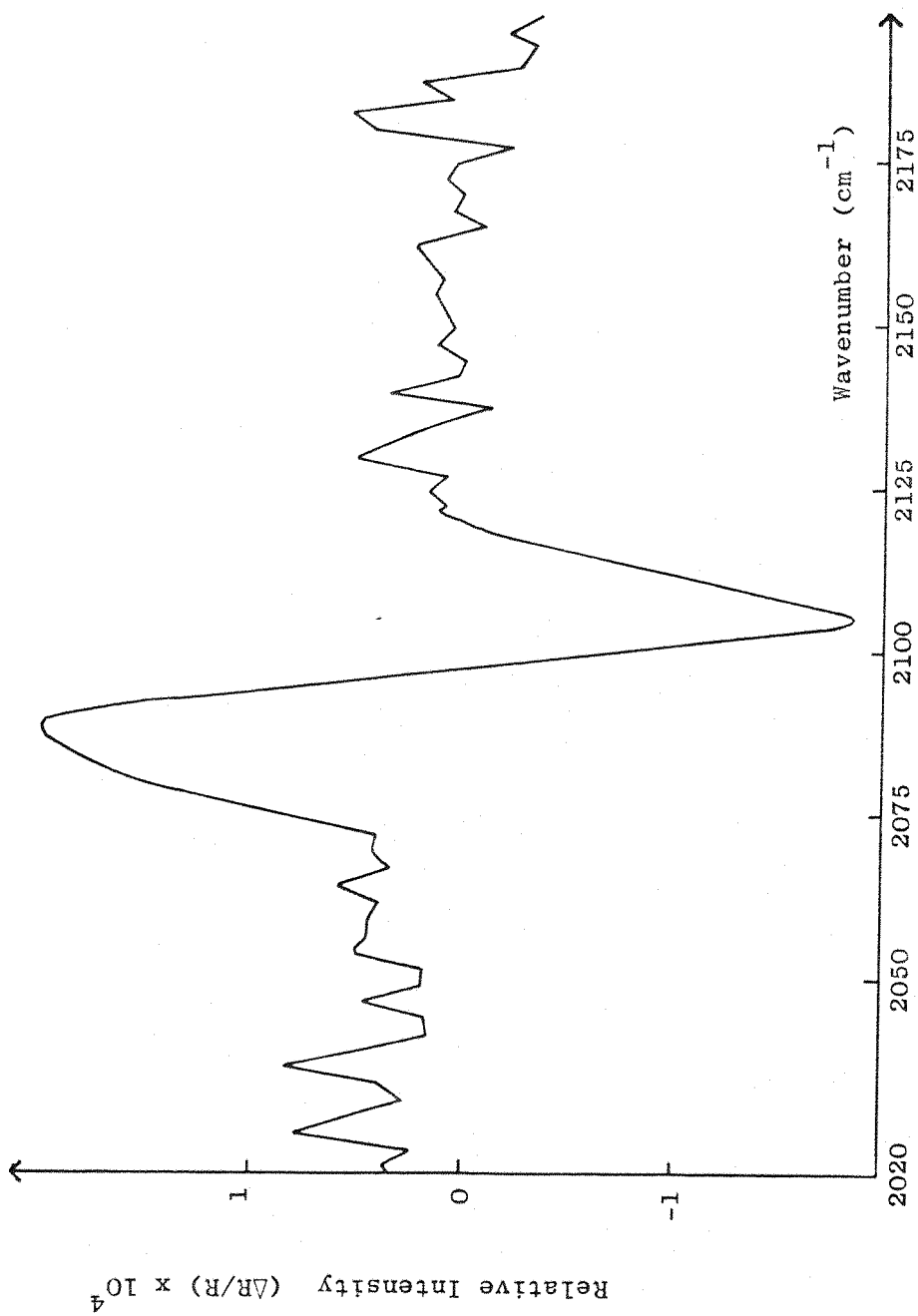


Figure V. 6 — EMIRS spectrum from Ag electrode in 0.5 M KCN solution.  
Modulation from -1.4 to -1.0 V (SCE).



*Figure 7* — EMIRS spectrum from Ag electrode in 0.5 M KCN solution. Modulation from -1.4 to -1.2 V (SCE).

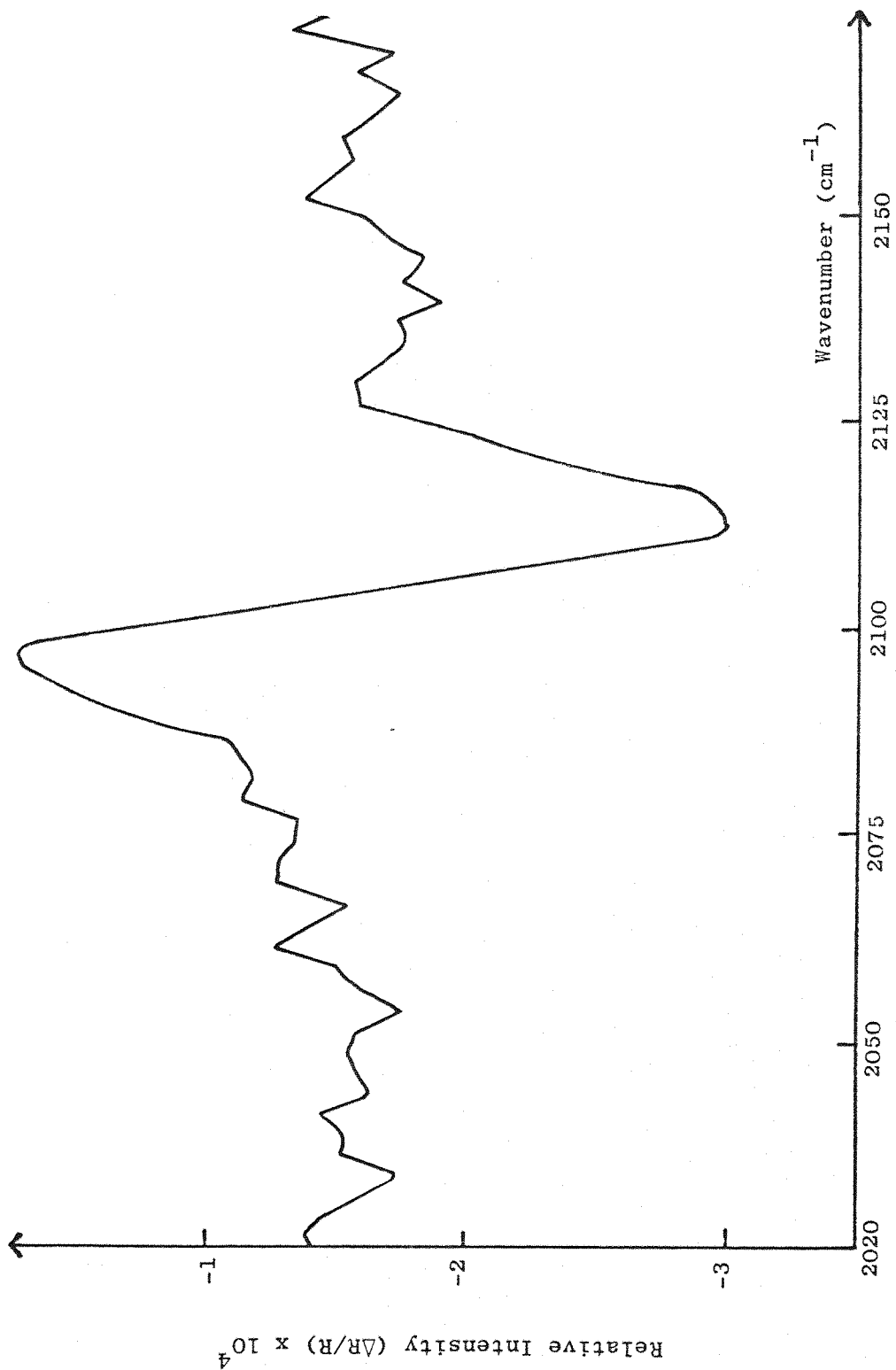


Figure 7. 8 — EMIRS spectrum from Ag electrode in 0.5 M KCN solution.

Modulation from -1.40 to -0.75 V (SCE).

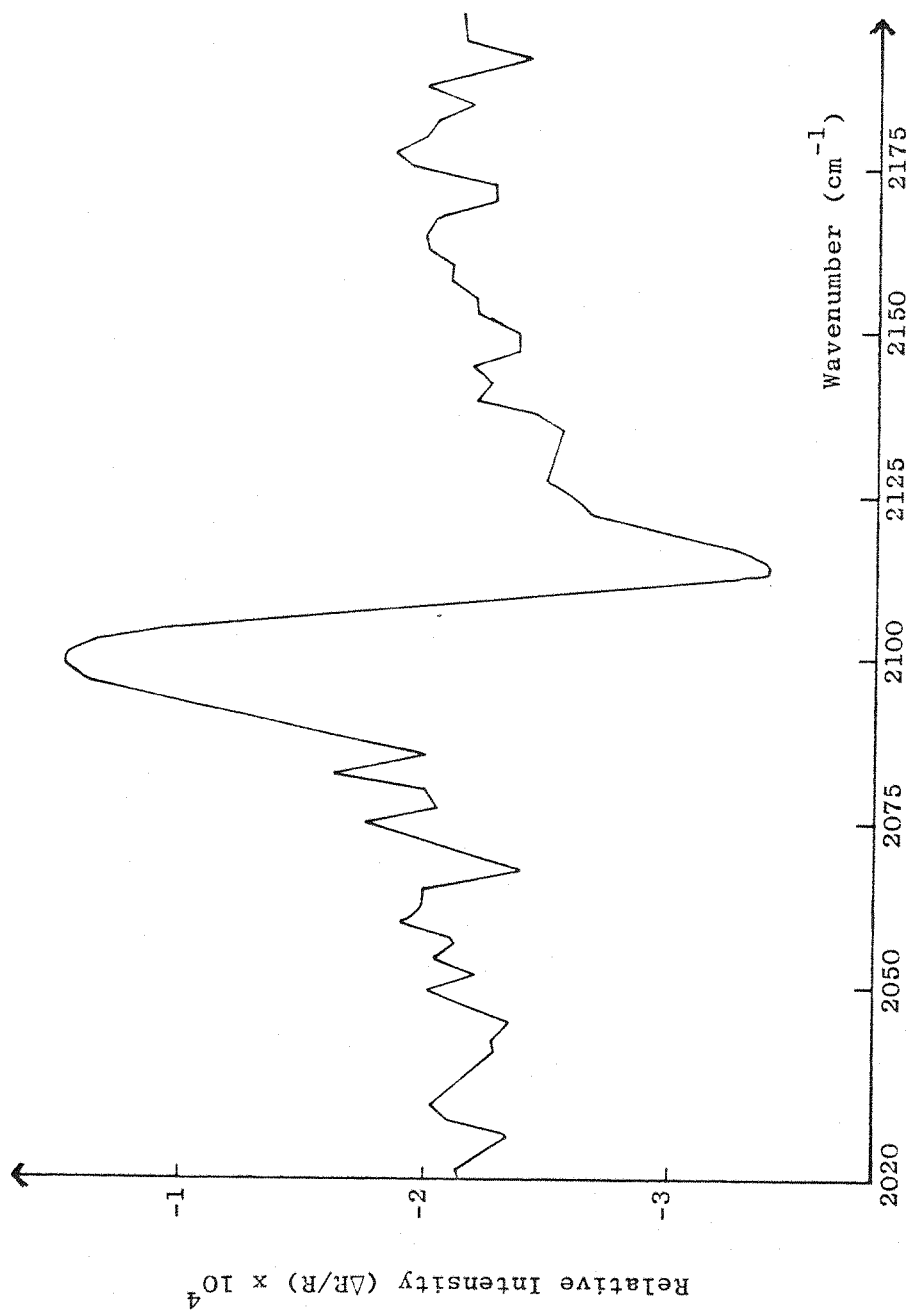


Figure V. 9 — EMIRS spectrum from Ag electrode in 0.5 M KCN solution.  
Modulation from -1.4 to -0.6 V (SCE).

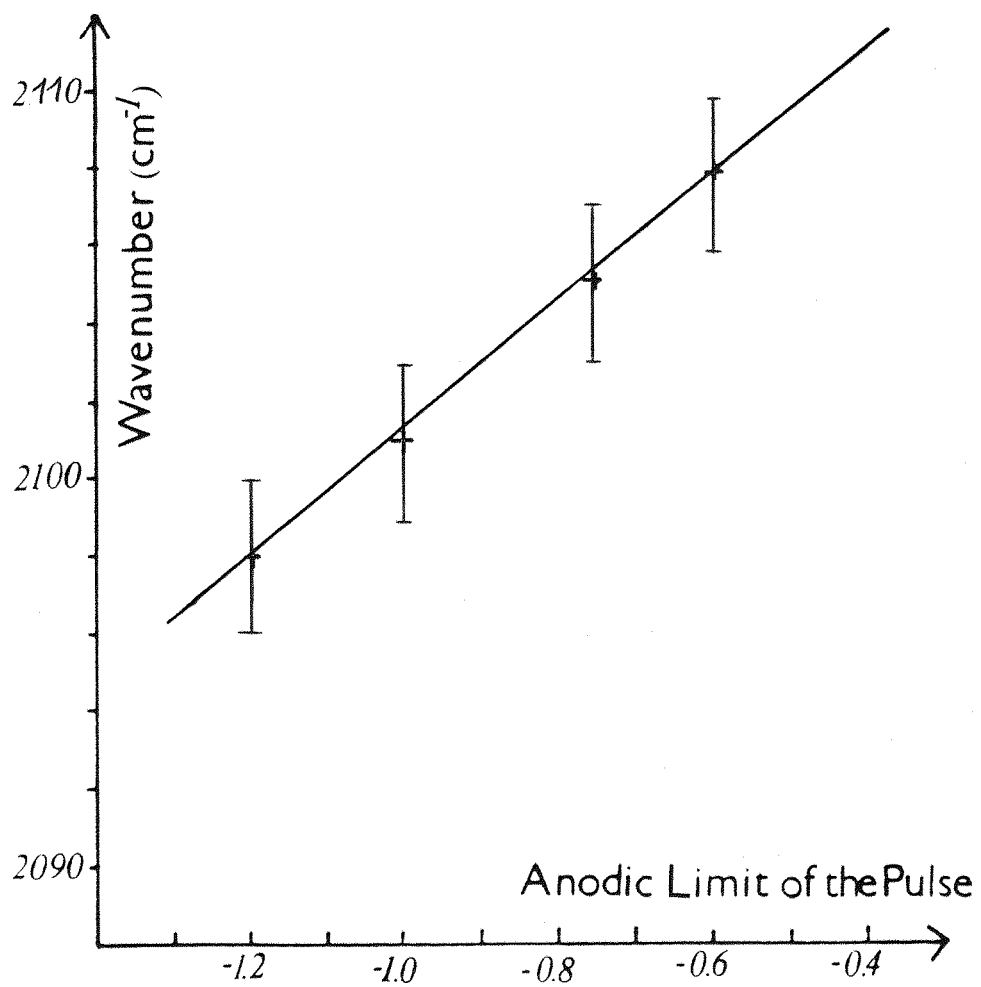


Figure V.10 - Frequency shifts of the observed absorption band in EMIRS spectra for the silver/cyanide system.

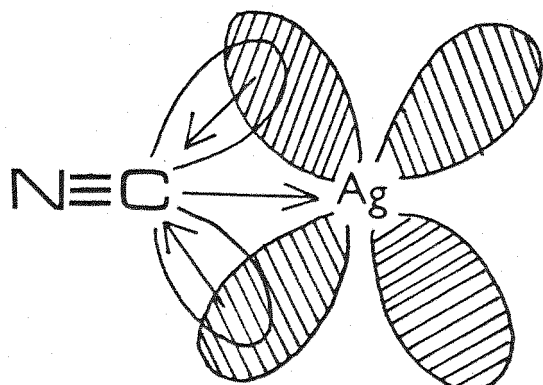
From these results, together with the conclusions reached by Otto et al<sup>(162)</sup> and Fleischmann and coworkers<sup>(164)</sup> from their in-situ Raman studies of this system, the following remarks can be made.

Contrary to all the previous work on Raman scattering from silver electrodes where the formation of a new silver surface with atomic scale roughness was the crucial precondition for the occurrence of surface enhanced Raman scattering<sup>(162)</sup>, the infra red EMIRS absorption band described above was obtained from a smooth silver surface. An electrochemical activation or a mechanical or electrochemical pretreatment was not found necessary.

For the silver cyanide complex ions, which may exist in aqueous solution, i.e.  $\text{Ag}(\text{CN})_4^{3-}$ ,  $\text{Ag}(\text{CN})_3^{2-}$  and  $\text{Ag}(\text{CN})_2^-$ , the frequency of the  $\nu(\text{C}\equiv\text{N})$  stretching vibration increases as the degree of interaction between the silver atom and the  $\text{CN}^-$  ligand increases,

$$\nu(\text{CN})^- < \nu_{\text{Ag}/(\text{CN})_4}^{3-} < \nu_{\text{Ag}/(\text{CN})_3}^{2-} < \nu_{\text{Ag}/(\text{CN})_2}^- < \nu_{\text{AgCN}}^{\text{solid}}$$

This phenomenon arises from the fact that the  $5\sigma$  orbital of the cyanide ion is used to form the metal-ligand bond. This orbital is anti-bonding with respect to the  $\text{C}\equiv\text{N}$  bond and therefore, an increase in the bonding character of the  $5\sigma$  metal-ligand interaction results in a net increase in the bonding of  $\text{C}\equiv\text{N}$ <sup>(181)</sup>. Electron back-donation from the filled metal d-orbitals to vacant anti-bonding orbitals of  $\text{C}\equiv\text{N}$  does occur, but this effect does not fully compensate the first one.



Back-Donation Effect

Thus an increase in the vibrational frequency of the  $\nu(\text{C}\equiv\text{N})$  stretching mode is observed with increasing Ag-C interaction.

However, for the surface complex species, an increase in the negative charge on the electrode can lead to increased back-donation from the filled metal d-orbitals<sup>(164)</sup> lowering the bond character of  $\text{C}\equiv\text{N}$ , and hence, as seen in our study, its stretching frequency.

We now turn to the problem of identifying the specific surface complex present at the electrode/electrolyte interphase in our experiments. The infra red spectra of the complexes  $\text{Ag}(\text{CN})_2^-$ ,  $\text{Ag}(\text{CN})_3^{2-}$  and  $\text{Ag}(\text{CN})_4^{3-}$  in solution show bands at 2135, 2105 and 2092  $\text{cm}^{-1}$  respectively, whereas the  $\text{C}\equiv\text{N}$  stretching mode of  $\text{AgCN}$  is at 2164  $\text{cm}^{-1}$  and that of  $\text{CN}_{\text{aq}}^-$  is at 2080  $\text{cm}^{-1}$  (179).

In our case the EMIRS difference spectrum shows a bisignate band which is assigned to the cyanide stretching mode of the adsorbed species. This band might result from: (1) the combination of two different absorption bands from two different adsorbed species. A species being present at only one of the two selected electrode potentials and the other one being adsorbed only at the other potential limit, (2) the shift with potential of one absorption band corresponding to two non-resolved absorption bands from two different species present at the two potential limits of the modulation, or (3) the shift with potential of one absorption band from a species adsorbed at the two potential limits of the modulation. In fact, the shape of the bisignate band remains the same as the potential range of the modulation is varied and, in every case, the shape and amplitude of the positive and the negative lobes of the band are quite similar. Therefore, the first two possibilities are most unlikely as the relative concentrations of the two different species involved would have almost certainly changed with the variation of potential range of the modulation.

Assuming the presence of only one complex species at the surface, whose coordination number does not change with electrode potential, three different possibilities should be considered: (1) a pyramidal  $\text{Ag}(\text{CN})_3^{2-}$  complex, which would have kept its postulated solution geometry ( $\text{C}_{3v}$ ), (2) an  $\text{Ag}(\text{CN})_2^-$  surface



complex, which would have been distorted from its linear form in solution ( $D_{\infty h}$ ) to  $C_{2v}$  symmetry, or (3) a simple linear Ag-CN complex, perpendicular to the surface. From steric considerations, the tetrahedral  $Ag(CN)_4^{3-}$  surface complex possibility is not considered since it is unlikely to be present at the surface.

It appears, from all the Raman studies of this system, that it is quite difficult to know exactly what is the nature of the surface adsorbate from the three possibilities listed above. The following proposals have been made:

- The  $Ag(CN)_3^{2-}$  unit was proposed by Otto et al<sup>(162)</sup> from a comparison of the adsorbate C≡N stretching frequency observed in their SERS studies and the one reported in a Raman spectrum of the free  $Ag(CN)_3^{2-}$ .

- Fleischmann et al<sup>(164)</sup> have recently concluded that the complex formed on the silver electrode surface may be represented by an  $Ag(CN)_2^-$  unit.

- Furtak<sup>(161)</sup> proposed that  $CN^-$  was bonded to Ag through the 5σ orbital on the carbon end of the cyanide, leading to a model with CN groups individually coordinated with Ag sites and aligned perpendicularly to the metal surface.

From the results of the EMIRS study, reported at the beginning of this section, we are unable to unambiguously distinguish between these three different complexes. For each of these adsorbed species the C≡N stretching vibrational mode would have a non-zero component of the dipole derivative perpendicular to the surface (cf. section 2.4.2.2) and therefore could have given the absorption band observed. The spectrometer presently used does not permit experiments to be performed below  $700\text{ cm}^{-1}$  and, therefore, we could not look at the Ag-C stretching and bending mode regions which is around  $400\text{ cm}^{-1}$ . These low-frequency bands would give valuable information as in SERS. In order to obtain additional spectroscopic data on this silver/cyanide system an EMIRS study of isotopic cyanide mixtures would be interesting as an IRRAS study which would permit one to obtain direct infra red spectra from the adsorbed species at different



electrode potentials (cf. section 2.4.5).

Finally, two different remarks should be made:

- As it has been noted by different researchers, silver is slowly dissolved by a cyanide solution, forming the most stable silver/cyanide complex ion:  $\text{Ag}(\text{CN})_2^-$ . An  $\text{Ag}(\text{CN})_2^-$  unit seems therefore to have more opportunity to be the adsorbed species.

- Some EMIRS experiments were carried out in 0.01M and 0.1M KCN solutions instead of the 0.5M KCN solution used for the results previously reported in this section. With the 0.01M KCN solution, no infra red absorption band could be detected in the  $\nu\text{C}\equiv\text{N}$  frequency range. With the 0.1M KCN solution, a bipolar band appeared at the same position as with the 0.5M KCN solution, but the intensity of this band was at least 2.5 times smaller. This surprising behaviour, knowing that even for the most diluted solution a high surface concentration of cyanide anions is certainly reached, can only be explained if different adsorbed species are considered. We suggest that for the lower concentrated solutions, ordinary (specifically)  $\text{CN}^-$  ions are adsorbed at the surface with their dipole moment parallel to the electrode surface which would explain why no  $\nu\text{C}\equiv\text{N}$  absorption band could have been detected. As the  $\text{CN}^-$  concentration increases it is believed that complexed species are formed at the surface; these adsorbed surface species with a non zero surface normal derivative component will therefore give rise to the absorption band observed. These observations and the explanation proposed can be related to the recent results reported by Hupp *et al* (169). They have shown that the surface roughening procedure which is crucial to SERS has a relatively small influence on the average surface concentration of the Raman scatterers.

#### 5.2.2.2 The Gold/Cyanide System

Figure V.11 shows the current-potential linear sweep voltammogram obtained for the Au/0.5M KCN aqueous system. A broad anodic current wave begins at about -0.1V (SCE) showing two peaks: a sharp peak at +0.45V and a small maximum at +0.675V after which the current decays rapidly with increasing potential. The reverse scan shows a small anodic current peak at +0.125V

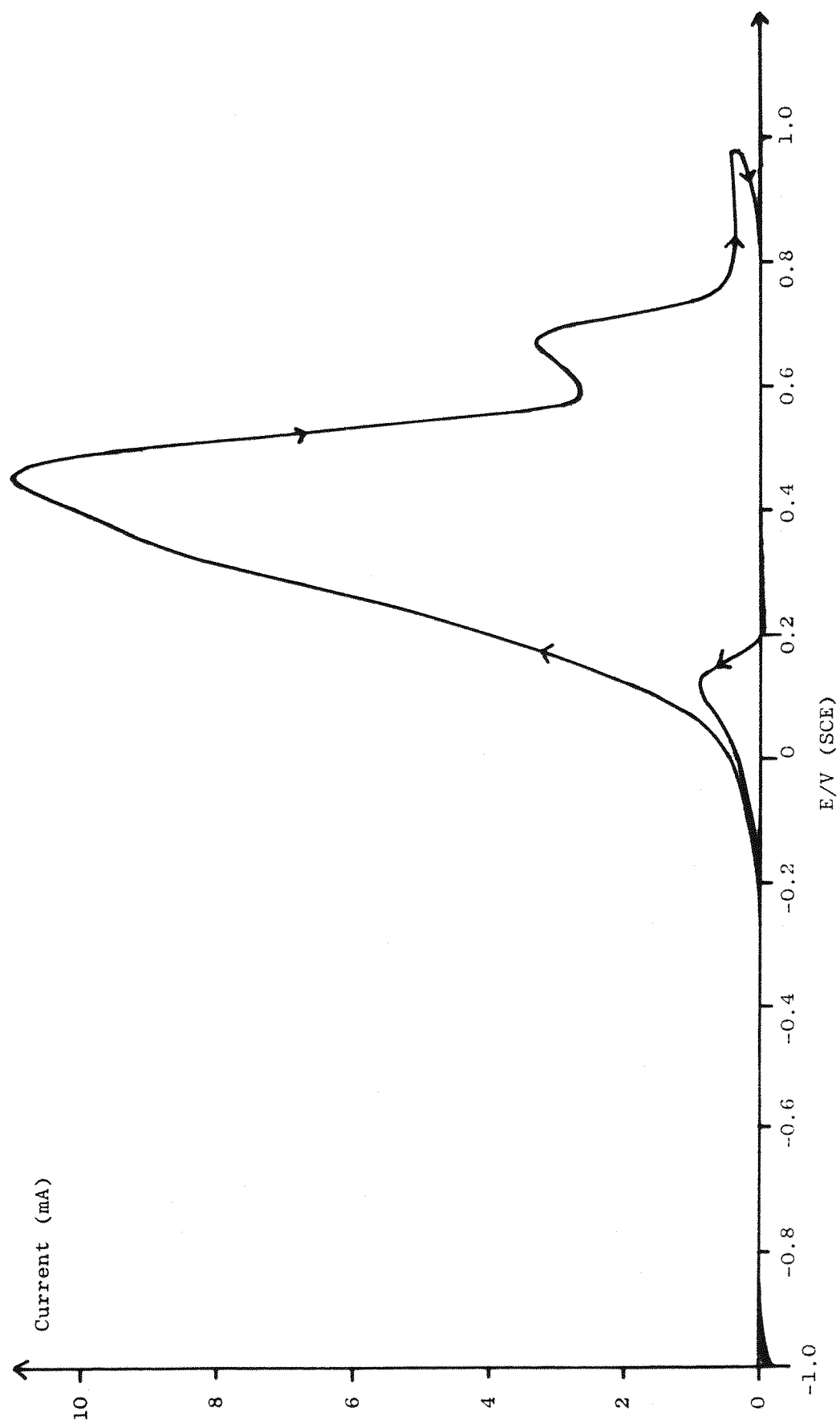


Figure V.11 - Cyclic voltammogram for Au electrode in 0.5 M KCN solution.  
Sweep rate 0.05 V/s.

after which the current decays slowly to zero. We can deduce from this cyclic voltammogram that a complex oxidation process is occurring after  $-0.1V$ . This process involves certainly gold dissolution.

Figures V.12 to V.14 show the EMIRS spectra obtained for the gold/cyanide system over the range from  $2020$  to  $2200\text{ cm}^{-1}$  for modulation from a fixed potential of  $-0.8V$  to various more positive values. As for the silver/cyanide study, these spectra were obtained from a smooth electrode surface. A strong bipolar absorption band centred between  $2119$  and  $2125\text{ cm}^{-1}$ , assigned to the  $C\equiv N$  stretching vibrational mode of adsorbed cyanide species can be seen. The intensity of this band appears to be at least 2.5 times greater than the similar band obtained from the Ag/cyanide system.

The spectra obtained by modulating the electrode potential between  $-0.8V$  and  $+0.550V$ , shown in Figure V.15, display in addition to the strong bipolar band a much weaker single-sided band with a maximum at  $2040\text{ cm}^{-1}$ . The positive sign of  $\Delta R/R$  for this band indicates stronger infra red absorption at the negative potential. The appearance of this new band might be related to the fact that the positive potential of the relative modulation was found to correspond to the dissolution of gold (cf. Figure V.11). This process may have permitted another type of adsorbate species to be formed.

The bipolar absorption band is seen to shift in a roughly linear fashion to lower wavenumbers, whilst retaining almost constant intensity and shape, as the electrode potential is made more positive. The frequency shifts of the band with potential are plotted in Figure V.16. For this system the shift observed for the crossing point of the band is about  $6.5\text{ cm}^{-1}$  per Volt, which is very small compared to the shift reported in the previous section for the silver/cyanide system. The changing relative intensities of the positive and negative lobes of the band appear to indicate a decrease in the coverage by adsorbed species at the more negative potential with increasing pulse amplitude. It should be noted that the absorption band observed by modulating

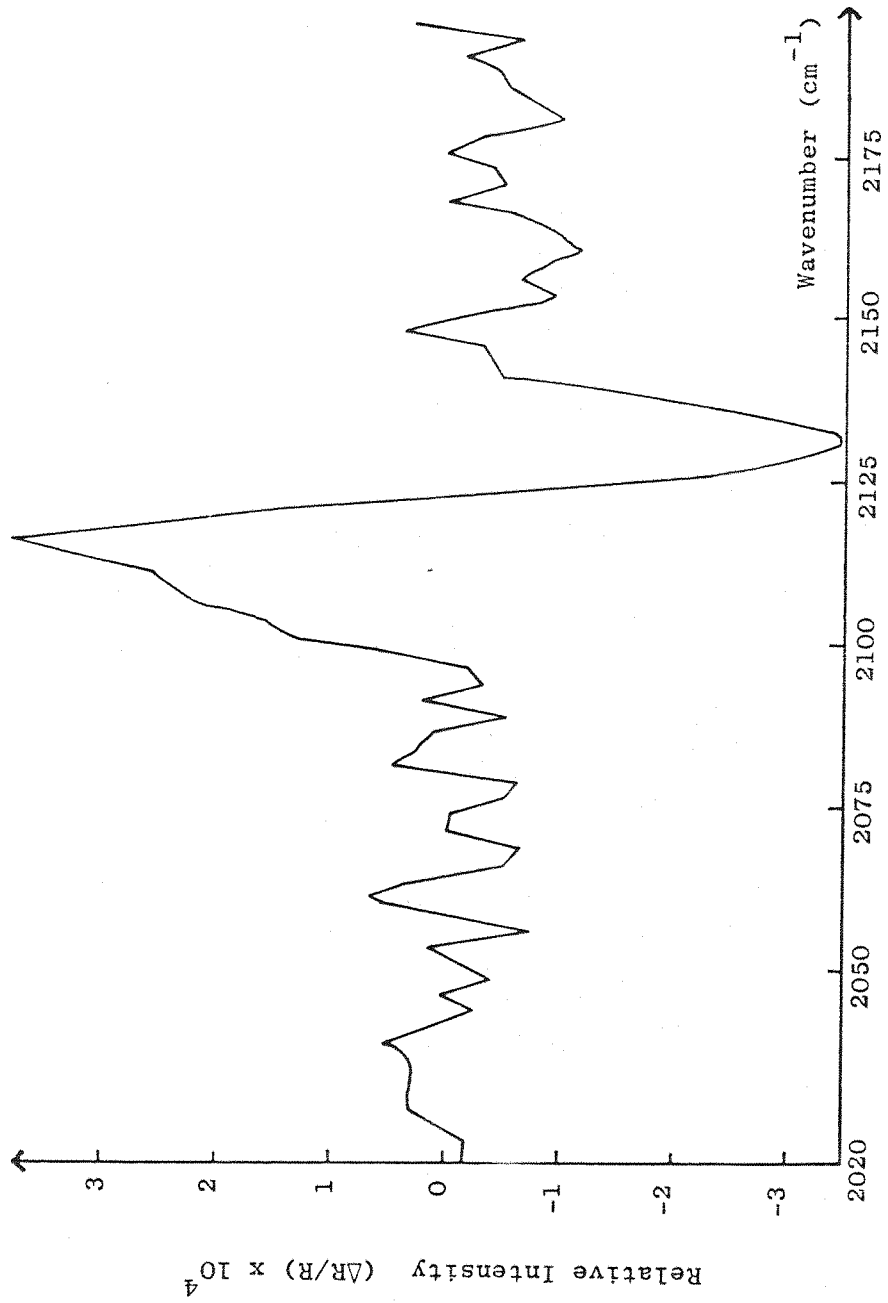


Figure I. 12 — EMIRS spectrum from Au electrode in 0.5 M KCN solution.  
Modulation from -0.8 to -0.6 V (SCE).

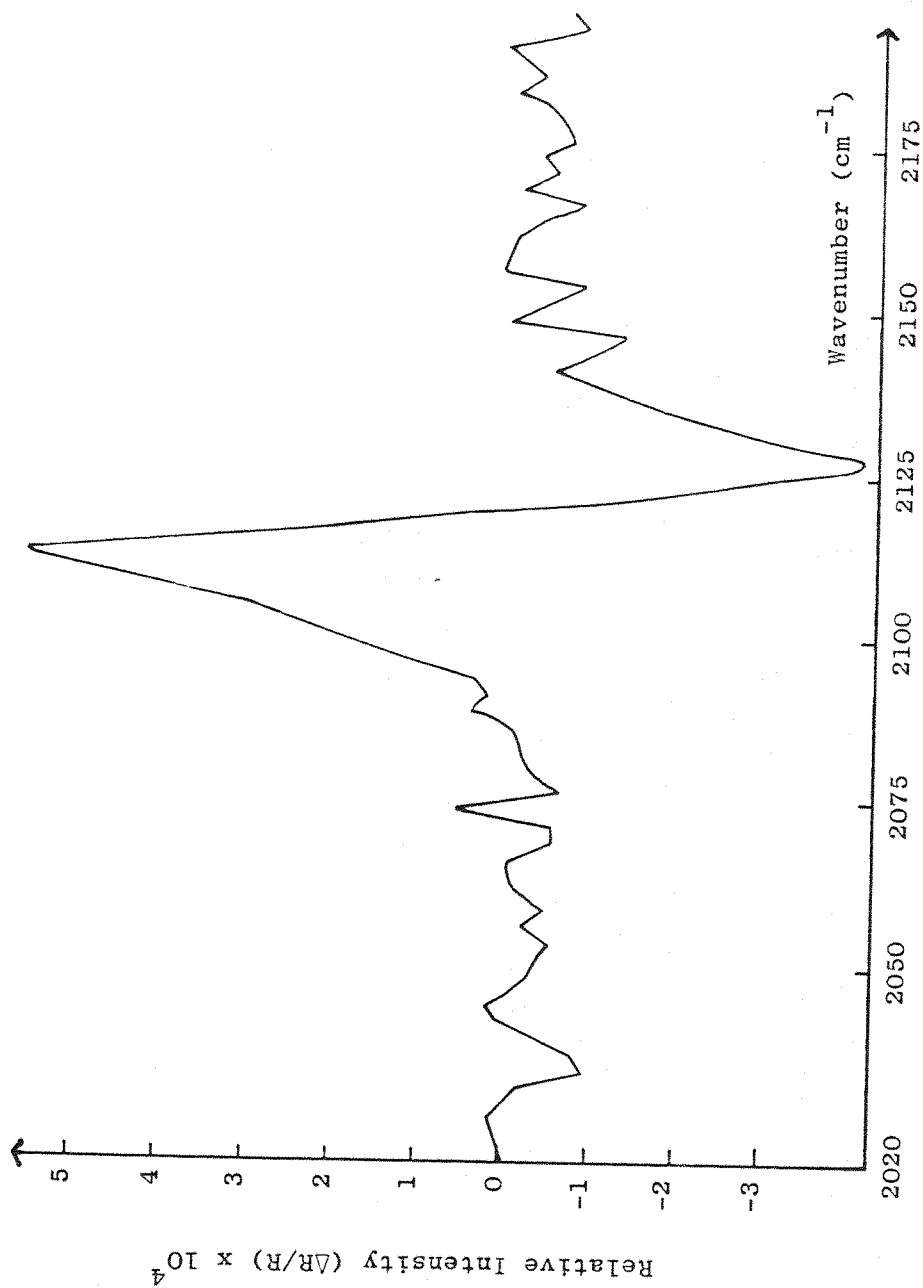


Figure 13 -- EMIRS spectrum from Au electrode in 0.5 M KCN solution.  
Modulation from -0.8 to -0.2 V (SCE).

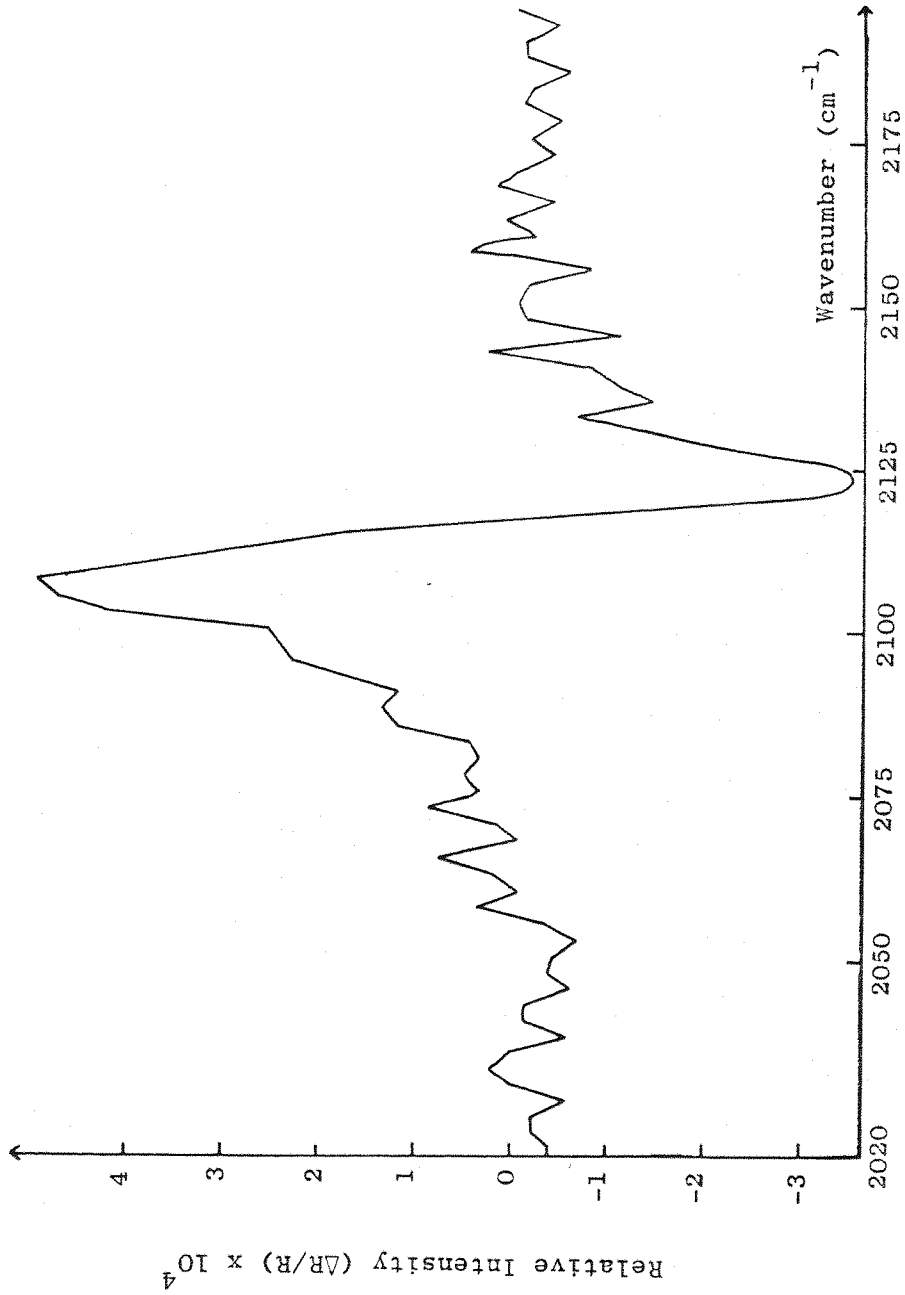


Figure 14 — EMIRS spectrum from Au electrode in 0.5 M KCN solution.  
Modulation from -0.8 to +0.2 V (SCE).

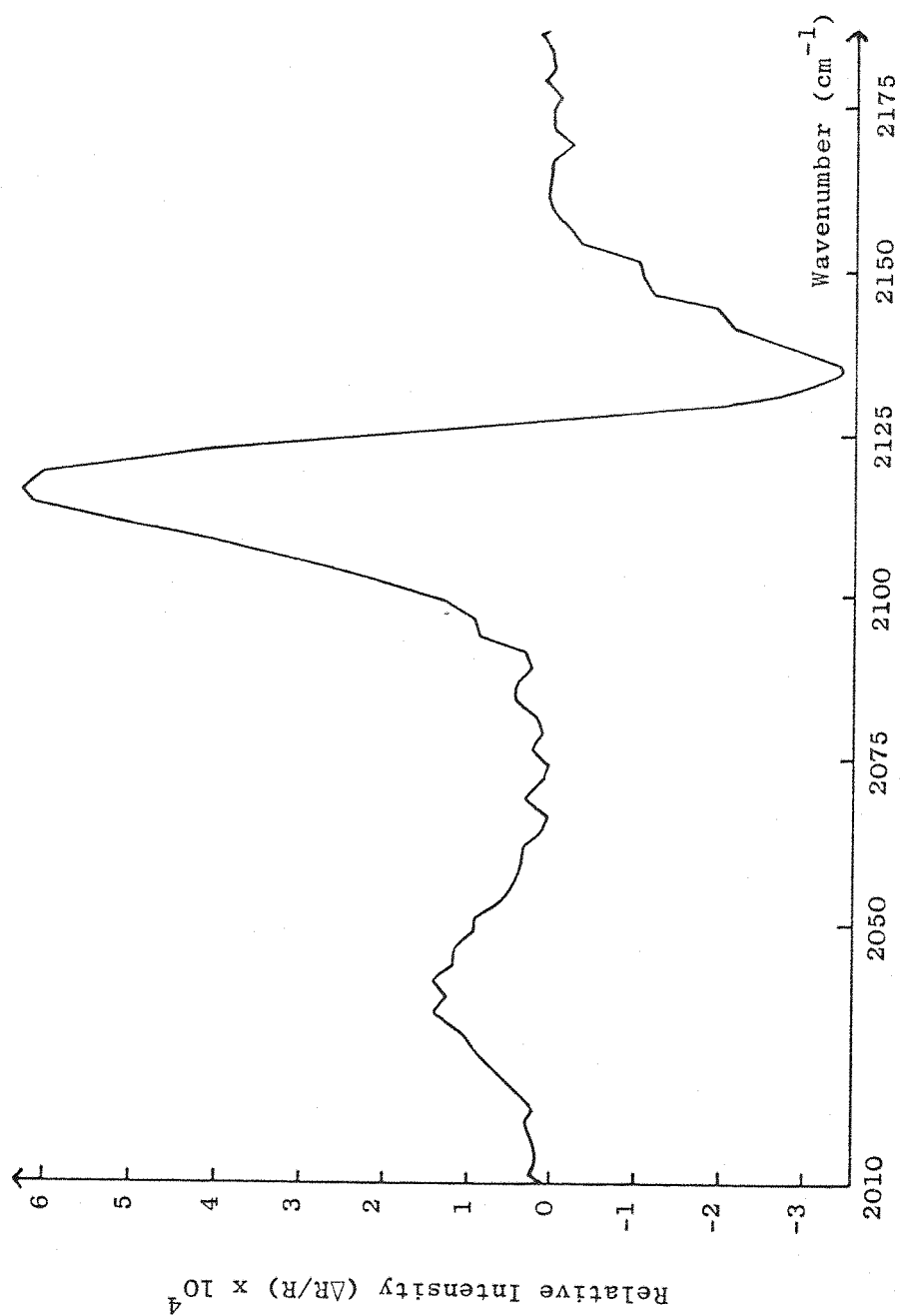


Figure V. 15—EMIRS spectrum from Au electrode in 0.5 M KCN solution.  
Modulation from -0.80 to +0.55 V (SCE).



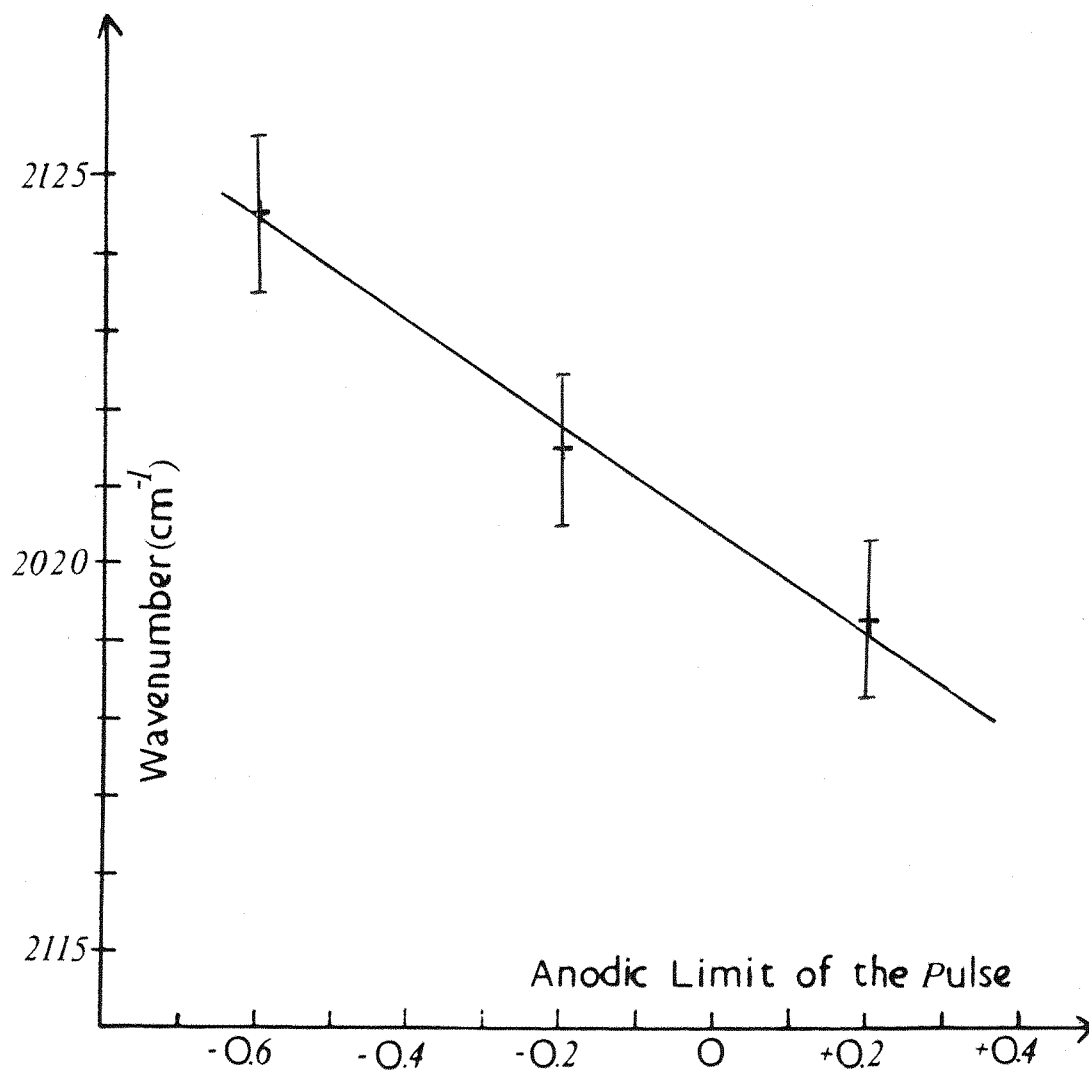
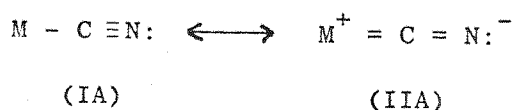


Figure V.16 - Frequency shifts of the observed bipolar absorption band in EMIRS spectra for the gold/cyanide system.

the electrode potential between -0.8 and +0.550V, cf. Figure V.15 does not follow the linear potential shift shown for the other modulation ranges.

As shown in Table V.2, for the gold cyanide complex ions which may exist in aqueous solution, i.e.  $\text{Au}^{\text{I}}(\text{CN})_2^-$ ,  $\text{Au}^{\text{III}}(\text{CN})_4^-$ , the  $\nu(\text{C}\equiv\text{N})$  stretching frequency increases with the oxidation state of the gold atom involved in the complex. According to El-Sayed and Sheline<sup>(182)</sup> the  $\text{C}\equiv\text{N}$  stretching frequencies of the cyano complexes lies between  $\text{C}=\text{N}$  and  $\text{C}\equiv\text{N}$  frequencies showing the resonance between the following resonance forms:



It has been shown<sup>(183)</sup> that  $\text{Au}^{\text{III}}$  has a high "effective nuclear kernel charge", i.e. due to their spatial orientation and extension the eight 5d electrons do not shield the metal from the ligands very efficiently and thus the metal appears to the cyanides to have a high positive charge. This "positive" charge on the metal increase the contribution of structure IA to the total structure of the complex. The gold tetracyanide complex ( $\text{Au}(\text{CN})_4^-$ ) is therefore a strong metal-ligand sigma bond and weak metal-ligand pi bond system. This fact explains the high  $\text{C}\equiv\text{N}$  stretching frequency observed in solution for  $\text{Au}^{\text{III}}(\text{CN})_4^-$  compared to  $\text{Au}^{\text{I}}(\text{CN})_2^-$  which shows a stronger, although probably rather small, metal-carbon  $\pi$ -bonding.

In our study, for the spectra given in Figures V.12 to V.14, we can assume that only one and the same complex species is present at the surface. From spatial considerations, only two different possibilities should be considered: (1) an  $\text{Au}^{\text{I}}(\text{CN})_2^-$  surface complex which would have changed its postulated symmetry from  $D_{\infty h}$  in solution to  $C_{2v}$  symmetry or (2) a simple linear  $\text{Au}^{\text{I}}-\text{CN}$  complex perpendicular to the surface, i.e. with CN groups individually coordinated with Au sites and aligned perpendicularly to the metal surface.

For each of these adsorbed species the  $\text{C}\equiv\text{N}$  stretching

vibrational mode would have a non-zero component of the dipole derivative perpendicular to the surface and therefore could have given the strong absorption band observed. Whatever the complex species considered, the shift observed for the bipolar band to higher frequencies as the potential of the electrode is made more negative cannot be simply explained. It has been shown<sup>(184)</sup> that for cyanide complex species an increase in the negative charge on the metal leads to an increase of the back-donation effect (see previous section), resulting in an increase of the contribution of structure IIA for the complex. Therefore, as the potential of the electrode is made more negative, a shift to lower frequency for the  $C\equiv N$  stretching mode should have been observed. However, the relative small shift observed, compared with the one reported in the previous section for the silver/cyanide system, may suggest that competitive effects are involved.

The spectra obtained by modulating the electrode potential between -0.8V and +0.550V (cf. Figure V.15) shows two different absorption bands. The strong bipolar band is assumed to arise from the same adsorbed species as that which gave a similar band in the experiments performed with smaller modulation amplitudes. The much smaller single-sided band demonstrates that another type of species is also adsorbed at the surface. By comparison of the infra red CN stretching frequencies reported for the free cyanide complexes (cf. Table V.2) with those observed in our study and assuming that the adsorbed species will show relatively lower  $C\equiv N$  stretching vibration frequencies, as is usually the case, we can suggest that: (1) the strong bipolar band can probably be assigned to the simple linear  $Au^I-CN$  complex species ( $\Delta\bar{\nu} = \bar{\nu}_{AuCN_{solid}} - \bar{\nu}_{observed} = 2239 - 2128 = 107 \text{ cm}^{-1}$ ) and (2) the single-sided band can probably be assigned to  $Au^I(CN)_2^-$  complex species ( $\Delta\bar{\nu} = \bar{\nu}_{Au(CN)_2_{aq}} - \bar{\nu}_{observed} = 2147 - 2040 = 107 \text{ cm}^{-1}$ ) These conclusions would have to be confirmed by further studies (EMIRS and/or IRRAS).

### 5.3 Conclusion

In view of the fact that the adsorption of cyanide at the silver metal/aqueous interphase has been widely studied by Raman spectroscopy, it was a very interesting system to investigate using electrochemically modulated infra red spectroscopy (EMIRS). The results presented in this chapter show very interesting similarities with those reported in the Raman work. However, it should be noted, that the difference spectra reported are inevitably more difficult to interpret than those obtained at a single potential in surface enhanced Raman spectroscopy (SERS).

The gold/cyanide system has been shown to behave differently than the silver/cyanide system and it was not possible to explain why, although it is well known that there are marked differences in the chemistry of silver and gold.

Because of its simplicity, compared with uncharged organic adsorbates, cyanide was expected to give easily interpretable spectra. In fact, this is not the case, as many different surface complex species could be formed at the surface, and further complementary EMIRS and/or IRRAS experiments are needed to identify unambiguously the surface adsorbate species.

## CHAPTER SIX

### Conclusion

The results presented in this thesis have firmly established Electrochemically Modulated Infra Red Spectroscopy (EMIRS) as a good technique at the molecular level for examining the chemical structure of electrochemical interphases.

As a simple infra red reflectance method, EMIRS does not need very sophisticated equipment. The only non-standard equipment used; a thin-layer spectroelectrochemical cell suitable for use with aqueous solutions throughout the infra red region, and an appropriate monochromator sampling chamber, have been designed to collect the highest possible throughput of energy which has been reflected from the electrode surface.

EMIRS has been demonstrated as being a very sensitive technique capable of detecting infra red bands of submonolayer amounts of adsorbate species and being also sensitive towards their orientation at the surface.

However, since EMIRS spectra are difference spectra, it is important to be aware of the limitations placed upon spectral observations and interpretations. In terms of interpretations it has been recently demonstrated that the use of the complementary useful IRRAS technique can be very efficient.

In order to be able to programme lower data acquisition times and thus to decrease the overall time of an EMIRS experiment, the noise produced by stepping the grating would have to be minimized and/or the detector chamber of the spectrometer would have to be separate from the grating unit of the monochromator.

An apparent violation of the surface selection rule has been observed in the study of the adsorption of acrylonitrile on gold electrodes. However, the results obtained can only be explained by the formation of a dipole change perpendicular to the electrode surface. This induced surface normal dipole component is likely to have been produced by the interaction of the static electric field present at the electrode with the parallel

vibrational modes of the adsorbed acrylonitrile molecules.

In the study of the adsorption of cyanide on silver and gold electrodes very interesting results have been obtained. However, further complementary investigations are needed to permit valuable suggestions on the nature of the adsorbed species.

REFERENCES

1. K.R. WILLIAMS,  
"An Introduction to Fuel Cells", Elsevier, Amsterdam,  
(1966).
2. J. O'M BOCKRIS, S. SRINIVASAN,  
"Fuel Cells: Their Electrochemistry", McGraw-Hill,  
New York, (1969).
3. B.G. BAKER,  
in "Modern Aspects of Electrochemistry", Vol. 10, Eds.  
J. O'M. Bockris and B.E. Conway, Plenum Press, New  
York (1975) 93.
4. E. YEAGER,  
Surf. Sci., 101 (1980) 1.
5. E. YEAGER,  
J. Electrochem. Soc., 128 (1981) 159c.
6. Symposia of the Faraday Society,  
"Optical Studies of Adsorbed Layers at Interfaces",  
4 (1970).
7. Journal de Physique,  
"Optics at the Solid-Liquid Interface", Colloque  
International du CNRS (France), C-5, 38 (1977).
8. T.E. FURTAK, K.L. KLIEWER and D.W. LYNCH, Eds.,  
"Non-Traditional Approaches to the Study of the Solid-  
Electrolyte Interface", Proceedings of an International  
Conference, Colorado (North-Holland, Amsterdam, 1980).  
Printed as Surf. Sci., 101 (1980).
9. E. PASSAGLIA, R.R. STROMBERG and J. KRUGER, Eds.,  
"Ellipsometry in the Measurement of Surfaces and Thin  
Films", Proc. Symposium, Washington, 1963. Nat. Bur.  
Stand. Misc. Publ., 256 (1964).
10. N.M. BASHARA, A.B. BUCKMAN and A.C. HALL, Eds.,  
"Recent Developments in Ellipsometry", Symposium  
Proceedings, University of Nebraska, (North-Holland,  
Amsterdam, 1969). Printed as Surf. Sci., 16 (1969).
11. R.H. MULLER,  
in "Adv. in Electrochem. and Electrochem. Eng.",  
Wiley, 9 (1973) 167.

12. J. KRUGER,  
in "Adv. in Electrochem. and Electrochem. Eng.", Wiley,  
9 (1973) 227.
13. N.M. BASHARA, R.M.A. AZZAM, Eds.,  
"Proceedings of the Third International Conference on  
Ellipsometry", University of Nebraska, (North-Holland,  
Amsterdam, 1976). Printed as Surf. Sci., 56 (1976).
14. A.J. BARD and L.R. FAULKNER,  
"Electrochemical Methods", Wiley (1980) New York,  
Chap. 14.
15. W.-K. PAIK and J. O'M BOCKRIS,  
Surf. Sci., 28 (1971) 61.
16. J. HORKANS, B.D. CAHAN and E. YEAGER,  
Surf. Sci., 46 (1974) 1.
17. B.D. CAHAN,  
Surf. Sci., 56 (1976) 354.
18. A.C. HALL,  
Surf. Sci., 16 (1969) 1.
19. L. TRONSTAD,  
Trans. Faraday Soc., 29 (1933) 502.
20. F.L. McCRACKIN,  
"A Fortran Program for Analysis of Ellipsometer  
Measurements", Nat. Bur. Stand., Tech. Note 479,  
(April 1969).
21. P. DRUDE,  
Ann. Phys. Chem., 36 (1889) 865.
22. Y.C. CHIU and M.A. GENSHAW,  
J. Phys. Chem., 72 (1968) 4325.
23. Y.C. CHIU and M.A. GENSHAW,  
J. Phys. Chem., 73 (1969) 3571.
24. W.-K. PAIK, M.A. GENSHAW and J. O'M BOCKRIS,  
J. Phys. Chem., 74 (1970) 4266.
25. W.-K. PAIK and J. O'M BOCKRIS,  
Surf. Sci., 27 (1971) 191.
26. M.J. DIGNAM, B. RAO, M. MOSKOVITS and R.W. STOBIE,  
Can. J. Chem., 49 (1971) 1115.
27. M.J. DIGNAM, B. RAO and R.W. STOBIE,  
Surf. Sci., 46 (1974) 308.



28. M.W. HUMPHREYS and R. PARSONS,  
J. Electroanal. Chem., 82 (1977) 369.
29. K. KUNIMATSU and R. PARSONS,  
J. Electroanal. Chem., 100 (1979) 335.
30. F.L. BAUDAIS, A.J. BORCHKE, J.D. FEDYK and M.J. DIGNAM,  
Surf. Sci., 100 (1980) 210.
31. D.J. WHEELER, B.D. CAHAM, C.T. CHEN and E. YEAGER,  
in "Passivity of Metals, Eds. R.P. Frankenthal and  
J. Kruger, The Electrochemistry Society, Princeton,  
N.J. (1978) 546.
32. N.J. HARRICK,  
"Internal Reflection Spectroscopy", Interscience,  
Publishers, Inc., New York (1967).
33. H.B. MARK, Jr and E.N. RANDALL,  
Symposia of the Faraday Society, 4 (1970) 157.
34. W.N. HANSEN,  
in "Adv. in Electrochem. and Electrochem. Eng.",  
Wiley, 9 (1973).
35. T. KUWANA,  
Ber. Bun. Ges. Phys. Chem., 77 (1973) 858.
36. W.N. HANSEN,  
Symp. of the Faraday Soc., 4 (1970) 27.
37. J.W. STROJEK and T. KUWANA,  
J. Electroanal. Chem., 16 (1968) 471.
38. B.S. PONS, J.S. MATTSON, L.O. WINSTROM and H.B. MARK, Jr.,  
Anal. Chem., 39 (1967) 685.
39. A. PROSTAK, H.B. MARK, Jr. and W.N. HANSEN,  
J. Phys. Chem., 72 (1968) 2576.
40. A. YILDIZ, P.T. KISSINGER and C.N. REILLEY,  
Anal. Chem., 40 (1968) 1018.
41. W. VON BENKEN and T. KUWANA,  
Anal. Chem., 42 (1970) 1114.
42. W.N. HANSEN, R.A. OSTERYOUNG and T. KUWANA,  
J. Am. Chem. Soc., 88 (1966) 1062 and Anal. Chem.,  
38 (1966) 1810.
43. D. LASER and M. ARIEL,  
J. Electroanal. Chem., 41 (1973) 381.
44. A.Z. TRIFONOV and I.D. SCHOPOV,  
J. Electroanal. Chem., 35 (1972) 415.

45. A.M. TUXFORD,  
Ph.D Thesis, Southampton University (1972).
46. J. ROBINSON,  
Ph.D Thesis, Southampton University (1976).
47. H.B. MARK, Jr. and B.S. PONS,  
Anal. Chem., 38 (1966) 119.
48. W.R. HEINEMAN, J.N. BURNETT and R.W. MURRAY,  
Anal. Chem., 40 (1968) 1974.
49. A.H. REED and E. YEAGER,  
Electrochim. Acta, 15 (1970) 1345.
50. D.R. TALLANT and D.H. EVANS,  
Anal. Chem., 41 (1969) 835.
51. J.S. MATTSON and C.A. SMITH,  
Anal. Chem., 47 (1975) 1122.
52. N.R. ARMSTRONG, A.W.C. LIN, M. FUJIHIRA and T. KUWANA,  
Anal. Chem., 48 (1976) 741.
53. M. PETEK, T.E. NEAL and R.W. MURRAY,  
Anal. Chem., 43 (1971) 1069.
54. W.R. HEINEMAN, T.P. DEANGELIS and J.F. GOELZ,  
Anal. Chem., 47 (1975) 1364.
55. M.L. MEYER., T.P. DEANGELIS and W.R. HEINEMAN,  
Anal. Chem., 49 (1977) 602.
56. T. KUWANA and W.R. HEINEMAN,  
Acc. Chem. Res., 9 (1976) 241.
57. W.R. HEINEMAN,  
Anal. Chem., 50 (1978) 390A.
58. J.D.E. McINTYRE and D.M. KOLB,  
Symp. Faraday Soc., 4 (1970) 99.
59. D.F.A. KOCH and D.E. SCAIFE,  
J. Electrochem. Soc., 113 (1966) 302.
60. J.D.E. McINTYRE,  
in "Adv. in Electrochem. and Electrochem. Eng.," Wiley,  
9 (1973) 61.
61. M.A. BARRETT and R. PARSONS,  
Symp. Faraday Soc., 4 (1970) 72.
62. A. BEWICK and A.M. TUXFORD,  
Symp. Faraday Soc., 4 (1970) 114.
63. W.J. PLIETH,  
Symp. Faraday Soc., 4 (1970) 137.

64. T. TAKAMURA, K. TAKAMURA, W. NIPPE and E. YEAGER,  
J. Electrochem. Soc., 117 (1970) 626.
65. T. TAKAMURA, K. TAKAMURA and E. YEAGER,  
J. Electroanal. Chem., 29 (1971) 279.
66. D.M. KOLB and J.D.E. McINTYRE,  
Surf. Sci., 28 (1971) 321.
67. J.D.E. McINTYRE and D.E. ASPNES,  
Surf. Sci., 24 (1971) 417.
68. A. BEWICK and A.M. TUXFORD,  
J. Electroanal. Chem., 47 (1973) 255.
69. A. BEWICK, F.A. HAWKINS and A.M. TUXFORD,  
Surf. Sci., 37 (1973) 82.
70. A. BEWICK and J. ROBINSON,  
J. Electroanal. Chem., 60 (1975) 163, Surf. Sci.,  
55 (1976) 349 and J. Electroanal. Chem., 71(1976) 131.
71. B.D. CAHAN, J. HORKANS and E. YEAGER,  
Symp. Faraday Soc., 4 (1970) 36.
72. D.C. WALKER,  
Can. J. Chem., 45 (1967) 807.
73. B.O. SERAPHIN, Ed,  
"Modulation Spectroscopy". Proceedings of the first  
international conference on modulation spectroscopy,  
Arizona (North-Holland, Amsterdam, 1973), Printed as  
Surf. Sci., 37 (1973).
74. J.D.E. McINTYRE and W.F. PECK, Jr., Faraday Disc. Chem.  
Soc., 56 (1973) 122.
75. R.M. LAZORENKO-MANEVICH, E.B. BRICK and Y.M. KOLOTYRKIN,  
Electrochim. Acta, 22 (1977) 151.
76. T.E. FURTAK and D.W. LYNCH,  
J. Electroanal. Chem., 79 (1977) 1.
77. R. KÖTZ and D.M. KOLB,  
Z. Phys. Chem., 112 (1978) 69.
78. R. KOFMAN, R. GARRIGOS and P. CHEYSSAC,  
Surf. Sci., 101 (1980) 231.
79. R. ADZIC, E. YEAGER and B.D. CAHAN,  
J. Electrochem. Soc., 121 (1974) 474.
80. T. TAKAMURA, F. WATANABE and K. TAKAMURA,  
Electrochim. Acta, 19 (1974) 933.

81. D.M. KOLB, D. LEUTLOFF and M. PRZASNYSKI,  
Surf. Sci., 47 (1975) 622.
82. A. BEWICK and B. THOMAS  
J. Electroanal. Chem., 65 (1975) 911; 70(1976) 239;  
84 (1977) 127; 85 (1977) 329.
83. M. FLEISCHMANN and I.R. HILL,  
"Surface Enhanced Raman Scattering" Ed. Furtak and  
Chang, Plenum Press, N.Y. to be published.
84. B.A. MORROW,  
in "Vibrational Spectroscopies for Adsorbed Species",  
A.T. Bell and M.L. Hair (Eds). American Chemical  
Society, Symposium 137 (1980) 119.
85. G. HERZBERG,  
"Infra-Red and Raman Spectra of Polyatomic Molecules"  
Van Nostrand, New York (1945).
86. M. DAVIES,  
"Infra-Red Spectroscopy and Molecular Structure",  
Elsevier, New York (1963).
87. C.V. RAMAN and K.S. KRISHNAN,  
Nature, 121 (1928) 501.
88. M. FLEISCHMANN, P.J. HENDRA and A.J. McQUILLAN,  
J.C.S. Chem. Comm. (1973) 80.
89. H.A. SZYMANSKI, Ed,  
"Raman Spectroscopy", Plenum Press, New York,  
Vol. 2 (1970).
90. D.L. JEANMAIRE, R.P. VAN DUYNE,  
J. Am. Chem. Soc., 98 (1976) 4029.
91. M. FLEISCHMANN, P.J. HENDRA and A.J. McQUILLAN,  
Chem. Phys. Lett., 26 (1974) 163.
92. T.H. WOOD and M.V. KLEIN,  
J. Vac. Sci. Technol., 16 (1979) 459.
93. A.W. CZANDERNA, Ed,  
"Methods of Surface Analysis", Elsevier, Amsterdam,  
(1975).
94. C.R. BRUNDLE,  
in "Surface and Defect Properties of Solids", The  
Chemical Society, 1 (1972) 171.
95. C.S. FADLEY,  
in C.R. Brundle and A.D. Daker, Eds, "Electron  
Spectroscopy: Theory, Techniques and Applications",  
Academic Press, London, Vol. 2 (1978).

96. K.S. KIM, A.F. GOSSMAN and N. WINOGRAD,  
Anal. Chem., 46 (1974) 197.
97. S.J. ADKINSON, C.R. BRUNDLE and M.W. ROBERTS,  
J. Electron Spectroscopy, 2 (1973) 105.
98. J.S. HAMMOND and N. WINOGRAD,  
J. Electroanal. Chem., 80 (1977) 123;  
J. Electrochem. Soc., 124 (1977) 826.
99. C.R. BRUNDLE and A.D. BAKER, Eds,  
"Electron Spectroscopy: Theory, Techniques and  
Applications", Academic Press, London, Vol. 4 (1981).
100. C.C. CHANG, B. SCHWARTZ and S.P. MURARKA,  
J. Electrochem. Soc., 124 (1977) 922.
101. P.W. PALMBERG,  
in "The structure and Chemistry of Solid Surfaces",  
G.A. Somorjai, Ed., Wiley, New York (1969).
102. P.W. PALMBERG,  
Surf. Sci., 25 (1971) 598.
103. G.A. SOMORJAI and H.H. FARELL,  
Adv. Chem. Phys., 20 (1971) 215.
104. J.B. PENDRY,  
"Low Energy Electron Diffraction" Academic Press,  
New York (1974).
105. R.M. ISHIKAWA and A.T. HUBBARD,  
J. Electroanal. Chem., 69 (1976) 317.
106. W.E. O'GRADY, M.Y.C. WOO, P. HAGANS and E. YEAGER,  
J. Electrochem. Soc., 125 (1978) 348.
107. P.N. ROSS, Jr.,  
J. Electrochem. Soc., 126 (1979) 67.
108. J.S. HAMMOND and N. WINOGRAD,  
J. Electroanal. Chem., 78 (1977) 55.
109. B. BEDEN, A. BEWICK, K. KUNIMATSU and C. LAMY,  
J. Electroanal. Chem., in press.
110. A. BEWICK, K. KUNIMATSU AND B.S. PONS,  
Electrochim. Acta , 25 (1980) 465.
111. R. PARSONS,  
In "Adv. in Electrochemistry and Electrochemical Engineering",  
Vol. 1 , Interscience, New York (1961).
112. P. DELAHAY,  
"Double Layer and Electrode Kinetics", Interscience, New York  
(1965).

113. R.M. REEVES,  
in "Modern Aspects of Electrochemistry", Vol. 9,  
B.E. Conway and J. O'M Bockris, eds., Plenum Press,  
New York (1974).
114. B.E. CONWAY,  
"Theory and Principles of Electrode Processes", Ronald  
Press (1965) chapter 3.
115. O. STERN,  
Z. Elektrochem., 30 (1924) 508.
116. D.C. GRAHAME,  
J. Am. Chem. Soc., 63 (1941) 1207; 68 (1946) 301.
117. D.C. GRAHAME,  
Chem. Rev., 41 (1947) 441.
118. J.R. MACDONALD AND C.A. BARLOW, Jr.,  
J. Chem. Phys., 36 (1962) 3062.
119. R.G. BARRADAS and B.E. CONWAY,  
J. Electroanal. Chem., 6 (1963) 314.
120. R. PEAT,  
in "Advanced Instrumental Methods in Electrode Kinetics",  
University of Southampton, July 1982.
121. A.W.B. AYLMER-KELLY, A. BEWICK, P.R. CANTRILL and  
A.M. TUXFORD,  
Faraday Disc. Chem. Soc., 56 (1973) 9.
122. A. BEWICK, G.J. EDWARDS and J.M. MELLOR,  
Tetrahedron Letters, 52 (1975) 4685; Electrochim. Acta.  
21 (1976) 1101; J.C.S. Perkin II, 2 (1977) 1952; Lebig's  
Ann. Chem., 1 (1978) 41.
123. A. BEWICK, J. MELLOR and B.S. PONS,  
Electrochimica Acta, 25 (1980) 931.
124. O.P. de MARQUEZ,  
Ph.D Thesis, Southampton University (1982).
125. B.S. PONS,  
Ph.D Thesis, Southampton University (1979).
126. A.M. BRODSKY,  
I.S.E. 33<sup>rd</sup> meeting ; Extended abstracts ; Vol. 11; France (1982).
127. R.M. LAZORENKO-MANEVICH and T.N. STOYANOVSKAYA,  
Sov. Electrochem. 8 (1972) 1079.
128. B.E. CONWAY and S. GOTTESFELD,  
J.C.S. Faraday I, 70 (1974) 1793.

129. T. TAKAMURA, K. TAKAMURA and F. WATANABE,  
Surf. Sci., 44 (1974) 93.
130. J.S. CLARKE, A.T. KUHN, W.J. ORVILLE-THOMAS and M. STEDMAN,  
J. Electroanal. Chem. 49 (1974) 199.
131. T. DAVIDSON, S. PONS, A. BEWICK and P.P. SCHMIDT,  
J. Electroanal. Chem., 125 (1981) 237.
132. S. PONS, T. DAVIDSON and A. BEWICK,  
Anal. Chem., submitted.
133. J.W. RUSSELL, J. OVEREND, K. SCANLON, M.W. SEVERSON and  
A. BEWICK,  
J. Phys. Chem., 86 (1982) 3066.
134. J.W. RUSSELL, J. OVEREND, K. SCANLON, M.W. SEVERSON and  
A. BEWICK,  
J. Phys. Chem., submitted.
135. W.G. GOLDEN, D.S. DUNN, J. OVEREND and M.W. SEVERSON,  
J. Catal., 65 (1980) 271 ; J. Phys. Chem. 84 (1980) 336.
136. J.H. VAN DER MAAS,  
"Basic Infrared Spectroscopy", Heyden and Son, London  
(1969).
137. C.N. BANWELL,  
"Fundamentals of Molecular Spectroscopy", Second Edition,  
McGraw-Hill, London (1972).
138. E.B. WILSON, Jr., J.C. DECIUS and P.C. CROSS,  
"Molecular Vibrations", McGraw-Hill, New York (1955).
139. N.V. RICHARDSON,  
Surf. Sci., 87 (1979) 622.
140. J. PRITCHARD,  
in "Chemical Physics of Solids and their Surfaces",  
The Chemical Society, Vol. 7 (1978) 157.
141. A. BEWICK, K. KUNIMATSU, B.S. PONS and J.W. RUSSELL,  
Anal. Chem., submitted.
142. A. BEWICK, K. KUNIMATSU, J. ROBINSON and J.W. RUSSELL,  
J. Electroanal. Chem., 119 (1981) 175.
143. A. BEWICK and J.W. RUSSELL,  
J. Electroanal. Chem., 132 (1982) 329.
144. B. BEDEN, A. BEWICK, K. KUNIMATSU and C. LAMY,  
J. Electroanal. Chem., 121 (1981) 343.

145. B. BEDEN, A. BEWICK, K. KUNIMATSU and C. LAMY,  
32nd I.S.E. Meeting, Dubrovnik/cavtat, Yugoslavia,  
September (1981).
146. B. BEDEN, A. BEWICK, M. RAZAQ and J. WEBER,  
J. Electroanal. Chem., 139 (1982) 203.
147. A. BEWICK and T. SOLOMUN,  
in preparation.
148. S.B. BRUMMER,  
J. Electrochem. Soc., 113 (1966) 1043.
149. M.W. BREITER,  
Electrochim. Acta, 12 (1967) 1213.
150. M.W. BREITER,  
J. Electroanal. Chem., 101 (1979) 329.
151. A. BEWICK and K. KUNIMATSU,  
Surf. Sci., 101 (1980) 131.
152. M.F. KIMMITT,  
"Far-Infrared Techniques", Pion, London (1970).
153. M.M. BAIZER,  
"Organic Electrochemistry", M. Dekker, N.Y. (1973).
154. A. CAPON and R. PARSONS,  
J. Electroanal. Chem., 39 (1972) 275.
155. E. GILEADI (Ed),  
"Electrosorption", Plenum Press, N.Y. (1967) Chapter 2.
156. J.P. DELVIN and K. CONSANI,  
J. Phys. Chem., 85 (1981) 2597.
157. Working Atlas of Infrared Spec.,  
Published by Butterworth and Co. Ltd., London, (1972).
158. A. OTTO,  
in "Proc. Conf. on Vibrations in the Adsorbed Layer",  
Jülich, Germany (1978) 162.
159. A. OTTO,  
Surf. Sci., 75 (1978) L392.
160. A. OTTO,  
Surf. Sci., 92 (1980) 145.
161. T.E. FURTAK,  
Solid State Commun., 28 (1978) 903.
162. J. BILLMANN, G. KOVACS and A. OTTO,  
Surf. Sci., 92 (1980) 153.



163. R.E. BENNER, R. DORNHAUS, R.K. CHANG and B.L. LAUBE,  
Surf. Sci., 101 (1980) 341.
164. M. FLEISCHMANN, I.R. HILL and M.E. PEMBLE,  
J. Electroanal. Chem., 136 (1982) 361.
165. R. DORNHAUS, M.B. LONG, R.E. BENNER and R.K. CHANG,  
Surf. Sci., 93 (1980) 240.
166. M.E. PEMBLE,  
Ph.D. Thesis, Southampton University, 1980.
167. J. TIMPER, J. BILLMANN, A. OTTO and I. POCKRAND,  
Surf. Sci., 101 (1980) 348.
168. T.E. FURTAK, G. TROTT and B.H. LOO,  
Surf. Sci., 101 (1980) 374.
169. J.T. HUPP, D. LARKIN and M.J. WEAVER,  
to be published in Surf. Sci.
170. J.G. BERGMAN, J.P. HERITAGE, A. PINCZUK, J. WORLOCK  
and J.H. McFEE,  
Chem. Phys. Lett., 68 (1979) 412.
171. R.M. NEXTER and M.G. ALBRECHT,  
Spectrochim. Acta, 35A (1979) 233.
172. R. KÖTZ and E. YEAGER,  
J. Electroanal. Chem., 123 (1981) 335.
173. U. WENNING, B. PETTINGER and H. WETZEL,  
Chem. Phys. Lett., 70 (1980) 49.
174. B.H. LOO and T.E. FURTAK,  
Chem. Phys. Lett., 71 (1980) 68.
175. B.B. DAMASKIN, O.A. PETRII and V.V. BATRAKOV,  
"Adsorption of Organic Compounds on Electrodes",  
Plenum Press, N.Y. (1971).
176. B. PETTINGER, U. WENNING and H. WETZEL,  
Surf. Sci., 101 (1980) 409.
177. D.L. JEANMAIRE and R.P. VAN DUYNE,  
J. Electroanal. Chem., 84 (1977) 1.
178. H. WETZEL, H. GERISCHER and B. PETTINGER,  
Chem. Phys. Lett., 80 (1981) 159.
179. J.M. SMITH, L.H. JONES, I.K. KRESSIN and R.A. PENNEMAN,  
Inorg. Chem., 4 (1965) 369.
180. A.Z. GENACK, D.A. WEITZ and T.J. GRAMILA,  
Surf. Sci., 101 (1980) 381.

181. R.L. DEKOCK, A.C. SARAPU and R.F. FENSKE,  
Inorg. Chem., 10 (1971) 38.
182. M.F.A. EL-SAYED and R.K. SHELINE,  
J. Inorg. Nuclear Chem., 6 (1958) 187.
183. L.H. JONES and J.M. SMITH,  
J. Chem. Phys., 41 (1964) 2507.